

THE GEOLOGY OF BASEMENT ROCKS IN THE
SOUTHEASTERN TARARUA RANGE, NORTH ISLAND
NEW ZEALAND.

LISA ANN FOLEY

Submitted in fulfilment for the degree of Master of Science
in geology, Victoria University of Wellington, September 1984.



FRONTISPIECE. View of the Tauherenikau River looking east.

ABSTRACT

Basement rocks within the southeastern Tararua Range belong to two associations: a sedimentary association (greywacke, argillite, calcareous siltstone, conglomerate and olistostrome) and a volcanogenic association (metabasite, chert, red argillite and limestone). Rocks of the sedimentary association are more abundant and have been deposited by turbidity currents and debris flows in a deep water, marine environment. Three turbidite and two intercalated non-turbidite lithofacies are recognized. Sedimentological data suggest that the sediment was deposited in a submarine fan system (mid-fan environment), probably in a trench. The alternating greywacke-argillite beds have detrital compositions which are essentially quartzo-feldspathic. Framework mode and geochemical analyses indicate that the sediment was derived from an active continental margin that was shedding detritus of mainly acid-volcanic and metamorphic origin.

Rocks of the volcanogenic association, although volumetrically minor, are widely distributed. Geochemical analyses of metabasites suggest that they were erupted in an oceanic environment, both at a mid-ocean ridge and an intra-plate setting. The presence of radiolaria skeletons in red argillite and chert indicates a hemiplagic depositional environment for these rocks. Rocks of the volcanogenic association often have conformable contacts. These rocks have a related depositional environment and represent seafloor material. Where observed, contacts between rocks of the two associations are always faulted.

Deformation in the field area is characterized by development of the following types of structures: several generations of folds, faults at both a low angle and high angle to bedding, shear foliation and melange. The region has undergone the following deformational events, outlined from oldest to youngest:

- 1) folding with at least two fold generations present.
- 2) fragmentation and disruption of the beds by faults. Low-angle to bedding faults and high-angle to bedding faults have disrupted the bedding. Where these structures have occurred to a great extent, a chaotically disrupted unit, melange, has formed.
- 3) post-melange folding.
- 4) recent faulting related to the present strike-slip regime in New Zealand. Rocks have undergone prehnite-pumpellyite facies metamorphism. The rock types, their field relationships and the deformation that the area has undergone is consistent with accretion at a convergent plate margin.

Radiolaria were extracted from two red chert samples. In the study the radiolaria define a Middle Jurassic age, which indicates that the sediments in the southeastern Tararua Range must be of Middle Jurassic in age or younger (possibly Cretaceous). A similar sample from the Manawatu Gorge to the north of the study area contained radiolaria of Late Jurassic-Early Cretaceous age. Sediments in both areas therefore belong to fossil zone 5 (Late Jurassic-Early Cretaceous) of MacKinnon (1983).

ACKNOWLEDGEMENTS

Special thanks to my supervisor Dr. R.J. Korsch, who aided my understanding of the geology of New Zealand during both field trips and numerous discussions. I am grateful for his encouragement, continuous help and constructive reviews.

This study has also benefitted from discussions with Drs. B. Roser, J. Begg and R. Grapes, all of whom read sections of this thesis. I would also like to thank:

Claire and Peter Rumble, for their help, use of their word processor and for a place to stay.

Alan Ross, for numerous meals and the use of his house and car, during my field work.

Duncan Watson and family, for allowing me to work on their property.

Featherston Borough Council for access to the Boar Creek area.

The staff, both academic and technical, and students of the Geology Department.

The New Zealand Geological Society for the student research award in 1983.

June and Tom Orr for transport to and from the field area, and for general support and encouragement over the last nineteen months.

My family for their encouragement and a months enforced holiday.

I especially thank Thomas Orr, without whom I would not have started or finished this thesis.

CONTENTS

AKNOWLEDGEMENTS	iii
<hr/>	
LIST OF FIGURES	vii
<hr/>	
LIST OF TABLES	x
<hr/>	
CHAPTER ONE : INTRODUCTION	1
<hr/>	
1.1: Regional geology	1
1.2: Field area	4
CHAPTER TWO : ROCK TYPES	8
<hr/>	
2.1: Sedimentary association : Sediment, lithologies and depositional environment	8
2.1.1 Turbidites	9
2.1.2 Conglomerate and olistostrome	11
2.1.3 Lithofacies	12
2.1.4 Environment of deposition	15
2.2: Petrography and geochemistry	18
2.2.1 Greywacke	18
2.2.2 Argillite	24
2.2.3 Calcareous siltstone	25
2.2.4 Polymict conglomerate	25
2.2.5 Olistostrome	26
2.2.6 Geochemistry	28
2.3: Provenance and tectonic setting	35
2.3.1 Tectonic setting using geochemical analysis	39
CHAPTER THREE : VOLCANOGENIC ASSOCIATION	45
<hr/>	
3.1: Introduction	45
3.1.1 Metabasite	45
3.1.2 Red argillite	48
3.1.3 Chert	49
3.1.4 Limestone	49

3.2: Metabasite geochemistry	50
3.2.1 Tectonic setting	53
3.3: Original environment of formation	60
 CHAPTER FOUR : METAMORPHISM	 64
<hr/>	
4.1: Vein mineral assemblages	68
4.2: Metamorphic grade	70
 CHAPTER FIVE : PALEONTOLOGY	 71
<hr/>	
5.1: Fossils localities within the study area	71
5.1.1 Radiolaria	73
5.2: Systematic paleontology	77
 CHAPTER SIX : STRUCTURE	 87
<hr/>	
6.1: Mesoscopic structures	87
6.1.1 Folds	87
6.1.2 Shear foliation	89
6.1.3 Low-angle faults	91
6.1.4 High-angle faults	91
6.1.5 Lozenges	93
6.1.6 Melange	93
6.2: Mesoscopic deformation events	99
6.2.1 Pre-melange structure	100
6.2.2 Structures produced during melange formation	100
6.2.3 Post-melange structure	101
6.3: Macroscopic structures	103
6.4: Macroscopic geometric analysis	105
6.4.1 High-angle faults	111
6.4.2 Conclusions	111
6.5: Recent deformation	115
6.6: Summary	120
6.6.1 Comparisons with other areas	121

CHAPTER SEVEN : DISCUSSION	124
<hr/>	
7.1: Source of the sedimentary association	124
7.1.1 Possible source of Tararua greywacke	126
7.1.2 Depositional environment for rocks of the sedimentary association	126
7.2: Origin of the volcanogenic association	127
7.3: Origin of the Torlesse Supergroup	128
7.3.1 Proposed model of formation of the Torlesse	128
7.4: Subduction zones	131
7.4.1 Style of accretion	131
7.4.2 Mechanisms of emplacement	132
7.5: Data from the field area	133
REFERENCES	138
<hr/>	
APPENDIX I : Maps	146
<hr/>	
APPENDIX II : Major and trace element geochemistry	147
<hr/>	
APPENDIX III : Modal point counting technique	148
<hr/>	
APPENDIX IV : Determination of grain size for sandstone	149
<hr/>	
APPENDIX V : Samples	150
<hr/>	
APPENDIX VI : Electron microprobe method	153
<hr/>	
APPENDIX VII : Carbonate determination	154
<hr/>	
APPENDIX VIII: Electron microprobe analysis	155
<hr/>	

LIST OF FIGURES

Figure	Page
1-1: Basement rocks of New Zealand	2
1-2: Location map of field area	5
2-1: Rock sequences	10
(a) Typical rock sequence in study area	
(b) Bouma sequence.	
2-2: Sedimentary lithofacies	13
(a) Lithofacies 2: sandstone with thin interbeds of argillite.	
(b) Lithofacies 3: Interbedded sandstone and argillite.	
2-3: Sedimentary lithofacies	16
(a) Lithofacies 4: olistostrome	
(b) Lithofacies 5: dominantly argillite.	
2-4: Marine environments	17
2-5: Lithofacies associations in the study area	19
2-6: Major oxide vs SiO ₂ chemical variation diagrams	32
2-7: Trace element vs SiO ₂ chemical variation diagrams	34
2-8: QFL and QmFlt diagrams	37
2-9: QpLvmLsm and LmLvLs diagrams	38
2-10: Comparative QFL diagrams for other areas in the Torlesse Supergroup	41
2-11: Determination of tectonic setting of greywacke-argillite using an alkali ratio - silica discriminant	44
3-1: Geological map of metabasite and sediment in Abbots Creek . .	46
3-2: Metabasite outcrops	47
(a) Sheared contact between metabasite and sediment.	
(b) Pillows in metabasite.	
3-3: Magma type discriminant plots	54
(a) Y/Nb ratio.	
(b) Histograms of discriminant function values.	
3-4: Ti-V discriminant plot for metabasites	55

3-5:	Discrimination plots for metabasites	57
	(a) Ti-Zr-Y discriminant diagrams.	
	(b) Ti-Zr discriminant diagram.	
	(c) Zr/Y-Zr discriminant diagram.	
3-6:	La-Nb discriminant plot for metabasites	59
3-7:	TiO ₂ -MnO-Na ₂ O discriminant plot for clinopyroxenes	61
4-1:	Variation diagrams for metamorphic minerals	67
	(a) Al-Ti-Fe variation diagram for sphene.	
	(b) Al-Fe-Mg variation diagram for pumpellyite.	
4-2:	CaO-Al ₂ O ₃ -Fe ₂ O ₃ (total iron) variation diagram for prehnite	69
5-1:	Age ranges of radiolaria	75
	(a) Southeastern Tararua Range.	
	(b) Manawatu Gorge.	
5-2:	Photomicrograph of radiolaria	84
5-3:	Photomicrograph of radiolaria	85
5-4:	Photomicrograph of radiolaria	86
6-1:	Folds	88
	(a) Folded radiolaria rich chert block that has been refolded.	
	(b) Folded melange.	
6-2:	Mesosopic structures	90
	(a) Folded block within melange.	
	(b) Shear foliation.	
6-3:	Faults	92
	(a) Faults at a high angle to bedding.	
	(b) Faults at a low angle to bedding.	
6-4:	Cartoon interpretation of the development of lozenges	94
6-5:	Beds showing a "kinked" outline	95
6-6:	Melange fabric	97
6-7:	Melange matrix	98
6-8:	Flinn diagram	102
6-9:	Structural "belts" in the field area	104

6-10: Structural "domains" and nets of bedding and shear foliation accreditations for each domain	106
6-11: Synoptic net of poles to π So	107
6-12: Possible methods by which pattern seen in the synoptic net (Fig. 6-11) can be produced	109
(a) Early fold.	
(b) Refolding an early fold.	
6-13: Mesoscopic folds	110
(a) Fold axes of both mesoscopic and macroscopic folds.	
(b) Axial surfaces.	
6-14: High-angle fault orientation data for each domain	112
6-15: Geometry of simultaneous cylindrical folding of two planar surfaces	113
6-16: Net which shows great circle girdles which contain the fold axis at π So and π Sf for domains 2, 3, 8, 12, 13	114
6-17: Recent faults as planes on Wulff net	116
6-18: Lineaments in field area	119
7-1: Subduction system	129
7-2: Delineation of fossil zones using data from this study	137

LIST OF TABLES

Table	Page
2-1: Facies association and relative environments of sedimentation .	17
2-2: Modal analyses from 15 sandstones	21
2-3: Major and trace element analyses for sandstone and argillite . .	29
2-4: Correlation matrix for sediments	31
2-5: Modal analysis of sandstone from known tectonic settings	40
2-6: Tectonic shedding of sediment using geochemical data	42
3-1: Metabasite major and trace element analyses	51
4-1: Representative analyses of metamorphic minerals	65
6-1: Deformation sequence in other areas	123

CHAPTER ONE

INTRODUCTION

1.1 REGIONAL GEOLOGY

New Zealand basement geology is divided into Western and Eastern Provinces, separated by the Median Tectonic Line and the active Alpine Fault (Landis & Coombs 1967) (Fig. 1-1). The Western Province of Precambrian to Cretaceous age, consists of Paleozoic sediments and crystalline rocks of Late Precambrian to Cretaceous age (Coombs *et al.* 1976). In the Eastern Province two associations are recognized, the Hokonuni and Alpine (Wellman 1952). Transitionally between the two associations occurs the Haast Schist, a metamorphosed equivalent of the surrounding rocks.

The most western association of the Eastern Province, the Hokonuni, abuts the Median Tectonic Line and contains predominantly volcanoclastic sediments and volcanics (Coombs *et al.* 1976). Based on lithologies, the Hokonuni association consists of four units, these being from west to east:

- 1) Brook Street Volcanics- consists predominantly of calc-alkaline to tholeiitic volcanics and intrusives,
- 2) Maitai group and Murihiku group- consists of dominantly volcanogenic siltstone with minor sandstone, conglomerate, breccia and limestone,
- 3) Dun Mountain Ophiolite- consists mainly of ultramafic (now mostly serpentinite) rocks, gabbros and pillow lavas,
- 4) Caples group, Pelorus group and Waipapa group- consists of poorly fossiliferous volcanogenic sandstone and siltstone with minor metabasite, chert and limestone.

The Alpine association, contains quartzo-feldspathic sediments of the Torlesse Supergroup (Suggate 1961). The Torlesse Supergroup is a complexly deformed, sparsely fossiliferous, interbedded sequence of

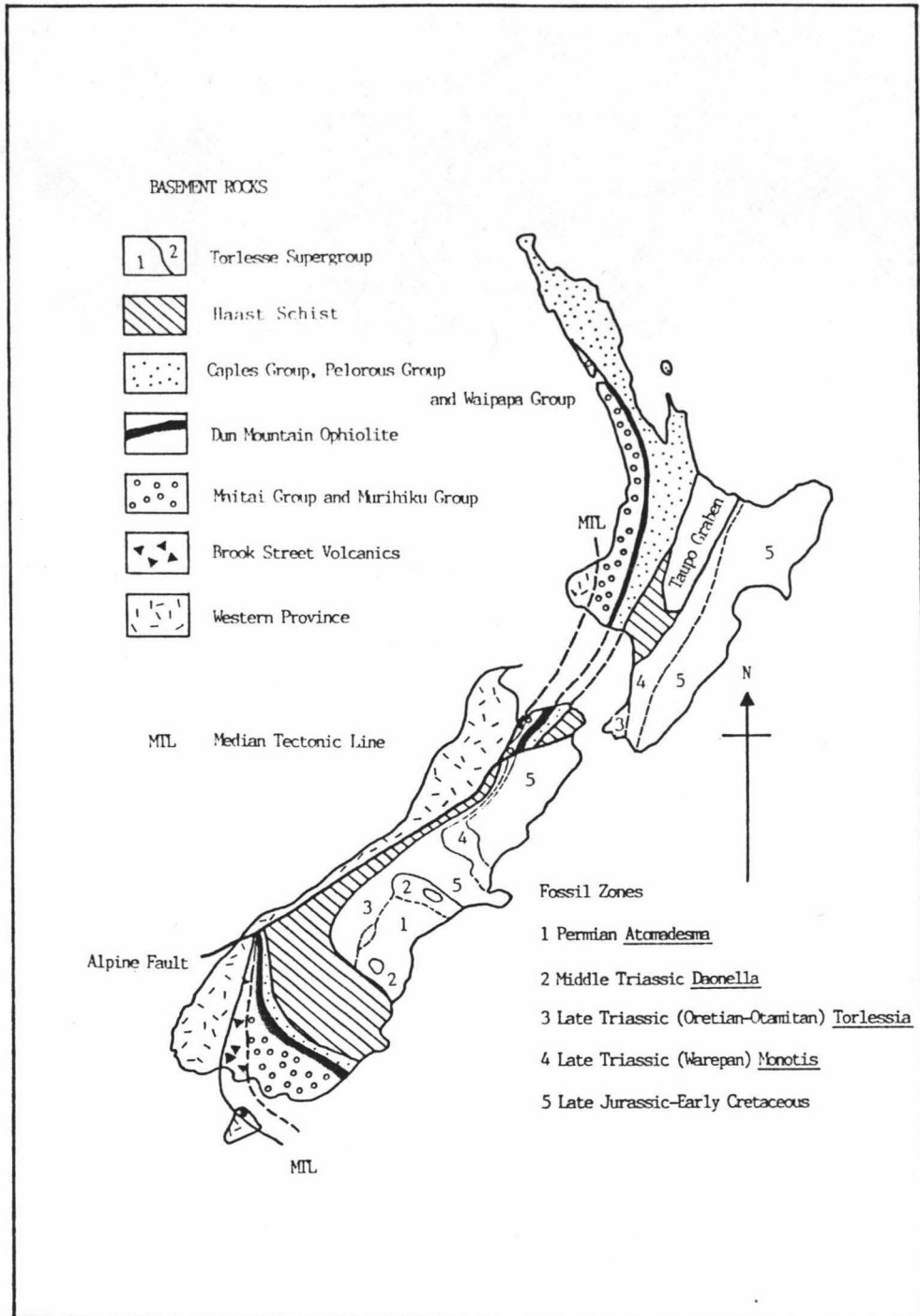


Figure 1-1: Basement rocks of New Zealand (after Sporli 1978). Fossil zones in the Torlesses Supergroup are from Landis & Bishop (1972); Speden (1976) and MacKinnon (1983).

sandstone and siltstone, usually referred to in New Zealand as greywacke and argillite, with minor associated conglomerate, basalt, tuff, coloured argillite, chert and limestone.

Five fossil zones have been recognized in the Torlesse Supergroup. They are: 1) Atomadesma, Permian; 2) Daonella, Mid-Triassic; 3) Torlessia, Late Triassic (Oretian-Otamitan); 4) Monotis, Late Triassic (Warepan); 5) Late Jurassic-Early Cretaceous (Campbell & Warren 1965; Webby 1967; Bradshaw 1973; Speden 1976; Andrews et al. 1976; MacKinnon 1983). In the North Island only fossil zones 3-5 have been recognised and these young towards the east, but within each zone the dominant younging direction is westward. The fossils, being both shallow water marine and deep water marine in origin, have led to differing opinions as to the site of Torlesse sediment deposition. Some workers (Bradshaw 1973; Bradshaw & Andrews 1973) have argued for a dominantly shallow marine origin, although now, the general consensus is that the Torlesse is dominantly deep water marine with some shallow marine and fresh water sediments (Carter et al. 1978).

The model currently favoured by many workers is that the Torlesse Supergroup represents an accretionary prism, forming as a result of turbidite deposition within trench, slope and borderland basins. These sediments were accreted to the inner trench wall, along with oceanic crust, during subduction (Sporli 1978; MacKinnon 1983; Korsch & Wellman in press). Subduction would have scraped the turbidity deposits, along with some oceanic crust, from the sea floor and stacked the rocks into imbricated "packets". Imbricated rock "packets" have been documented from many localities within the Torlesse (Sporli & Bell 1976; Sporli 1978). Fossil zones and younging directions are consistent with an accretionary prism model. The Torlesse has often been compared with the Franciscan Complex of California, U.S.A., (Landis & Bishop 1972; Blake et al.

1974), which is regarded as a type accretionary prism (Dickinson et al. 1982).

In the southern part of the North Island, the Torlesse Supergroup crops out in the Wellington area and the Rimutaka, Tararua and Ruahine Ranges. Age control is minimal. Fossils found in the Wellington area are Late Triassic (Oretian-Otamitan) Halobia lilliei (Campbell 1982), tube fossils Torlessia and Titahia (Webby 1967; Speden 1976) and the trace fossil Scalarituba (Rowe in prep.). At Otaki Forks, Late Triassic (Warepan) Monotis occur (Grant-Taylor & Waterhouse 1963; Speden 1976).

Due to complex deformation and a lack of marker beds in the Torlesse, most workers have made interpretations of the regional geology based on detailed studies of small areas. In 1888 McKay produced two geological reports on the south-eastern Tararua Range (McKay 1888a,b). The petrography of rocks in the Wellington area has been described by Reed (1957a) and Rowe (1980). Other studies have concentrated on structural and sedimentological aspects (Sporli & Bell 1976; Rattenbury 1983).

The main aims of this study are to: 1) geologically map an area, attempting to subdivide the rocks into lithofacies based on lithology and structure; 2) carry out detailed petrological and geochemical studies, to elucidate the provenance and tectonic setting; 3) outline the deformational history; 4) relate the area to regional tectonic interpretations.

1.2 FIELD AREA

The study area is situated in the eastern foothills of the southern Tararua Range, 55 kilometres north-east of Wellington (Fig.1-2).

The area is approachable by road along its eastern margin, (Underhill Road) and is bounded to the north and south by Waiohine Gorge

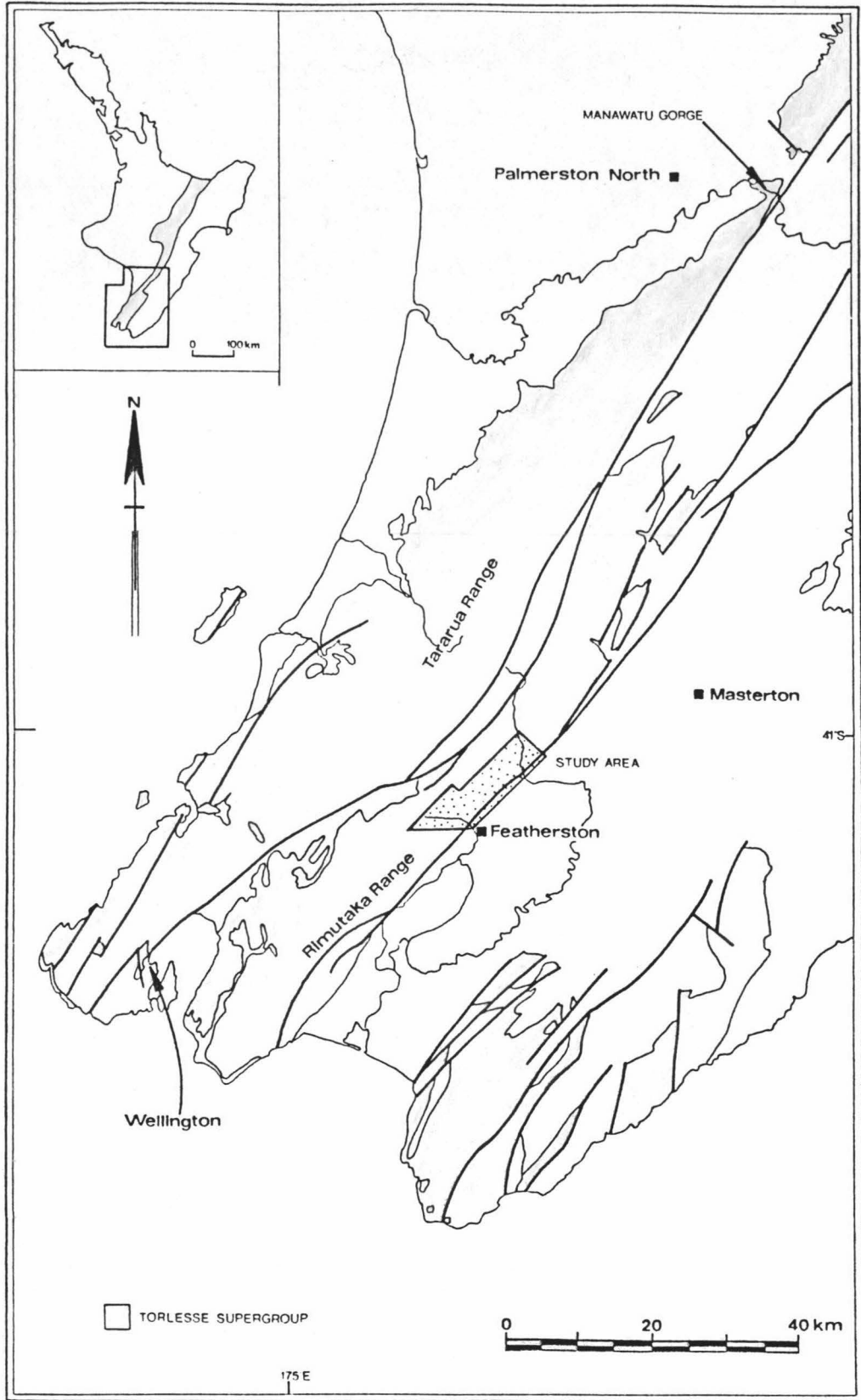


Figure 1-2: Map of the southern North Island showing the Torlesse Supergroup and the study area.

Road and State Highway 2 respectively. Over most of the area, (the western and central portions) walking tracks are few, with access often being restricted to river and stream beds.

Elevation in the study area ranges from 100m to 645m above mean sea level, resulting in steep and often rugged slopes. Along the eastern margin of the foothills these slopes have been cleared for farming. Immediately west, the ground cover is regenerated scrub, (mainly manuka and gorse) grading into beech forest with scattered rimu, miro and kahikatea. Most fresh rock outcrops are confined to river and stream beds.

Rocks in the study area are predominantly sedimentary, with alternating greywacke and argillite dominating over minor calcareous siltstone, conglomerate and olistostrome. Metabasite, with associated chert and red argillite occurs widely throughout the Tararua Range, and has sheared contacts with surrounding rocks.

Bedding strikes roughly north-northeast to northeast. The structure is complex, with shearing being pervasive and developed predominantly along bedding planes. Highly sheared tectonic melanges have developed, with shearing striking roughly parallel to the dominant strike. The melanges incorporate all rock types found in the area.

Kingma (1967) in mapping the Wellington 1:250,000 sheet, assigned the rocks of the study area to the Upper Jurassic. However when Speden (1976) designated fossil zones within the Torlesse, the Tararua Range fell within his Late Triassic (Warepan) Monotis zone. These assignments of conflicting ages, have been based on extrapolation from other areas in the Torlesse and therefore neither age can be taken as definitive.

All grid references cited refer to the 1975 metric grid of New Zealand, based on the NZMS 260 topographical series. Topographic maps and

aerial photographs used for the basis of maps and figures are listed in Appendix I.

CHAPTER TWO

ROCK TYPES

The rocks in the study area are predominantly sandstone (greywacke), and siltstone-mudstone (indurated to argillite) with minor associated conglomerate, olistostrome, metabasite, argillite, limestone and chert. For organisation purposes the rock types are examined in two sections. Chapter 2 provides a description and discussion of the main clastic sedimentary rocks, eg. greywacke, conglomerate. Chapter 3 provides a description and discussion of rocks of volcanogenic association, eg metabasite, chert, red argillite.

2.1 SEDIMENTARY ASSOCIATION: SEDIMENT, LITHOLOGIES AND DEPOSITIONAL ENVIRONMENT

Sedimentary rocks in the area are predominantly sandstone and argillite, with minor conglomerate and olistostrome. Initially the nature of the sediments are described, and a depositional environment is proposed, followed by detailed petrographic descriptions (including geochemistry) of the sediments.

Within the Tararua Range a common sequence of sandstone and argillite is of a massive fine-grained sandstone within a single graded unit, overlying a sharp base. This sandstone grades up into a laminated finer-grained sandstone and then siltstone-mudstone. Often the fine laminated sandstone is absent.

The sandstone portions are generally fine-grained, massive with grading being distinct in only a number of beds. The units range in size up to 20 metres in thickness, although these thicknesses may represent the amalgamation of a number of beds, where joint planes could represent the amalgamated surfaces. Amalgamated sandstone beds are a common feature to see in deep sea sediments but are usually difficult to observe (Ingersoll 1978). In the basal sections of the sandstone, clasts of

siltstone and mudstone occur. In the upper section, plane parallel laminations and ripple cross-laminations, often truncated, are occasionally seen.

The sandstone-argillite contact is frequently sheared with bedding plane shears, although gradations between the two can be seen in a large number of beds. Within the argillite unit, plane parallel laminations can be observed, grading into a finer mud-size sediment, devoid of any sedimentary structures. The massive fine mudstone is suggestive of deposition by suspension settling only.

Typical rock sequences with sedimentary structures can be seen in Fig. 2-1a.

2.1.1 Turbidites

The alternating sandstone and argillite beds within the Torlesse from the southern North Island have often been ascribed to turbidite deposits (Reed 1957a; Rowe 1980; Rattenbury 1983). Turbidite deposits are the result of density currents.

Practically all turbidites have been deposited in a marine environment, although turbidites from fresh-water environments are known eg. Lake Mead (Gould 1951); Lake Geneva (Bouma 1964). Fossils found in the Wellington area and the Tararua Range ie. Torlessia (Webby 1967), Titahia (Webby 1967) and Monotis (Grant-Taylor & Waterhouse 1963), indicate a marine depositional environment for the sediments.

Turbidity deposits and their features are often described in terms of the "ideal" turbidite model, proposed by Bouma (1962). The five sections of the "ideal" turbidite model (Fig 2-1b), have a fixed sequence, these being from bottom to top:

- 1) Graded interval (Ta)-sandstone which shows graded bedding, although grading may be indistinct or absent,
- 2) Lower interval of parallel lamination (Tb)-graded sandstone interval

Column 1= Devils Creek (S26D/ 1165 1884)
 Column 2= Waiohine Gorge Road (S26D/ 1200 1785)
 Column 3= State hightway 2 (S27A/ 0244 0859)

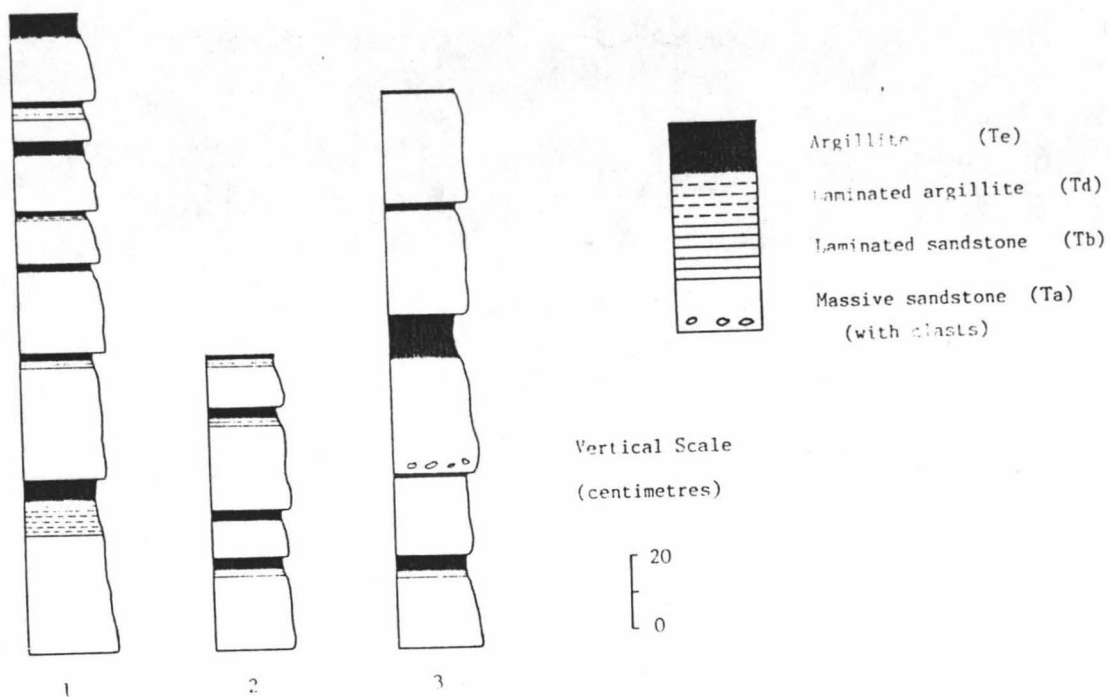


Figure 2-1a: Typical rock sequences in the field area.

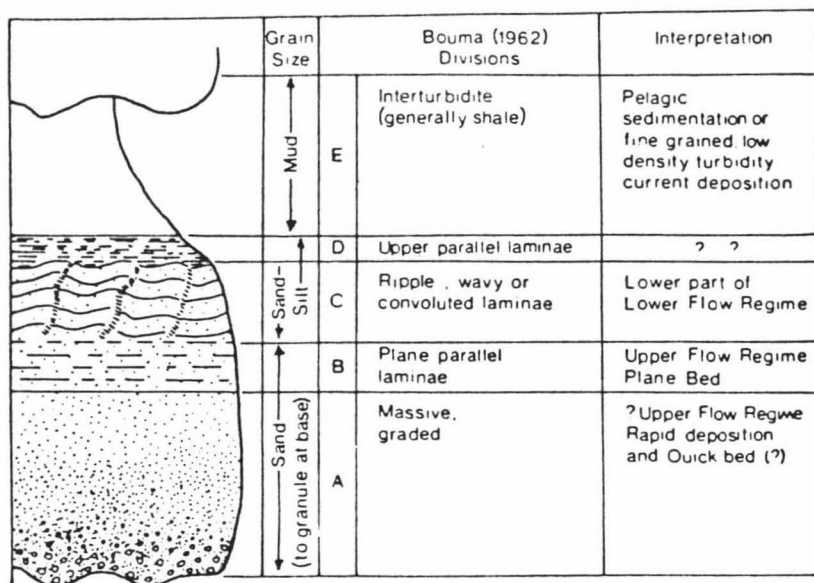


Figure 2-1b: Bouma model (from Middleton & Hampton 1973)

with coarse parallel laminations,

- 3) Interval of current ripple lamination (Tc)-sandstone featuring current ripples, crossbedding and convolute laminations,
- 4) Upper interval of parallel lamination (Td)-fine sandstone to siltstone with indistinct parallel lamination,
- 5) Pelitic interval (Te)-with no visible sedimentary structures.

Features of turbidites are commonly those which develop by the redeposition of sediment in a deep-water marine environment. Therefore turbidite sequences typically lack features indicative of proximity to sea-level or terrestrial sites eg. winnowed sands, beach structures, river deposits, megaripples, sun cracks, rain pits and reefs.

Throughout the Tararua Range, most of the typical features listed above for turbidites have been found. This, and the lack of features indicative of other depositional sites, make it reasonable to ascribe the beds to the action of turbidity currents.

2.1.2 Conglomerate and olistostrome

Other rocks of sedimentary association formed by sedimentary gravity flows (conglomerate and olistostrome) cannot be explained in the turbidite model of Bouma (1962). Several different types of sedimentary gravity flows are distinguished on the mechanism of grain support. As well as turbidity flows (by fluid turbulence) these are: debris flows (clasts supported by matrix), grain flows (by grain to grain interactions) and fluidized sediment flow (by expanding pore fluids) (Rupke 1978).

Conglomerates within the Tararua Range are clast supported, with some being normally-graded (Chapter 2.2.4). Walker (1975) stated that conglomerates associated with turbidites could be deposited by turbulent flows, or as mass movements (debris flows). Grading within the conglomerate implies deposition by turbulent flow, rather than debris

flows, with the deposition of clasts occurring because of decreased energy, rather than a "freezing" of mass moving sediment.

Alternatively, olistostromes (sedimentary chaotic deposits, sedimentary "melange") are formed by debris flows or slumps, with mass movements of sediments down slope. In the study area, olistostromes are internally structureless and consist of mainly rounded clasts in an unsheared matrix (Chapter 2.2.5). They are quite commonly found in other areas intercalated with turbidite deposits eg. Northern Appennines (Mutti & Ricci Lucchi 1972).

All rocks of the sedimentary association can be interpreted as having been deposited in a deep water marine environment, as the result of turbulent flows and debris flows.

2.1.3 Lithofacies

In the study of turbidites and other deep water marine deposits, facies analysis based on lithological and sedimentological observations, has been used to determine the nature of the depositional environment (eg. Walker 1979).

A simplified facies classification, after Mutti and Ricci Lucchi (1972), is used in this study area. Three turbidite and two intercalated non-turbidite lithofacies are recognized.

Lithofacies 1, consists of polymict conglomerate (clast-supported) and pebbly sandstone which corresponds to facies A of Mutti and Ricci Lucchi (1972). The conglomerate falls into the inverse- to normally-graded facies of Walker (1975). The Bouma sequence is not applicable to the description of these beds. Deposition has occurred by the process of turbulent flows.

Lithofacies 2, (fig.2-2a) consists of medium grained sandstone with thin interbeds of argillite. Sandstone beds range from 30cm to metres thick, and the sandstone to argillite ratio is high, ranging from 4:1 to

Figure 2-2a: Lithofacies 2; massive sandstone with thin interbeds of argillite. Note the crushed appearance of the sandstone due to the outcrops proximity to the Wairarapa Fault.

Waiohine River S26D/ 1150 1494,
geological hammer 31 cm long.

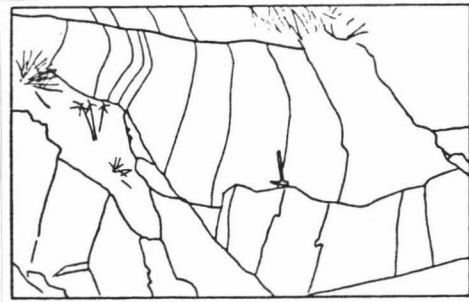
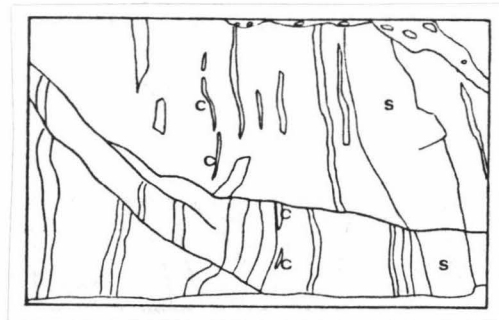
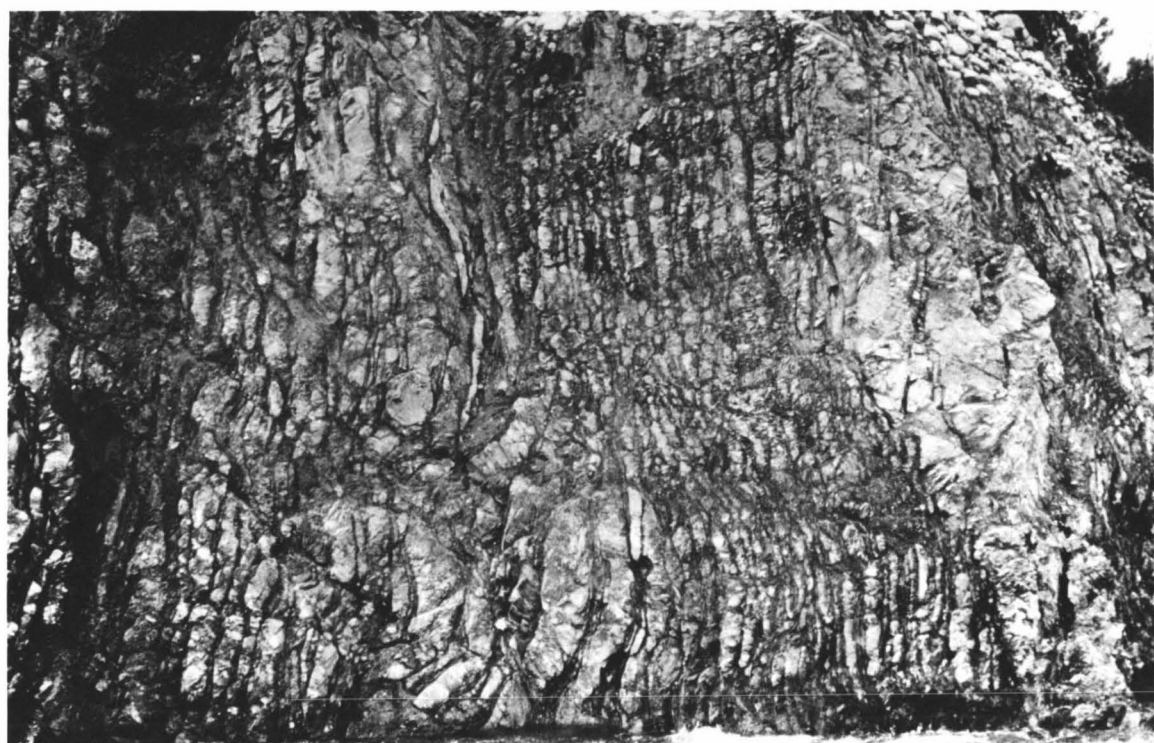
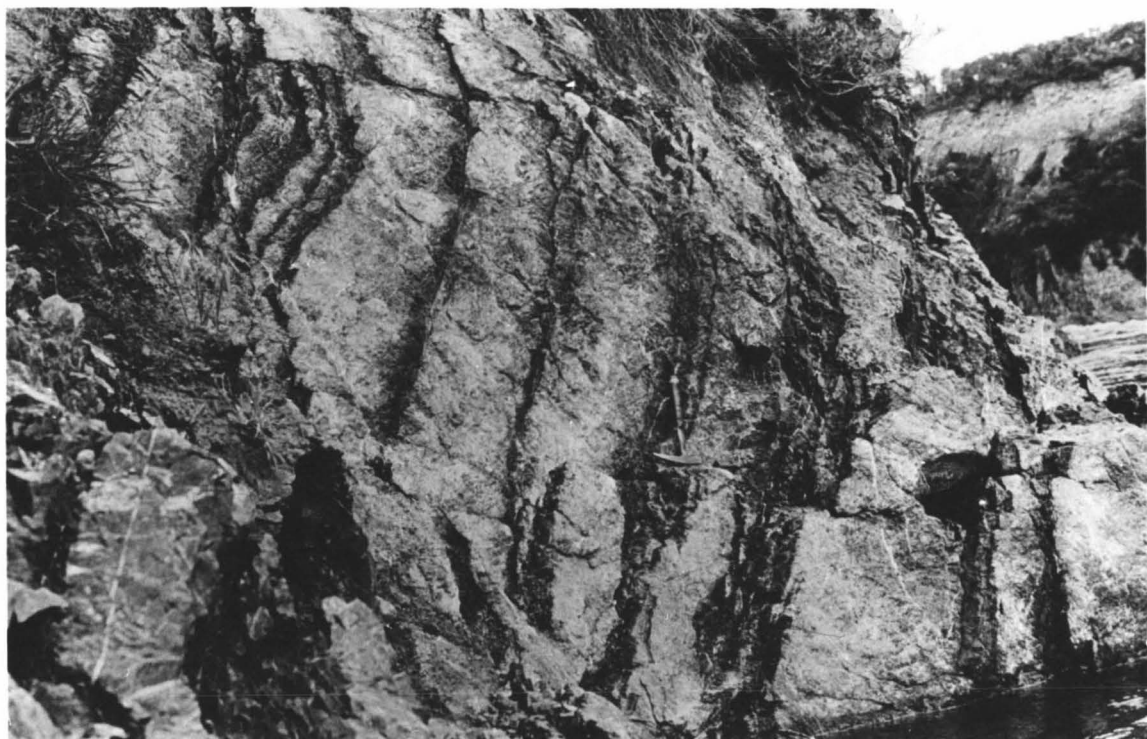


Figure 2-2b: Lithofacies 3; interbedded sandstone and argillite with minor calcareous beds (C) and massive sandstone beds (S). Note that a number of the sandstone beds wedge out.

Waiohine River S26D/ 1140 1591, width of
photograph 15 metres.





20:1; commonly 8:1. Massive beds are jointed and may be an amalgamation of a number of sandstone beds. Beds are poorly sorted with occasional laminae developed in the fine sandstone-argillite portions. Ripped-up and redeposited argillite chips are common. This is equivalent to facies B of Mutti and Ricci Lucchi (1972). These flows, being deposited by turbidity flows, can be applied to the Bouma model, where sequences Tade and less commonly Tabde and Tabe occur.

Lithofacies 3, (fig.2-2b) consists predominantly of interbedded medium to fine grained sandstone and argillite. The sandstone beds are generally less than 30cm thick, whilst the argillite beds, on average, are less than 20cm thick. However, both types can be up to 1 metre thick. Lithofacies 3 can be subdivided into two types based on sandstone: argillite ratios. Lithofacies 3(i) has sandstone to argillite ratios greater than 1:1, but less than 4:1, while lithofacies 3(ii) has ratios less than 1:1, (corresponding with facies C and D respectively, of Mutti and Ricci Lucchi (1972)). Both lithofacies can show grading in the sandstone and laminae with minor ripple cross laminations in the upper sandstone interval. Bedding surfaces are commonly parallel. The Bouma sequence is applicable to these beds with sequences of Tabcde, Tadbe and Tade occurring, indicating that they were deposited by turbidity flows. Rare calcareous beds (10-15cm thick), conformable with surrounding very fine sandstone and argillite, occur. Rattenbury (1983) noted calcareous units within thin-bedded alternating sandstone and argillite sequences from the Otaki Forks region. Mutti and Ricci Lucchi (1972) found in some beds of their facies D (my facies 3ii), that the pelitic interval could be represented by micritic limestone. These calcareous beds of the Tararua Range could indicate such a fine pelitic layer within the turbidites.

Lithofacies 4, (fig.2-3a) consists of olistostromal units, (Flores 1955). Clasts within the olistostromes are highly variable in composition, shape, size and origin. The matrix (usually very fine sandstone or argillite) is generally massive but may show shearing (equivalent to facies F of Mutti and Ricci Lucchi (1972)), being deposited by mass debris flows. The Bouma model is not applicable.

Lithofacies 5, (fig.2-3b) consists dominantly of argillite with minor, interbedded, fine-grained sandstone. Argillite is often sheared and massive. Bedding is visible between fine sandstone and argillite layers. Within argillite, occasional pebble-size clasts of various lithologies can be found, as well as finely disseminated pyrite (equivalent to facies G of Mutti and Ricci Lucchi (1972)). These beds represent deposition of hemipelagic silt and mud.

2.1.4 Environment of deposition

Based on the study of modern and ancient marine environments, early workers were able to show, systematic changes in turbidite-beds characteristics (ie, sandstone:siltstone ratio, bed thickness, grain size), as a function of the distance from the source of the depositional site (either proximal or distal; Walker 1967).

Working in the Appennines, Mutti and Ricci Lucchi (1972) distinguished facies associations common to particular marine environments. Environments indicated by the facies associations of Mutti and Ricci Lucchi are:

- 1:Slope and scarp associations,
- 2:Deep sea fan or proximal association,
- 3:Deep sea plain or distal basin association.

Table 2-1 shows the facies associations suggested for these environments. Figure 2-4 illustrates the position of these marine environments.

Figure 2-3a: Lithofacies 4; olistostromal unit showing sandstone concretions (C) which weather to a light grey colour, surrounded by dark argillite. Tauherenikau River S26C/ 1788 1290, geological hammer head 17 cm long.

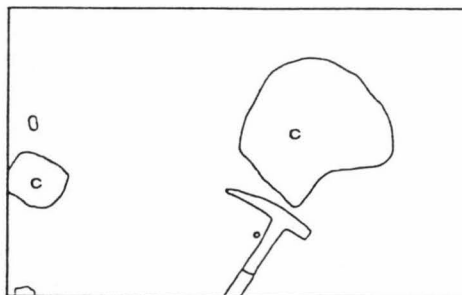
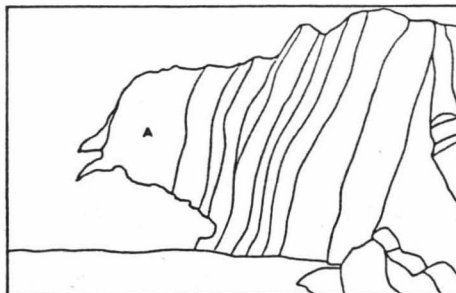


Figure 2-3b: Lithofacies 5; argillite (A) with minor interbedded sandstone, which passes into massive thick bedded sandstone with minor thin interbeds of argillite (Lithofacies 2).

Waiohine River S26D/ 1161 1875, width of photograph 15 metres.





Facies types (after Mutti & Ricci Lucchi 1972)	This studies lithofacies	General characteristics	Environments and subenvironments	
G (F)	5 (4)	Mudstone and slump textures	Slope	
A, F (B, E, G)	1, 4, 5 (2)	Major channel fill complexes, conglomerate	Fan	Inner
B, C, A, E (D, C)	2, 3i, 1 (3ii)	Predominance of thick channelized sandstone bodies; inter-channel deposits		Middle
C, D (B)	3i, 3ii (2)	Proximal to distal turbidite beds with little channelization		Outer
G, D (C)	4, 3ii (3i)	Hemiplagic mudstone with interbedded thin sandstone beds	Basin Plain	

Table 2-1: Facies associations and relative environments of sedimentation
(based on Ingersoll 1978, after Mutti & Ricci Lucchi 1972).

SUBMARINE FAN MODEL

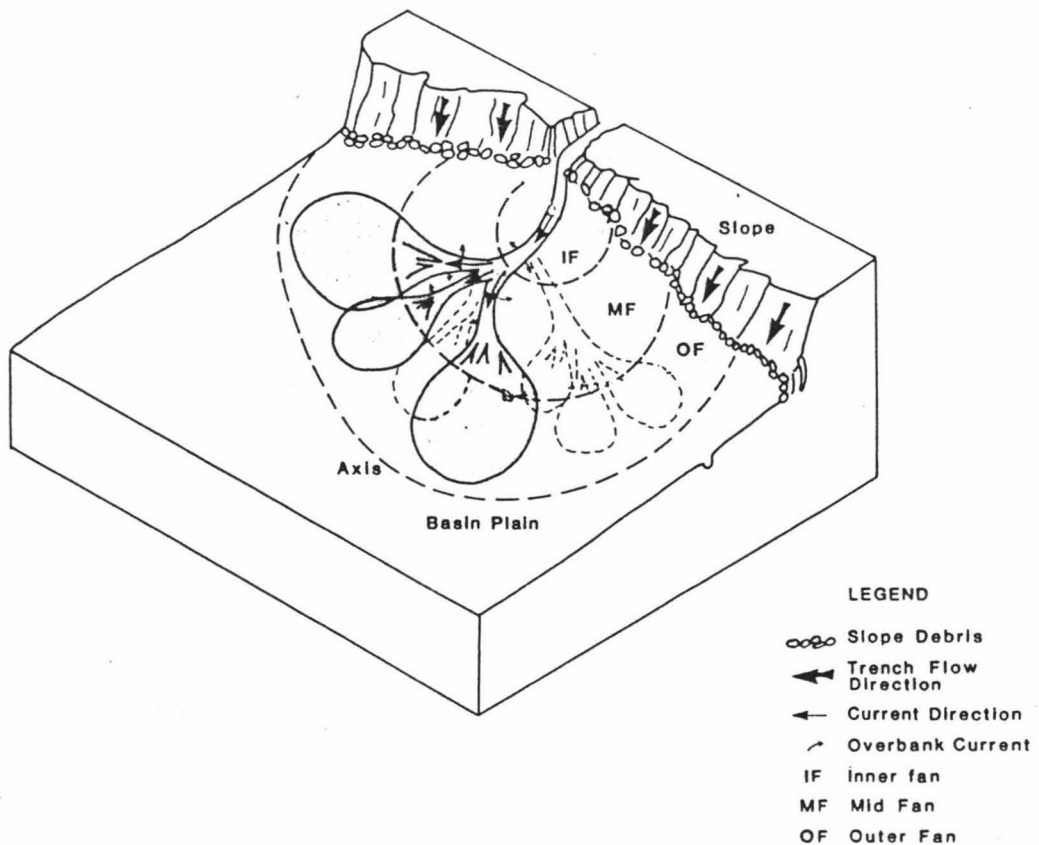


Figure 2-4: Submarine fan model

Throughout the study area, individual lithofacies occur in regions up to several tens of metres thick. On the bases of lithofacies associations, the study area can be divided into two broad "belts" (Fig. 2-5). These belts follow the general trend of the Tararua Range.

The lithofacies association occurring in the **eastern** belt is dominated by thin, alternating sandstone and argillite beds, with minor thick-bedded sandstone and massive argillite (lithofacies 3, minor 2,5).

The lithofacies association exposed in the **western** belt is dominated by massive, thick-bedded sandstone, with minor conglomerate, olistostrome, thin-bedded sandstone and argillite and minor massive argillite (lithofacies 2,1,4,3, minor 5).

Using criteria from Mutti and Ricci Lucchi (1972), both these lithofacies associations imply a submarine mid-fan depositional site for the sediments. The occurrence of olistostromal beds may represent changes to inner-fan depositional sites, or increased energy of the deposits, allowing gravity slide deposits to reach mid-fan sites. Submarine fan depositional sites have been suggested for several areas elsewhere in the Torlesse (Carter *et al* . 1978; Howell 1980a; Hicks 1981; MacKinnon 1983).

2.2 PETROGRAPHY AND GEOCHEMISTRY

The rocks of the clastic sedimentary association have been examined petrographically and some greywackes and argillites have been analysed for major and trace elements geochemistry (Analytical methods are given in Appendix II).

2.2.1 Greywacke

The greywackes are fine- to medium-grained, and well indurated, with fresh material being light to dark grey, and weathered surfaces a light yellow-brown colour.

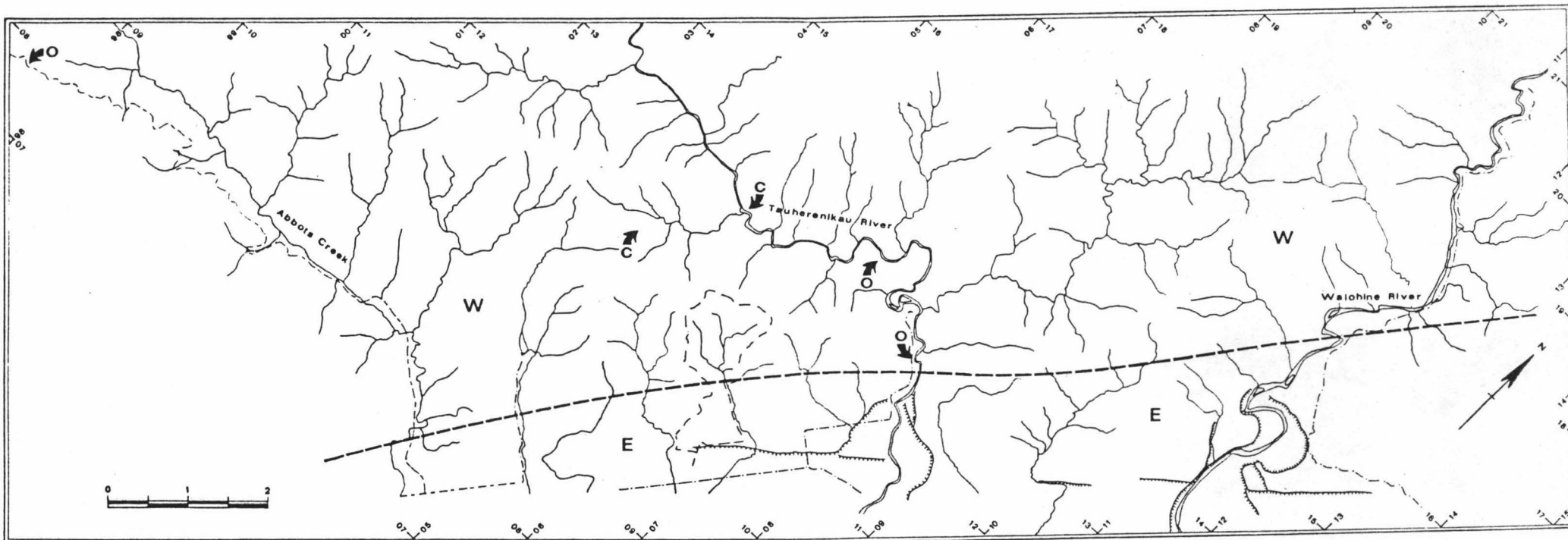


Figure 2-5: Lithofacies associations in the study area. The study area can be divided into two broad "belts" which follow the regional trend of the Tararua Range.

The western belt (W) is predominantly massive sandstone with minor conglomerate (C), olistostrome (O), thin interbedded sandstone and argillite and massive argillite.

The eastern belt (E) is predominantly thin interbedded sandstone and argillite, with minor massive sandstone and massive argillite.

Thin section examination reveals a poorly sorted fabric of angular detrital grains, predominantly quartz and feldspar (both plagioclase and K-feldspar) along with minor lithic fragments, epidote, biotite, muscovite, zircon and sphene. Representative modal analyses from 15 sands are listed in Table 2-2, with the average grain size for these sands being 0.16mm (modal technique and grain size determination are outlined in Appendix III & IV respectively). These grains ranged in size from 1.3mm to >0.01mm. As there is a gradation in grain size from detrital grains to clay-sized particles, an arbitrary figure of 0.02mm was taken as the maximum size for matrix components (after Reed 1957a).

Quartz

Detrital quartz occupies 19.2% to 41% of total rock and occurs as angular to sub-rounded grains. The larger grains, (>0.3mm) are more rounded in comparison with the smaller grains which are generally angular to sub-angular. Grains are predominately monocrystalline and strained with moderate to strongly undulose extinction. Polycrystalline quartz aggregates are common but only in minor amounts. Graphic intergrowths with feldspar are frequent (17010, 17014, 17020*). Inclusions within quartz are not common. These are in order of decreasing abundance, fine trains of opaque inclusions, zircon (17066, 17011) and acicular laths of rutile (17071, 17021).

Calcite occurs as overgrowths at grain boundaries, (17018) with silica being replaced with carbonate. Occasional grain boundaries are sutured, showing evidence of pressure solution (17018).

* Numbers refer to samples housed in the petrology collection, Geology Department, Victoria University of Wellington. All samples, with grid references and short descriptions are listed in Appendix V.

TABLE 2-2: Modal analyses of fifteen fine grained sandstones

Sample number	17012	17013	17014	17015	17016
Grain size (phi)	2.1	2.9	2.3	2.8	2.4
Monocrystalline Quartz	19.6	16.8	23.6	16.8	19.5
Polycrystalline Quartz	1.6	3.0	5.4	6.8	1.4
Chert	0.4	0.8	0.6	0.6	2.0
Plagioclase	31.2	30.2	32.6	36.0	34.1
Alkali Feldspar	3.4	5.6	4.6	5.8	8.0
Fe-Mg Minerals	1.8	0.8	0.6	0.6	0.0
Lithic Fragments	26.2	19.0	20.0	14.6	16.8
Other	5.8	7.2	4.2	5.2	6.6
Matrix	10.0	16.6	8.4	13.6	11.6
Lithic Fragments:					
Volcanic	66.0	45.5	51.0	44.0	29.6
Sedimentary	8.0	31.0	18.0	18.0	31.5
Metavolcanic	12.5	5.0	6.0	2.0	12.3
Metasedimentary	13.5	18.5	25.0	36.0	26.6
Sample number	17017	17018	17019	17020	17021
Grain size (phi)	3.1	2.3	2.8	1.9	2.7
Monocrystalline Quartz	20.4	18.6	25.2	23.6	30.2
Polycrystalline Quartz	2.4	2.8	3.2	5.6	10.8
Chert	0.8	0.8	0.6	0.6	1.4
Plagioclase	28.0	35.8	35.2	34.2	29.6
Alkali Feldspar	5.4	9.0	3.8	5.3	2.8
Fe-Mg Minerals	0.0	0.6	1.6	0.6	0.0
Lithic Fragments	11.8	13.4	14.2	10.8	10.4
Other	4.8	6.8	6.6	5.8	3.6
Matrix	26.4	12.2	9.6	13.0	11.2
Lithic Fragments:					
Volcanic	44.4	57.0	53.5	47.3	44.0
Sedimentary	18.6	8.0	12.0	14.4	20.0
Metavolcanic	9.0	22.0	10.5	12.3	11.0
Metasedimentary	28.0	13.0	24.0	26.0	25.0
Sample number	17022	17023	17024	17010	17011
Grain size (phi)	2.4	3.1	2.8	3.1	3.2
Monocrystalline Quartz	28.0	20.2	17.0	20.8	20.0
Polycrystalline Quartz	5.4	2.2	4.4	3.4	4.4
Chert	0.6	0.6	0.6	0.6	1.4
Plagioclase	32.4	31.2	32.4	35.6	26.0
Alkali Feldspar	5.6	5.2	4.6	7.0	4.6
Fe-Mg Minerals	0.2	0.2	1.2	0.4	0.2
Lithic Fragments	13.0	7.6	18.2	11.6	13.6
Other	6.8	7.2	7.4	6.4	6.4
Matrix	8.0	25.6	14.2	14.2	23.4
Lithic Fragments:					
Volcanic	52.0	66.3	37.0	48.6	56.2
Sedimentary	16.5	8.3	24.5	23.4	19.7
Metavolcanic	7.5	8.8	9.5	3.5	0.3
Metasedimentary	24.0	16.6	29.0	24.5	23.8

Plagioclase

Plagioclase grains comprises 26% to 36% of total rock.

Compositions of plagioclase using the Michel-Levy method ranged from An₀-An₃₀, the majority being andesine. Electron microprobe analysis (EPMA; analytical method is given in Appendix VI) of four plagioclase grains have albite compositions ranging from An_{0.4} Ab_{99.2} Or_{0.4} to An_{1.9} Ab_{97.4} Or_{0.7}. The original plagioclase compositions, as implied from the Michel-Levy method, have been albitized. The grains are elongate, lath like, angular to sub-rounded. Twinning is common, mainly albite and less commonly Carlsbad/albite and Carlsbad. Several grains display perthitic intergrowths (17019, 17024). Kinked albite twins are common (17063).

Only rare apatite inclusions (17011) are found, a feature which may be due to the masking affects of sericitic alteration. Sericite alteration varies from absent to total replacement and occurs preferentially along cleavage traces.

Alkali feldspar

The alkali feldspar grains (2.8% to 9.0% of total rock), are generally sub-angular to sub-rounded. Grains are of orthoclase and microcline, the latter shows characteristic cross hatched twinning (17011, 17107). Orthoclase is often covered with murky incipient alteration to sericite and carbonate containing inclusions of opaque oxides.

Lithic fragments

Three types of lithic fragments constituting 10.8% to 26.2% of the total rock occur in the greywackes. These are discussed in order of decreasing abundance.

Volcanic lithic fragments

Both acidic and basaltic volcanic fragments were noted. Grains are frequently sub-rounded, although they do vary from sub-angular to

rounded. The acid volcanic fragments display microporphyritic textures of euhedral sodic plagioclase grains set in a fine grained groundmass (17068).

The basaltic volcanic fragments generally show variolitic textures with plagioclase laths (euhedral, up to 0.07mm long in 17018) set in a dark cryptocrystalline groundmass. Devitrified volcanic fragments are also common (17076).

Metamorphic lithic fragments

The most common metamorphic fragments are schists and phyllites. These are generally angular grains, elongated parallel to their internal schistosity (17068). This schistosity is usually defined by the alignment of biotite and white mica, (17011, 17088) and, more rarely oxide minerals (17039). Deformation prior to incorporation in the greywacke is evident from kinked schistose layers (17071), although these are rare.

Other metamorphic fragments are, metaquartzites occurring as equant, sub-angular grains, some with distinct fabric orientation (17087) and metavolcanics.

Sedimentary lithic fragments

Sedimentary lithic fragments range from fine grained siltstone to medium grained sandstone, (based on Folk's 1974 classification) as well as chert fragments. Fine-grained siltstone grains are angular, often showing soft-sediment deformation, being elongated and moulded around other grains (17016, 17075, 17087). These are probably intraformational in origin. The siltstones are dark, with only rare individual grains of quartz and feldspar (0.06mm) being recognized.

Sandstone lithic fragments vary from sub-angular to rounded, with the medium-grained sandstone fragments tending to be more rounded relative to the fine-grained sandstone fragments. Individual fragments are consistent in their detrital components having quartz, feldspar and

lithic fragments in various amounts.

Chert fragments are generally sub-rounded to rounded, and form a small proportion of sedimentary lithics (17014, 17016). No radiolarian skeletons were observed.

Accessory minerals

Detrital epidote is a common accessory mineral. The grains are round, equant (0.1mm large) and range from colourless to pale yellow in colour. Electron microprobe analyses indicate compositional variations within grains of Pistacite values from Ps21.5 to Ps24.2. The grains are often fractured, resulting in aggregates of several grains (17108). Strontium occurs replacing Ca along fractures (determined by electron microprobe analyses).

Other common accessory minerals are, in order of decreasing abundance, biotite (17019, 17075), muscovite (17076, 17077), zircon (17015, 17019, 17069), sphene (17010, 17019), hornblende (17088, 17090), apatite (17069), zeolite (17014) and iron oxide minerals (17014).

2.2.2 Argillite

In outcrop argillite is dark grey to blue black in colour, well indurated and can be massive or laminated. The argillites range in grain size from siltstone to claystone (Udden-Wentworth size classes, in Folk, 1974).

The siltstone, a fine grained equivalent of the greywacke, has an average grain size of 0.04mm. They are poorly sorted, with detrital quartz, feldspar, biotite and less commonly epidote grains, scattered in a fine claysize matrix (17064, 17065, 17073, 17094). The detrital grains are angular and equant (except for biotite laths). Quartz occurs as monocrystalline, often strained grains (17070, 17073), and feldspars (some with albite twinning) are often altered, and partly obscured by matrix. In the matrix, micas are common and in laminated argillites are

orientated parallel to bedding.

The clay size argillite, has occasional detrital grains of quartz embedded throughout a dark matrix (17067).

Stylolites and opaque oxides are common throughout, indicating deformation through pressure solution mechanisms.

2.2.3 Calcareous siltstone

Calcareous siltstone crop out as thin beds (10cm to 13cm thick). These beds consist of ferroan-dolomite rich siltstone with minor grains of quartz and feldspar (carbonate determination methods are given in Appendix VII). Alternating quartz-rich and quartz-poor layers can be seen (17038). Quartz grains (less than 0.1mm) are monocrystalline, subrounded and with the exception of fine opaque minerals (17038), are inclusion free (17093). Feldspar laths are seen (17085) as are pyrite grains (17099).

2.2.4 Polymict conglomerate

Exposures occur in the Tauherenikau river, (site 1: S26C/ 0547 1280, site 2: S26C/ 0512 1274) and on the saddle between Mt. Frith and Mt. Finis (site 3: S26C/ 0420 1130). At site 1 beds range in thickness from 20cm to 60 cm and at site 2 from 50cm to several metres. The exposure at site 3 is poor, cropping out over 20 metres.

The clasts are pebble to cobble size, rounded to subrounded, poorly sorted and set in a medium-grained sand matrix. Post-depositional fracturing of some clasts has occurred. The clasts are, in order of decreasing abundance, sedimentary, volcanic and metamorphic. Grading is distinct at site 2, with the conglomerate beds grading into sandstone then argillite. No imbrication was observed.

A brief description of clasts are:

Sedimentary clasts vary from siltstone to coarse-grained sandstone. They display a similar mineralogy to the normal greywacke and

argillite, being poorly sorted, predominantly quartz, feldspar, lithic fragments, with minor epidote, biotite and mica grains. Rounded chert clasts are generally hematite-stained and cryptocrystalline.

Volcanic clasts are predominantly felsic with subordinate amounts being mafic. This may be due to the mafic volcanic fragments breaking up more readily and being incorporated into the matrix. The clasts show trachytic, ignimbritic and variolitic textures, and also have development of both prehnite and pumpellyite minerals (17072). Prior to incorporation within the conglomerate some volcanic clasts developed quartz veining.

Metamorphic clasts are predominantly phyllite with foliation defined by alignment of biotite and mica minerals. The clasts are elongated parallel to foliation. Some metaquartzites with recrystallized quartz showing an interlocked mosaic texture occur.

The matrix (25% of the total rock) has a similar composition to the greywacke, consists of medium sand size grains of detrital quartz, feldspar and lithic fragments with minor epidote, biotite, apatite and mica, set in a fine grained dark silt.

2.2.5 Olistostrome

Olistostromes (sedimentary melanges), are highly mixed rock bodies, which are interpreted as forming as results of sub-marine mass gravity flows (Rupke 1978). They feature rounded clasts set in a dominantly unsheared matrix, in comparison to tectonic melanges, which have pervasively deformed matrix and angular clasts surrounded by fracture surfaces (Hsu 1974). Within the study area these exposures consist of rounded to sub-angular clasts of a variety of rock types set in an unsheared matrix. It is hard to imagine any tectonic process which would result in the mixing of rock types, without being reflected in the matrix. Also the mixture and shape of clasts appear to be the result of a

mass debris flow and therefore the exposures are termed olistostromes.

Olistostromes are exposed in the Tauherenikau River (site 1: S26C/ 0787 1295; site 2: centered at S26C/ 0661 1359) and along State Highway 2 (site 3: S27A/ 970 0781). At site 1, the olistostrome crops out over 20 metres, within a sequence of thin bedded alternating sandstone and argillite. The olistostrome at site 2 is exposed over 80 metres of river bed. At site 3, the olistostrome crops out over 20 metres surrounded by massive sandstone and has been more intensely sheared than the other olistostromes. Clasts range in size from a few millimetres to several metres, are rounded to angular, poorly sorted and set in a fine grained sand to argillite matrix. Pre-depositional fracturing of some clasts has occurred.

The olistostromes are different in that two contains clasts of both sedimentary and volcanogenic association (sandstone, argillite, basalt, limestone and chert; site 1 & site 3), and the other contains only clasts of sedimentary association (sandstone, argillite and calcareous siltstone; site 2). Clasts of volcanogenic association are discussed in Chapter 3. Clasts of sedimentary association are similar to "normal" greywacke and argillite; brief descriptions are:

Sandstone clasts occur as round concretions or are angular to rounded. Concretions weather to a light grey colour (Fig. 2-3a), are up to 13cm in diameter, medium grained and poorly sorted. They contain a large amount of carbonate cement, with a detrital mineralogy of quartz, feldspar, lithic rock fragments, with minor epidote and biotite grains (17083). Sandstone fragments are medium to fine grained, poorly sorted and have a detrital mineralogy similar to that of concretions, with grains set in a fine silt matrix.

Argillite clasts are dark grey in colour, sub-angular to sub-rounded, and are fine grained equivalent of the sandstone clasts.

Calcareous siltstone clasts are usually angular but are uncommon.

The matrix (40%–75% of total rock), is dark grey to black in colour, and consists of very fine grained sand to silt size detrital grains of quartz, feldspar, lithic fragments (sedimentary, volcanic, metamorphic), epidote and biotite set in a fine dark silt (17080).

2.2.6 Geochemistry

To characterize the greywacke and argillite from the Tararua Range, and document geochemical variations between the rock types, nine greywacke and four argillite samples were analysed for major and trace elements.

Major elements:

The greywackes range in SiO_2 content from 64.62–77.03 weight percent (all analyses are given as hydrous values), with Al_2O_3 content between 11.13–16.91 weight percent (Table 2-3). In contrast, the argillites contain less SiO_2 , between 57.54–63.78 weight percent and significantly greater Al_2O_3 (16.69–20.28 weight percent). The chemical variation between all analysis is dominated by two components, SiO_2 and Al_2O_3 , which have abundances related to detrital quartz and clay content (phyllosilicates) respectively (Pettijohn 1957). The oxides which are concentrated in the clay content Al_2O_3 , TiO_2 , MgO , K_2O , P_2O_5 and Fe_2O_3 (total Fe) are all positively correlated in abundance, and all have a strong negative correlation with SiO_2 . Correlation coefficients are listed in Table 2-4. Chemical variation diagrams (Fig. 2-6) illustrate the affect. This variation can be explained as a function of grain size, where phyllosilicates are more abundant in the finer grained sediment. Although the specific grain size of the samples, for geochemical analysis in this study were not determined, variations in relative grain size from sand to argillite can be seen. These trends are similar to those observed by Rowe (1980) based on grain size.

TABLE 2-3a: Analyses of greywackes and argillites from the Tararua Range

Analysis	(1)	(2)	(3)	(4)	(5)	(6)	(7)
Sample No.	17027	17031	17036	17029	17026	17034	17037
Major Oxides (wt.%)							
SiO ₂	57.54	59.41	62.71	63.78	64.62	67.78	68.74
TiO ₂	0.82	0.80	0.72	0.67	0.64	0.47	0.51
Al ₂ O ₃	20.28	18.78	17.18	16.69	16.91	15.81	15.22
Fe ₂ O ₃ T	5.64	5.71	5.45	4.93	4.48	3.44	3.85
MnO	0.09	0.09	0.07	0.07	0.06	0.10	0.06
MgO	2.18	2.03	1.92	1.67	1.62	1.29	1.31
CaO	1.53	1.42	1.38	2.02	1.28	2.66	1.02
Na ₂ O	3.30	2.85	3.03	2.64	3.73	3.95	3.85
K ₂ O	4.54	4.10	3.19	3.43	3.34	2.44	2.83
P ₂ O ₅	0.19	0.18	0.16	0.15	0.15	0.11	0.11
Loss	4.04	4.38	3.73	3.76	3.20	3.04	2.37
TOTAL	100.15	99.75	99.54	99.81	100.03	99.09	99.87
Trace Elements (ppm)							
Ba	607	707	449	445	541	643	644
Ce	72	66	65	54	60	45	49
Cr	57	60	52	56	43	41	34
Cu	20	22	18	19	13	10	10
Ga	28	25	22	21	22	15	18
La	41	32	35	27	31	27	22
Nb	11	12	10	11	9	8	7
Ni	14	17	20	17	8	11	10
Pb	28	29	27	25	23	17	22
Rb	194	176	138	148	138	83	113
Sc	15	14	13	12	10	9	10
Sr	233	224	172	213	255	287	309
Th	17	16	15	13	15	10	11
U	4	4	3	3	3	2	2
V	125	120	111	105	89	71	74
Y	34	34	29	29	29	20	23
Zn	98	101	92	92	77	57	61
Zr	281	247	187	210	312	191	241

TABLE 2-3b: Analyses of greywackes and argillites from the Tararua Range

Analysis	(8)	(9)	(10)	(11)	(12)	(13)	(14)
Sample No.	17035	17028	17032	17030	17025	17014	17033
Major Oxides (wt.%)							
SiO ₂	69.69	70.15	70.97	72.84	73.10	73.53	77.03
TiO ₂	0.51	0.51	0.46	0.43	0.44	0.38	0.38
Al ₂ O ₃	14.61	13.56	13.66	13.05	12.87	12.91	11.13
Fe ₂ O ₃ T	3.66	3.90	3.29	3.32	3.18	2.68	2.62
MnO	0.05	0.06	0.08	0.06	0.06	0.04	0.05
MgO	1.28	1.36	1.17	1.01	1.04	0.91	0.86
CaO	1.04	1.61	1.02	0.97	0.99	0.85	1.11
Na ₂ O	3.52	3.82	4.29	3.56	3.87	3.79	3.43
K ₂ O	2.71	2.54	2.59	2.36	2.21	2.50	1.72
P ₂ O ₅	0.13	0.11	0.10	0.10	0.10	0.07	0.08
Loss	2.35	2.29	2.07	1.96	1.85	2.11	1.57
TOTAL	99.55	99.91	99.70	99.60	99.71	99.77	99.98
Trace Elements (ppm)							
Ba	526	593	596	549	493	700	506
Ce	47	52	44	43	45	39	47
Cr	34	51	34	29	25	22	21
Cu	9	8	10	8	9	6	4
Ga	18	14	15	15	13	13	11
La	23	25	24	18	18	16	25
Nb	8	6	6	7	5	5	5
Ni	7	10	9	7	6	3	2
Pb	19	19	18	20	15	19	14
Rb	105	89	99	86	84	85	62
Sc	8	9	8	7	7	6	6
Sr	244	235	248	271	244	265	266
Th	13	11	12	10	9	8	9
U	4	3	3	3	2	2	3
V	70	75	64	56	56	51	42
Y	22	22	19	21	20	17	19
Zn	63	56	52	55	50	39	38
Zr	242	255	221	220	261	150	333

	SI02	TI02	AL203	MNO	MGO	CAO	NA2O	K2O	P2O5	FE2O3T	BA	CE	CR	CU	GA	LA	NB	NI	PB	RB	SC	SR	TH	U	V	Y	ZN	ZR	
SI02	1.00000																												
TI02	-0.97744	1.00000																											
AL203	-0.99083	0.97528	1.00000																										
MNO	-0.65076	0.58055	0.57372	1.00000																									
MGO	-0.98588	0.99148	0.97234	0.62618	1.00000																								
CAO	-0.40131	0.33213	0.29449	0.69564	0.39250	1.00000																							
NA2O	0.52246	-0.64616	-0.54778	-0.11674	-0.58043	-0.20360	1.00000																						
K2O	-0.97101	0.94933	0.98384	0.55943	0.94000	0.26065	-0.53144	1.00000																					
P2O5	-0.96676	0.98385	0.96396	0.59121	0.97610	0.34818	-0.61695	0.92909	1.00000																				
FE2O3T	-0.96444	0.94025	0.95628	0.57143	0.98644	0.34980	-0.66168	0.91931	0.97133	1.00000																			
BA	-0.09006	-0.02310	0.08595	0.23955	0.00822	0.00122	0.33529	0.18092	-0.07779	-0.05904	1.00000																		
CE	-0.90892	0.95239	0.90746	0.49795	0.94973	0.25089	-0.58090	0.86918	0.93294	0.93395	-0.06919	1.00000																	
CR	-0.90059	0.90274	0.85048	0.64988	0.92301	0.56981	-0.56432	0.83431	0.88226	0.92404	0.00564	0.82903	1.00000																
CU	-0.94595	0.96385	0.94047	0.64364	0.94745	0.37643	-0.67217	0.92070	0.93936	0.96308	-0.03569	0.85435	0.88063	1.00000															
GA	-0.97250	0.96451	0.99147	0.52996	0.95399	0.23915	-0.56441	0.97180	0.96655	0.94216	0.03858	0.90468	0.81378	0.91925	1.00000														
LA	-0.85854	0.87165	0.83260	0.63103	0.89573	0.43114	-0.44945	0.78540	0.86709	0.84119	-0.07871	0.93045	0.79285	0.77288	0.83038	1.00000													
NB	-0.92831	0.93721	0.92227	0.61579	0.92299	0.46440	-0.71572	0.89289	0.94539	0.93653	-0.03864	0.82427	0.87279	0.94425	0.92577	0.77961	1.00000												
NI	-0.83010	0.84452	0.78961	0.65260	0.86481	0.50816	-0.59949	0.72977	0.81297	0.89718	-0.13204	0.73440	0.89221	0.89571	0.75139	0.69787	0.84680	1.00000											
PB	-0.92126	0.93200	0.94059	0.44249	0.91329	0.18870	-0.65442	0.92859	0.88846	0.94253	0.09347	0.84945	0.82895	0.91610	0.93399	0.72277	0.90074	0.82334	1.00000										
RB	-0.96641	0.96563	0.98635	0.52507	0.94640	0.21453	-0.58869	0.98967	0.94643	0.93843	0.07380	0.89320	0.82444	0.94153	0.98239	0.79746	0.90505	0.75099	0.93716	1.00000									
SC	-0.97485	0.97615	0.96016	0.65684	0.98513	0.41216	-0.59617	0.92978	0.94909	0.97827	0.03056	0.92343	0.91785	0.95310	0.93699	0.86946	0.91607	0.89231	0.92119	0.93998	1.00000								
SR	0.49709	-0.61398	-0.48714	-0.16787	-0.59767	-0.11132	0.61933	-0.44940	-0.58406	-0.63980	0.48308	-0.59101	-0.59527	-0.62225	-0.46838	-0.52247	-0.51929	-0.65683	-0.53427	-0.49816	-0.54138	1.00000							
TH	-0.93768	0.95507	0.94659	0.51266	0.94808	0.20085	-0.51675	0.91755	0.96758	0.93221	-0.02531	0.92492	0.82953	0.88345	0.95876	0.86770	0.88614	0.73815	0.87639	0.93558	0.90231	-0.57544	1.00000						
U	-0.63218	0.66674	0.63767	0.36203	0.66408	0.01949	-0.31977	0.66026	0.69670	0.62698	0.11685	0.70805	0.61264	0.53168	0.67709	0.71546	0.59392	0.39509	0.58788	0.65435	0.60634	-0.39773	0.79438	1.00000					
V	-0.98365	0.99017	0.97161	0.61232	0.99342	0.40325	-0.62715	0.94537	0.96803	0.99113	-0.00531	0.92152	0.93481	0.96831	0.95011	0.85534	0.93894	0.89160	0.93703	0.95362	0.98795	-0.61143	0.92847	0.62109	1.00000				
Y	-0.94716	0.98211	0.95520	0.51147	0.95716	0.27990	-0.68461	0.93282	0.97104	0.96766	-0.04962	0.95114	0.86135	0.93443	0.95834	0.84134	0.92839	0.77570	0.91926	0.95749	0.94279	-0.54757	0.93765	0.66034	0.95609	1.00000			
ZN	-0.95882	0.98275	0.95663	0.57304	0.96848	0.36632	-0.70160	0.92179	0.97697	0.98760	-0.10548	0.89767	0.90162	0.97760	0.95183	0.81109	0.97022	0.88583	0.93494	0.94632	0.96094	-0.62139	0.92768	0.60120	0.98139	0.96866	1.00000		
ZR	-0.03020	0.10671	0.04683	-0.08096	0.06456	-0.16813	-0.02844	0.03753	0.15859	0.04203	-0.22382	0.30807	-0.01092	-0.04974	0.10622	0.28759	-0.01255	-0.24955	-0.10167	0.09149	0.03387	0.11037	0.20334	0.37758	0.00406	0.22643	0.03245	1.00000	

Table 2-4: Correlation matrix for sediments.

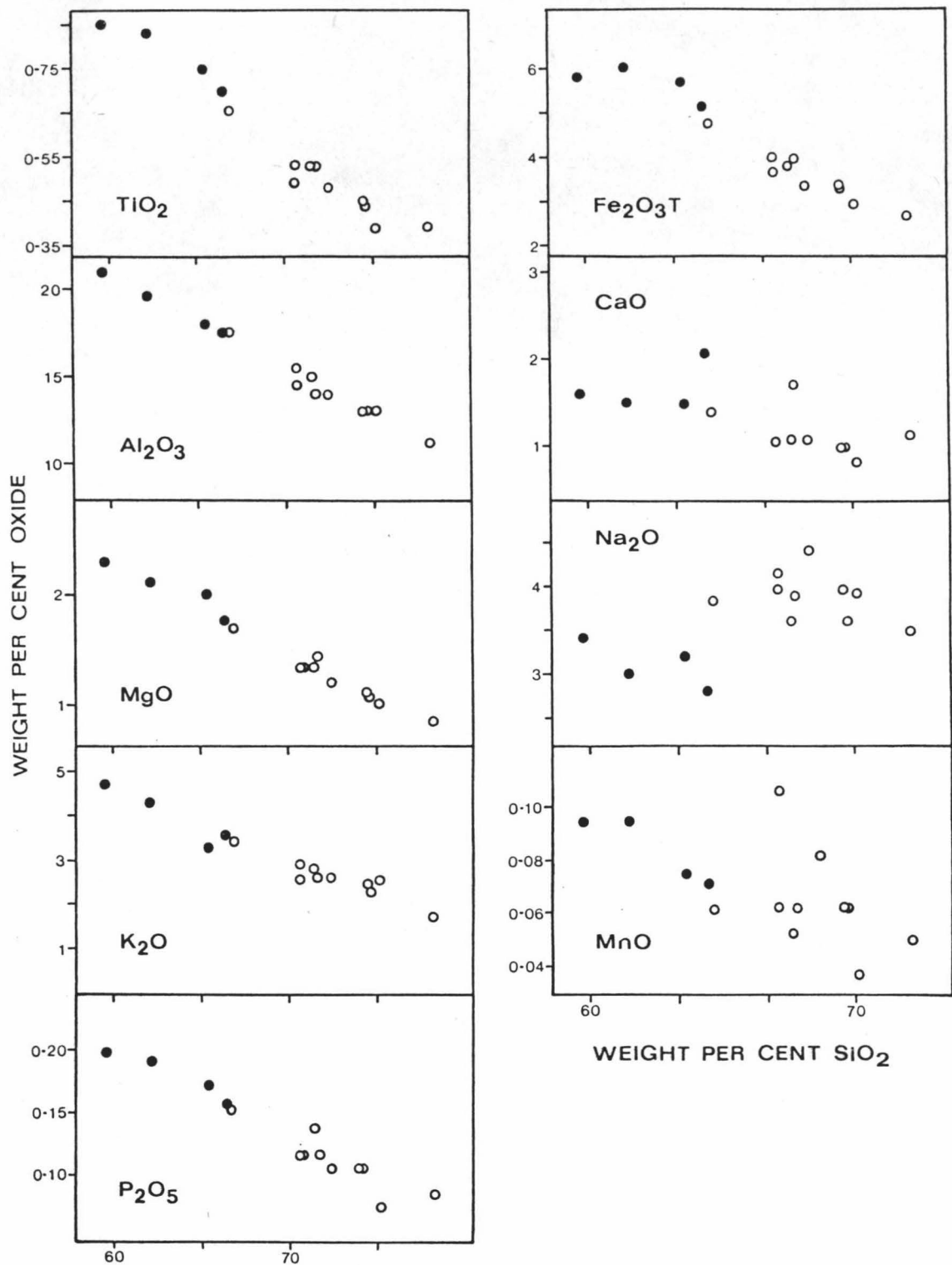


Figure 2-6: Major oxide variations in the sandstones and argillites from the study area.

○ = sandstone ● = argillite

The major oxides, CaO, Na₂O and MnO show no correlation with either SiO₂ or Al₂O₃ (Fig. 2-6). The scatter of CaO abundances is probably due to calcite veining. Na₂O values show an overall increase with SiO₂, and is probably related to an overall decrease in sodic plagioclase with grain size. In greywacke albitized feldspars are thought to be the main source of Na (Pettijohn et al. 1972), therefore with increased phyllosilicate content the abundance of feldspar and hence Na would decrease. MnO abundances decrease with increasing SiO₂ and may reflect weathering as manganese is readily mobilized in surface conditions (Roser 1983).

Trace elements:

Most trace elements tend to be concentrated in the fine grained argillite relative to greywacke. This is thought to be due to the increased amount of phyllosilicates in the argillite, where phyllosilicate minerals have a high capacity for chemical absorption eg. montmorillonite can have considerable atomic substitution where alumina can be replaced by Fe, Zn, Cr, Mn and Ni (Mason 1958). Thirteen of the 18 trace elements analyses show increased concentrations in the argillite, while the concentration of trace elements in both argillite and greywacke are similar to the average amounts for these rock types listed by Taylor (1965).

With decreasing abundance of SiO₂, (and hence grain size), the trace elements Sc, V, Cr, Ni, Cu, Zn, Ga, Rb, Y, Nb, La, Ce, Pb and Th (Fig. 2-7), all have significant negative coefficients with SiO₂ and show systematic increases. Uranium shows an ill-defined trend to increase with decreased SiO₂ content. Such elements are commonly present in phyllosilicates (Mason 1958, Pettijohn et al. 1972). Conversely Sr shows an overall increase in abundance with increasing SiO₂, while Ba and Zr have no significant correlation with any other elements (Fig. 2-7). Sr can

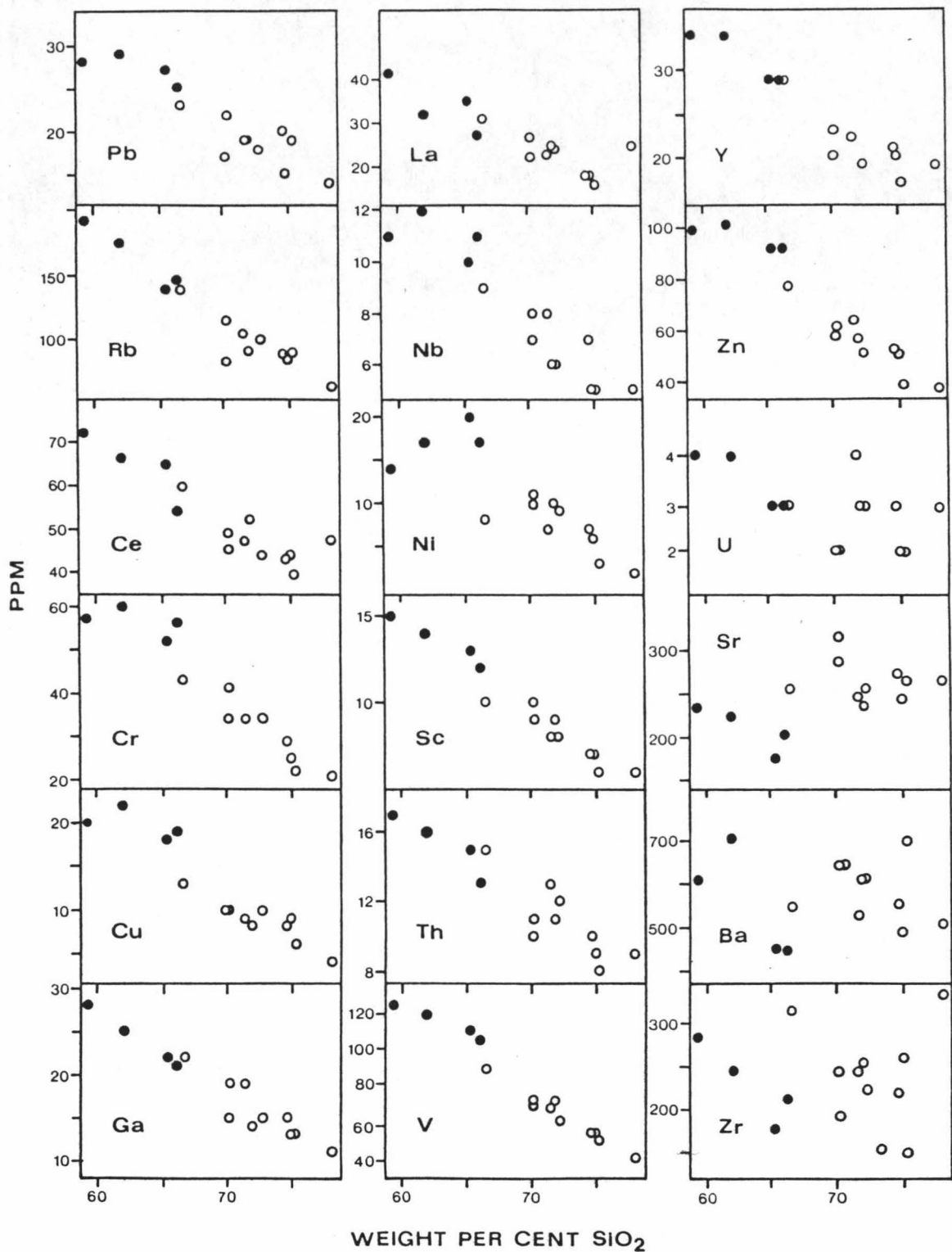


Figure 2-7: Trace element variations in sandstones argillites from the study area.

○ = sandstone ● = argillite

substitute for Ca^{2+} and K^+ in plagioclase and K-feldspar, while Ba^{2+} can substitute for K^+ in feldspar, and to a minor extent in micas (Taylor 1965). The variability of both Sr and Ba is therefore probably related to the presence of a minor feldspar component and is not directly related to quartz or phyllosilicate content. The lack of inter-element correlation for Zr implies that its abundance is dominated by detrital zircon. Rowe (1980) found zircon to have a preferred grain size range, with concentrations in coarse siltstones.

From the analyses, the chemistry is largely determined by SiO_2 and Al_2O_3 content, with the transition from greywacke to argillite being a chemical continuum, rather than discrete end-members. Such a chemical continuum can be explained by hydraulic sorting of turbidity currents, where the coarser detritus would be deposited initially, followed by the settling out of finer and more phyllosilicate rich sediment (ie. argillite).

Greywacke and argillite from other areas in the Torlesse show similar bulk chemical analyses (Reed 1957a; Rowe 1980; Roser 1983), implying that the Torlesse Supergroup is relatively homogeneous in terms of chemistry. Minor differences in chemistry may be related to variations in mineral compositions and/or to the relative amounts of minerals present.

2.3 PROVENANCE AND TECTONIC SETTING

The provenance of the greywacke in the study area can be inferred from petrographic and optic modal analysis. The main features of the provenance is reflected in the greywackes detrital mineralogy. Evidence of source terrane is:

- the presence of strained quartz, alkali feldspar and biotite,
- the occurrence of exsolution textures,

-the presence of metamorphic fragments (phyllite, schist, metaquartzite),

-the incidence of the heavy minerals, epidote, zircon, sphene and apatite. Pettijohn (1957) described detrital mineral suites characteristic of source rock types. He found that for rocks derived from an acid-igneous source the characteristic detrital mineralogy is of apatite, biotite, hornblende, sphene, zircon, quartz (igneous variety), microcline and magnetite, while rocks derived from a metamorphic source area have a detrital mineralogy of phyllite and quartzite fragments and quartz (metamorphic variety). From the above, the detrital mineralogy of major components in the greywacke indicates an acid-igneous to metamorphic source terrane. Sedimentary lithic fragments, which have similar detrital mineralogy to the greywackes, are most likely to be reworked Torlesse sediment.

Recently workers have concentrated on the use of detrital framework modes to distinguish the provenance of sediments (Dickinson 1970). Dickinson and Suczek (1979) found that the composition of sandstones derived from different source terranes tended to lie within discrete and separate fields on various ternary diagrams. Using the detrital framework modes of quartz, feldspar and lithic rock fragments, three provenances could be distinguished: 1) continental; 2) magmatic arc; 3) recycled orogen.

Detrital framework modes of 15 fine grained greywackes from the study area are listed in Table 2-2. On QFL and QmFLt diagrams (Dickinson and Suczek 1979, modified by Dickinson et al. 1983) Fig. 2-8a & b, the framework modal data fall within the dissected magmatic arc field. On QpLvmlsm and LmLvLs diagrams (after Ingersoll & Suczek 1979) the data fall within the broad field of magmatic arc source (Fig. 2-9a & b).

Framework modes have also been used to imply tectonic setting of

Figure 2-8a: QFL ternary diagram (after Dickinson et al., 1983)

- Q = Total quartzose grains, including polycrystalline lithic fragments such as chert and quartzite
- F = Monocrystalline feldspar grains
- L = Unstable polycrystalline lithic fragments of either igneous or sedimentary origin, including metamorphic varieties

Figure 2-8b: QmFLt ternary diagram (after Dickinson et al., 1983)

- Q_m = Quartz grains that are exclusively monocrystalline
- F = Monocrystalline feldspar gains
- L_t = Total polycrystalline grains (including quartzose varieties)

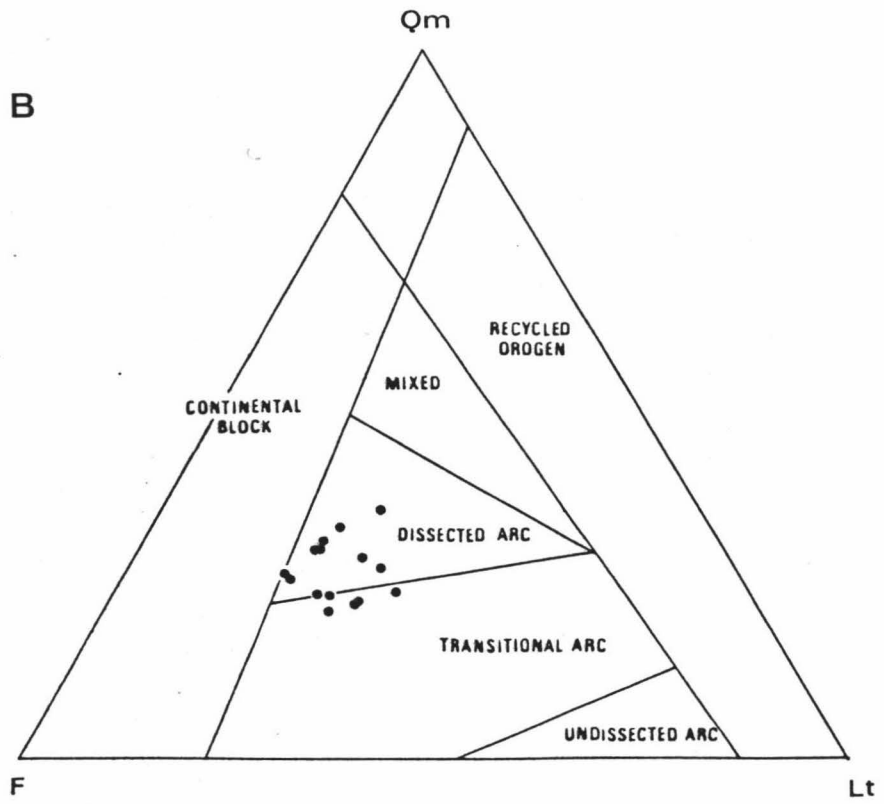
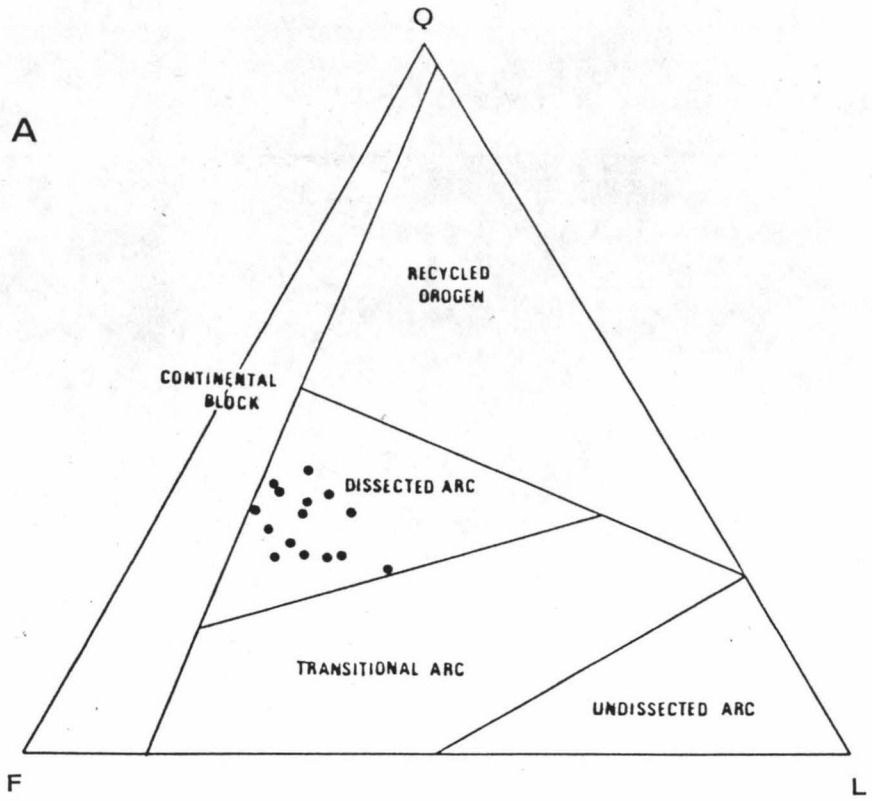


Figure 2-8

Figure 2-9b: L_mL_vL_s ternary diagram (after Ingersoll & Suczek, 1979)

L_m = Metamorphic Lithic fragments
L_v = Volcanic Lithic fragments
L_s = Sedimentary Lithic fragments

Figure 2-9a: Q_pL_{vm}L_{sm} ternary diagram (after Ingersoll & Suczek, 1979)

Q_p = Polycrystalline Quartz
L_{vm} = Volcanic and Metavolcanic Lithic fragments
L_{sm} = Sedimentary and Metasedimentary Lithic fragments

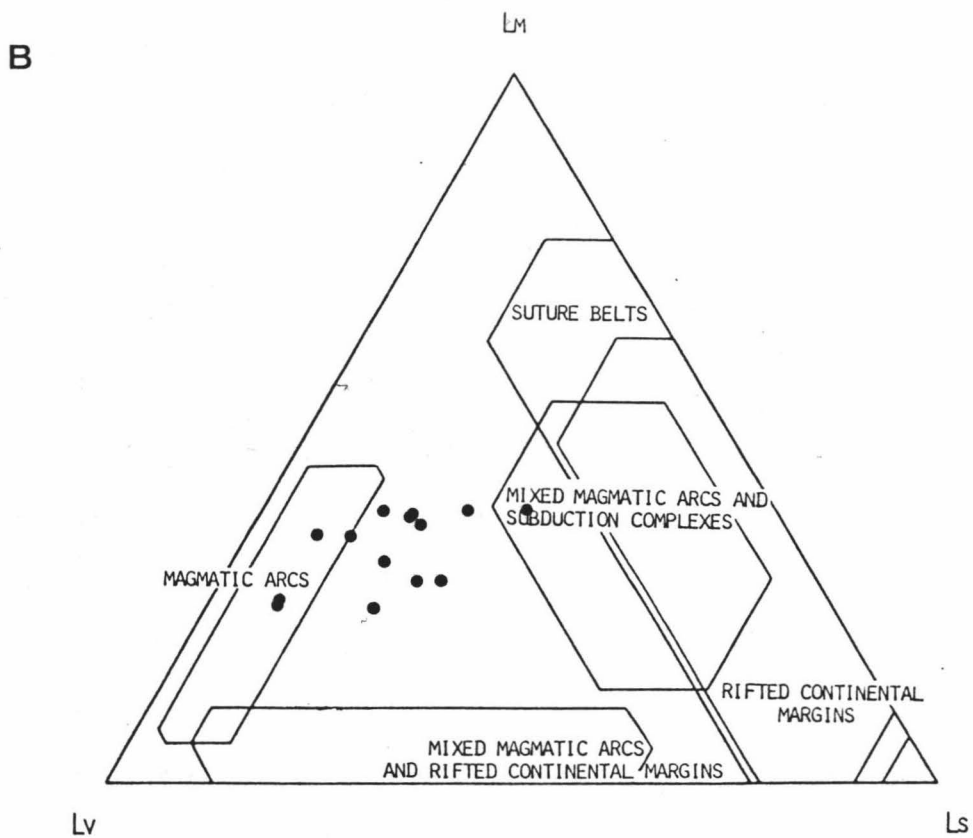
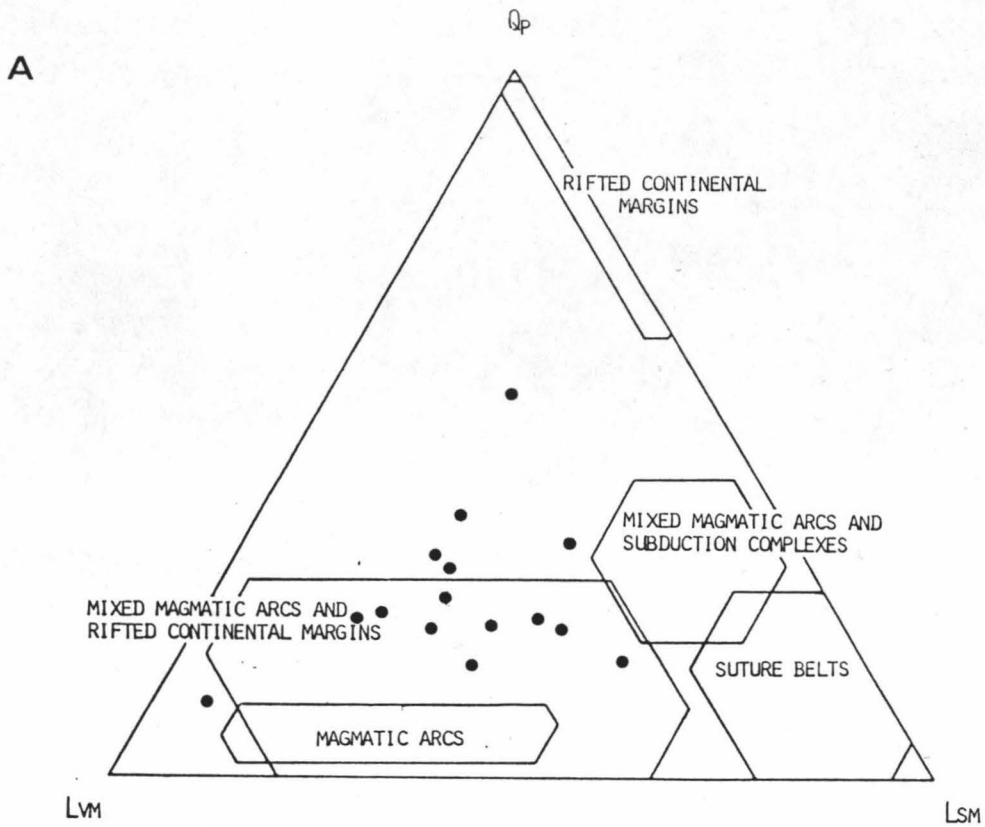


Figure 2-9

sediments. From analysis of modern sands, Valloni and Maynard (1981) defined five different tectonic settings, while Dickinson and Valloni (1980) determined detrital modes for three major tectonic settings (Table 2-5). Data from this study compare best with the leading edge mode of Valloni and Maynard (1981) and the active continental margin mode of Dickinson and Valloni (1980).

Detrital framework modes for other greywackes in the southern North Island (Rowe 1980; Orr in prep.), are shown in Fig.2-10a. Point counts of four thin sections of Rowe (1980) were repeated by me. The recounted sections, although lower in modal lithic fragments, still fall within the same field on a QFL diagram. The fields for QFL of Rowe (1980), Orr (in prep.) and myself all overlap (Fig.2-10a). The average grain size from thin sections for which modes were determined of Rowe (0.15mm), Orr (0.17mm) and myself (0.16mm) are similar, therefore, the difference is thought to be real, indicating a minor variation in the detritus derived from the source area.

On QFL diagrams, MacKinnon (1983) was able to define an evolutionary trend within his five Torlesse petrofacies from the South Island. Data from this study falls near the Triassic petrofacies field of MacKinnon (Fig.2-10b). Comparisons will be further discussed in Chapter 7.

2.3.1 Tectonic setting using geochemical analyses

A recent trend in the literature is to use geochemical analyses to distinguish tectonic settings of sands and this has met with limited success (Maynard *et al.* 1982). Maynard *et al.* (1982) are able to distinguish between passive margin and arc-related settings. Using their criteria (Table 2-6) the sands from the study area, could not have been derived from a passive margin.

Crook (1974) defined three tectonic settings of greywackes using

Table 2-5: Modal analysis of sandstone from known tectonic setting.

	No. of samples	Q	F	L
Tararua Range	15	33	48	19

From Valloni & Maynard (1981)				
Margin				

Trailing-edge	29	61	26	13
Leading-edge				
-subduction	8	16	53	31
-strike-slip	7	31	36	33
Back-arc	27	16	34	50
Fore-arc	9	3	16	81

From Dickinson & Valloni (1980)				
Ocean basin adjacent to				

Rifted continental margin				
-Cratonic block only	155	76	18	6
-Craton plus rift belt	15	69	26	5
-Craton plus orogenic belt	30	63	26	11
Orogenic continental margin				
-Transform arc orogen	35	31	45	24
-Continental-margin arc	40	20	41	39
Oceanic island chain				
-Oceanic island arc	85	11	34	55
-Intraplate archipelago	25	0	5	95

Figure 2-10a: Comparative QFL diagrams for other areas in the Torlesse Supergroup

Data from

R = Rowe (1980)

O = Orr (in prep.)

● = this study

Figure 2-10b: Comparative detrital framework modes for the South Island and the Tararua Range.

□ = Data from Mackinnon (1983) where numbers refer to sediment of known age. Numbers are the same as the fossil zones for the Torlesse Supergroup.

■ = Data from this study.

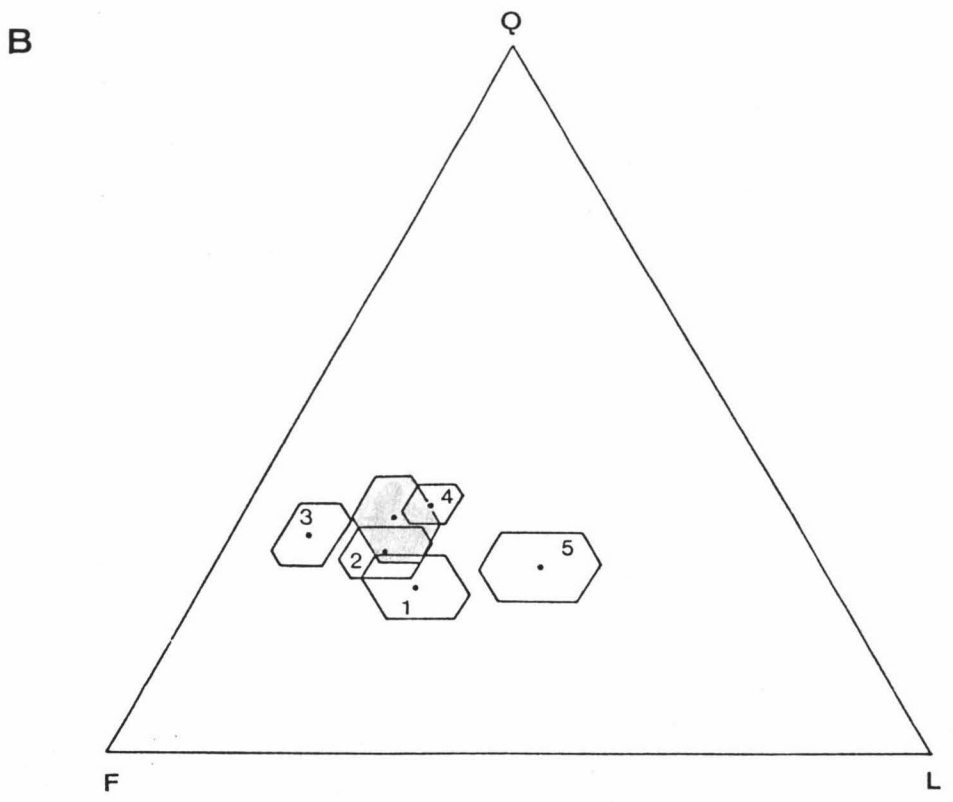
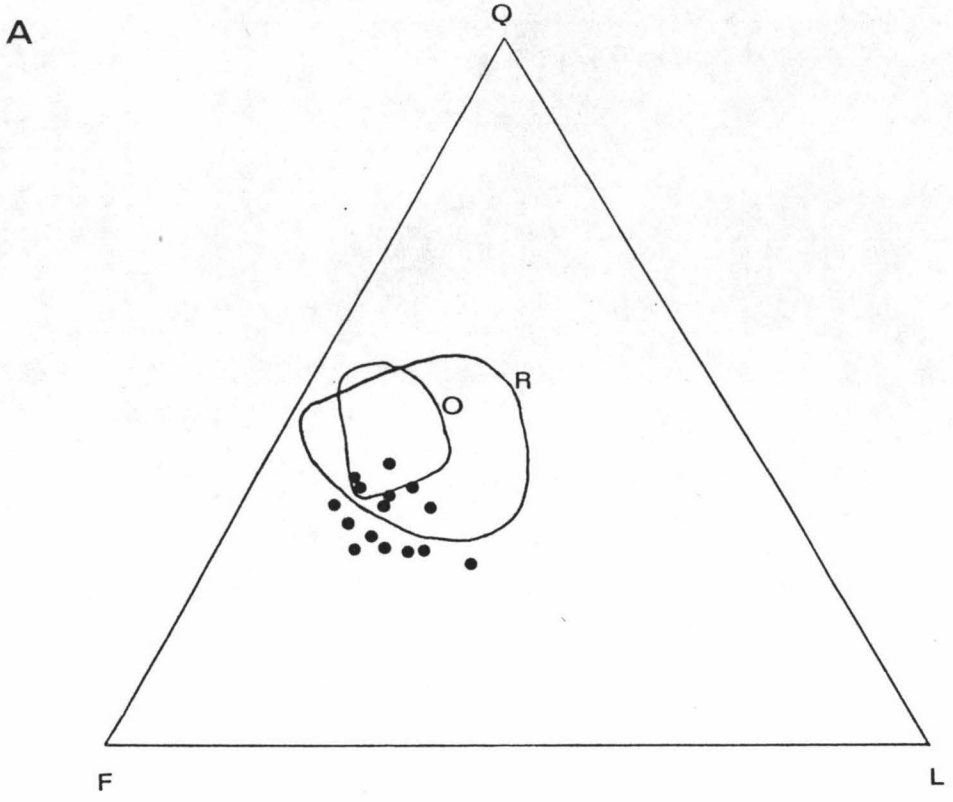


Figure 2-10

Tectonic setting	SiO ₂	Al ₂ O ₃	Fe ₂ O ₃	MgO	CaO	K ₂ O	Na ₂ O
1 Sands							
Trailing-edge	77.9	9.8	2.9	1.3	4.1	2.0	1.9
Strike-slip	67.8	15.6	3.7	2.3	3.6	2.9	3.9
Continental margin arc	69.5	14.1	3.9	1.9	4.4	2.6	3.6
Backarc	68.8	14.4	4.5	2.4	4.4	2.0	3.6
Forearc	61.5	15.2	7.7	3.8	6.7	1.4	3.8
2 Muds							
Trailing-edge	65.9	13.7	5.3	2.8	8.2	2.6	1.5
Strike-slip	65.8	14.4	6.8	3.4	4.9	2.0	2.7
Continental margin arc	66.1	16.9	6.4	3.2	3.0	2.5	2.4
Backarc	68.0	14.9	6.5	3.1	2.8	2.3	2.5
Forearc	68.9	12.1	7.2	3.0	4.9	1.5	2.6

Table 2-6: Bulk chemistry of modern deep-sea sands and associated muds
(from Maynard et al. 1982).

Using the criteria of Maynard et al. (1982), the sands and argillites from the study area, having SiO₂ ranges from 77.03 - 57.54 weight percent and Al₂O₃ ranges from 11.13 - 20.28 weight percent, could not have been derived from a trailing-edge (passive margin) tectonic setting.

SiO₂, K₂O and Na₂O contents, these being:

- 1) Atlantic types- greywacke that has been deposited at passive margins or in plate interiors,
- 2) Andean type- greywacke that are deposited at subducting plate margins (off active continental margins),
- 3) Pacific type- greywackes that are deposited in trenches off active volcanic island arcs.

Roser (1983) expanded on the work of Crook (1974) and discriminated greywacke types using a K₂O/Na₂O versus SiO₂ diagrams. On such a plot, data from the Tararua Range falls within an Andean margin field (Fig. 2-11), implying deposition of sediment at an magmatically active continental margin or strike-slip boundary.

The Torlesse sandstone and argillite samples analysed by Roser (1983) also fall within the Andean margin field.

Framework modes and geochemical analyses indicate that the greywacke from the study area was derived from an active continental margin, which was shedding sediment of acid-volcanic and metamorphic origin.

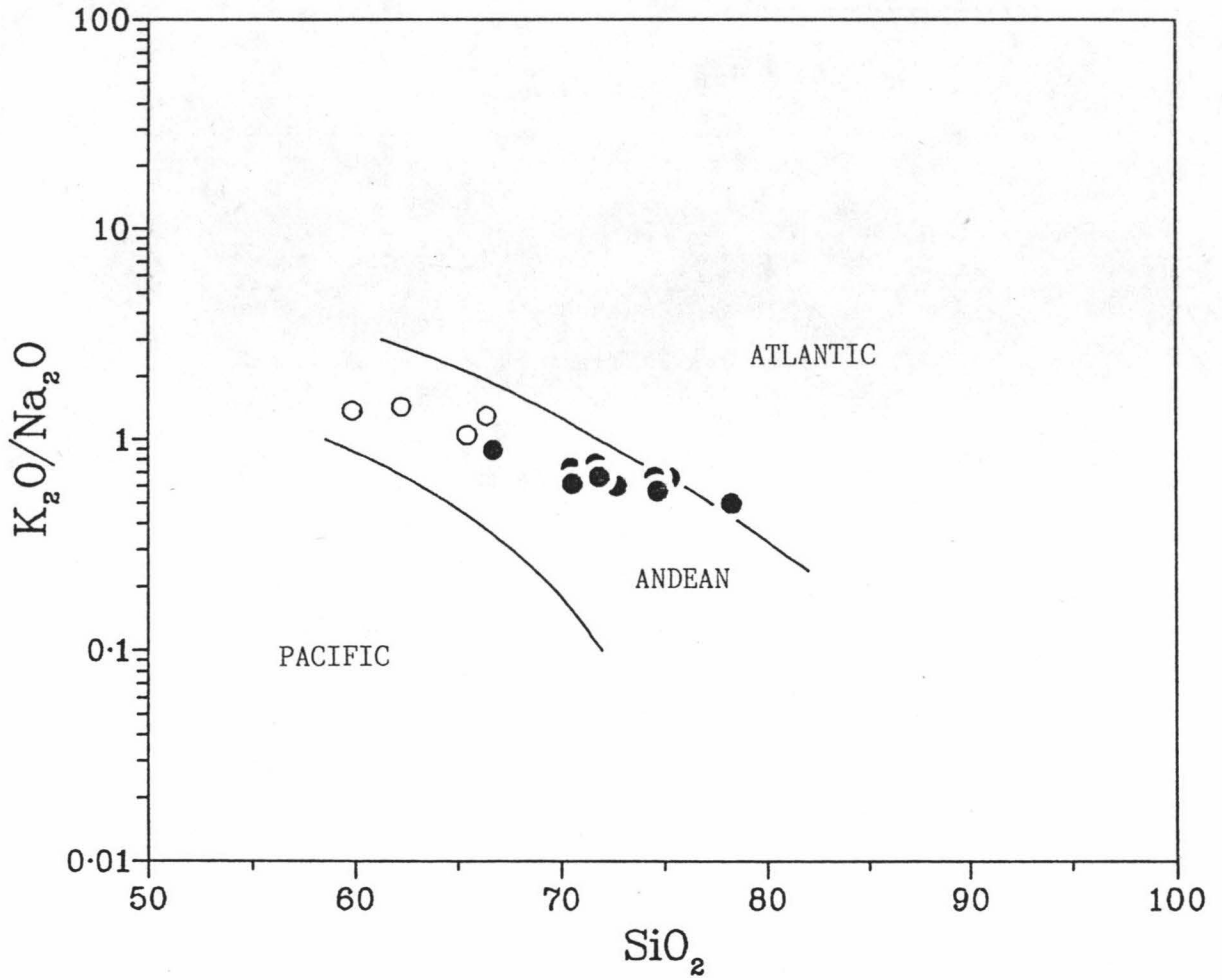


Figure 2-11: Tectonic setting of sediments using a volatile-free alkali/silica discriminant (after Roser 1983).

● = sandstone

○ = argillite

Data falls within the Andean field.

CHAPTER THREE

ROCKS OF THE VOLCANOGENIC ASSOCIATION

3.1 INTRODUCTION

Rocks of the volcanogenic association, although volumetrically minor (less than 3% of the total rock), are widely distributed. Many workers have noted the association of metabasite, red argillite, limestone and chert within the Torlesse Supergroup, although they may crop out alone in some places (Bradshaw 1972).

This section describes the petrology of volcanogenic association rocks and uses major element, trace element and electron microprobe analyses, to examine the possible original environment within which the metabasite and other rocks of volcanogenic association formed.

3.1.1 Metabasite

Metabasite within the Tararua Range, commonly termed spilite by earlier workers (Reed 1957a; Barnes 1979), is extensively altered, either being hematite stained to a red to red-brown colour, or chloritized and green in colour. They crop out as large slivers (up to 120m by 40m in Abbots Creek, S26A/ 9967 0880; Fig. 3-1) having sheared contacts with the surrounding greywacke and argillite (Fig. 3-2a), or as blocks (1.6m by 1.4m; S26D/ 1191 1799) or inclusions within melange. Hematite-red pillows up to 50cm in diameter are exposed within slivers in Abbots Creek (S27A/ 9967 0880; S27A/ 9970 0872) Figure 3-2b. Inter-pillow material is basaltic.

In thin section the mineral assemblage consists of predominantly sodic plagioclase and clinopyroxene grains set in a dark groundmass. Plagioclase grains are albite (ranges of six analyses from four samples by electron microprobe is $An_{0.2} Ab_{99.7} Or_{0.1}$ to $An_{2.1} Ab_{96.4} Or_{1.5}$), and are often covered with carbonate and incipient sericite alteration. Clinopyroxene grains are calcic in composition. Salite and some

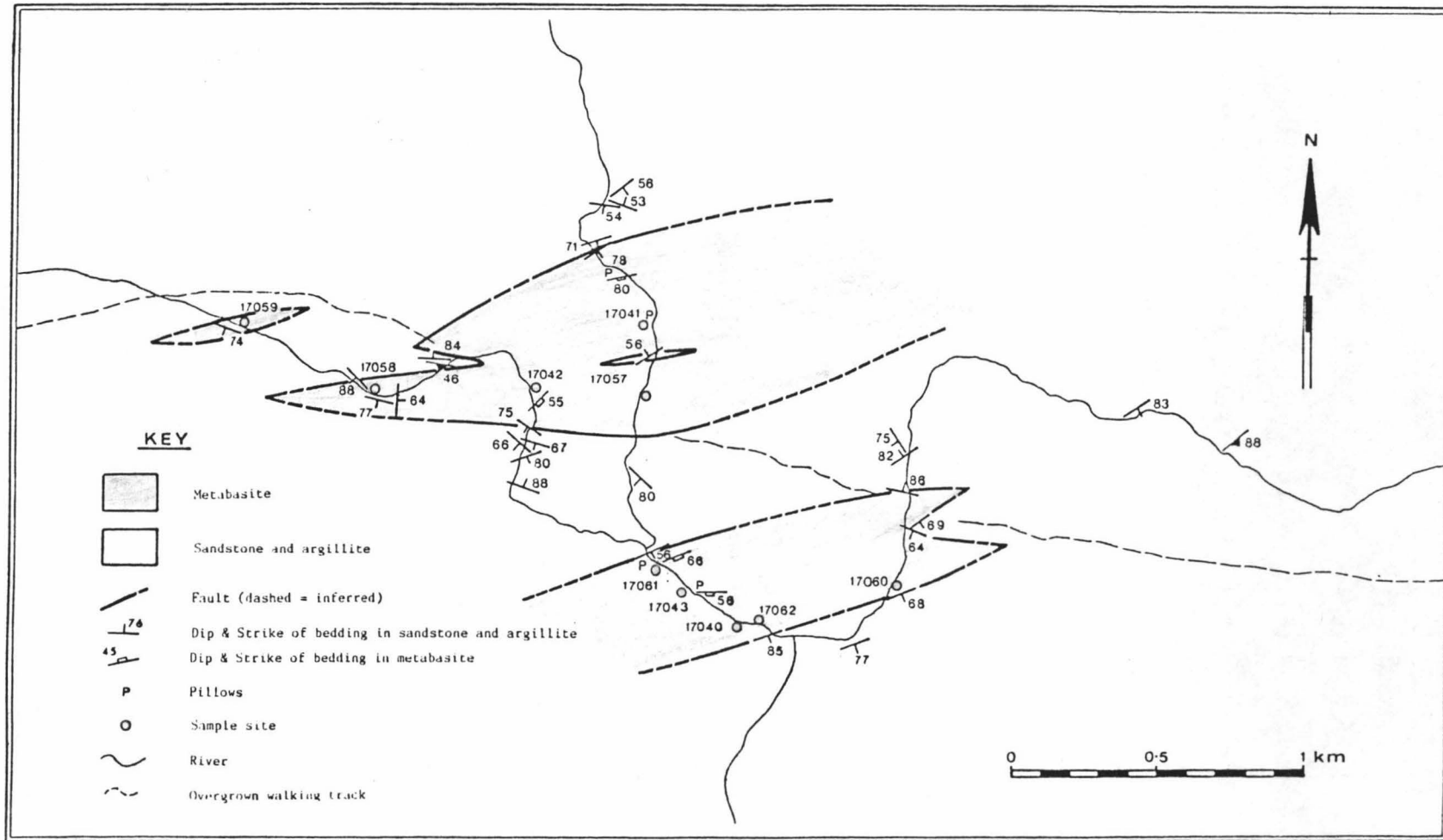


Figure 3-1: Map of metabasites in Abbots Creek.

Figure 3-2a: Large outcrop of green metabasite (M) with a faulted and sheared contact with the surrounding rocks of sedimentary association (predominantly argillite (A)).
Abbots Creek S27A/ 0401 0790, width of photograph 15 metres.

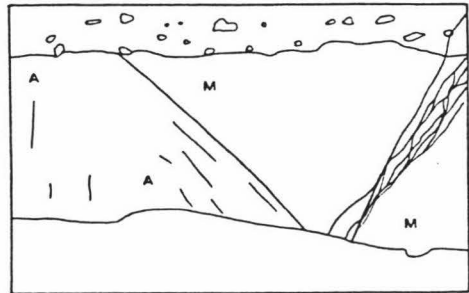
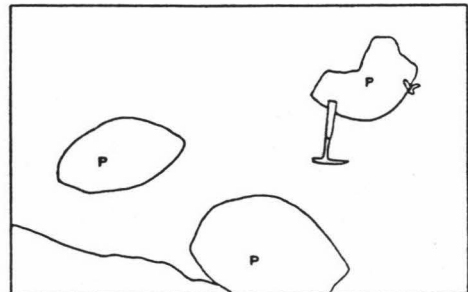
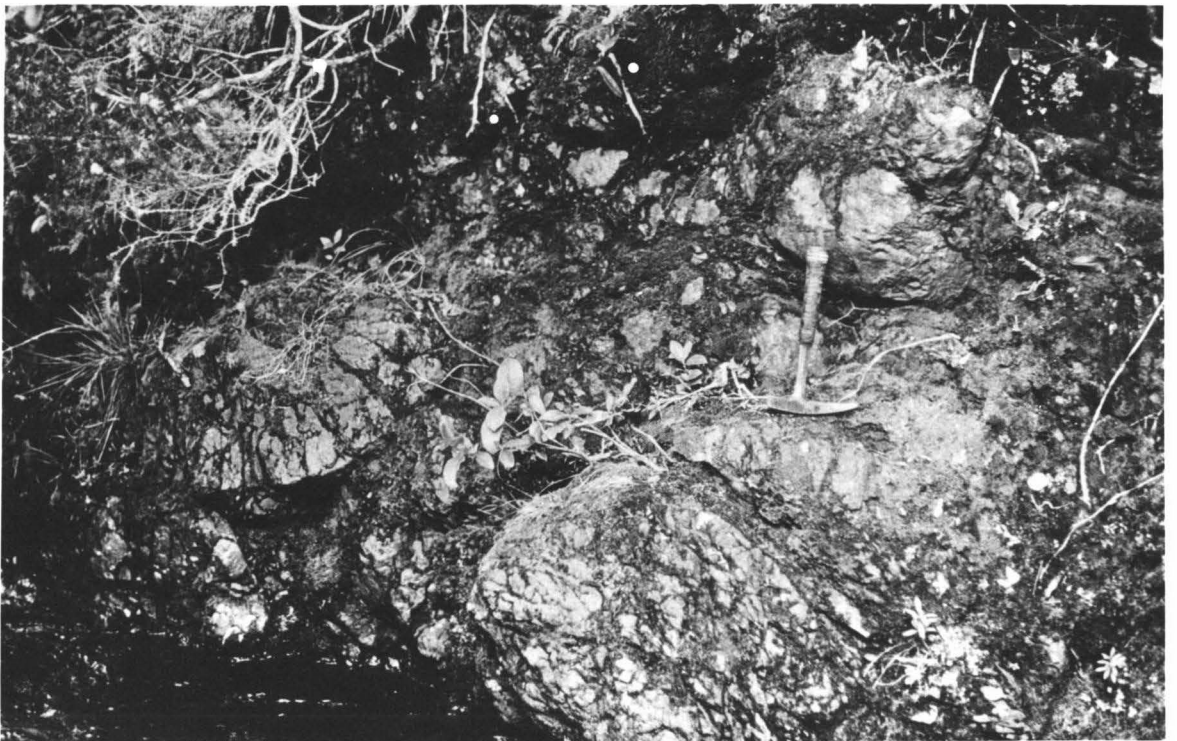
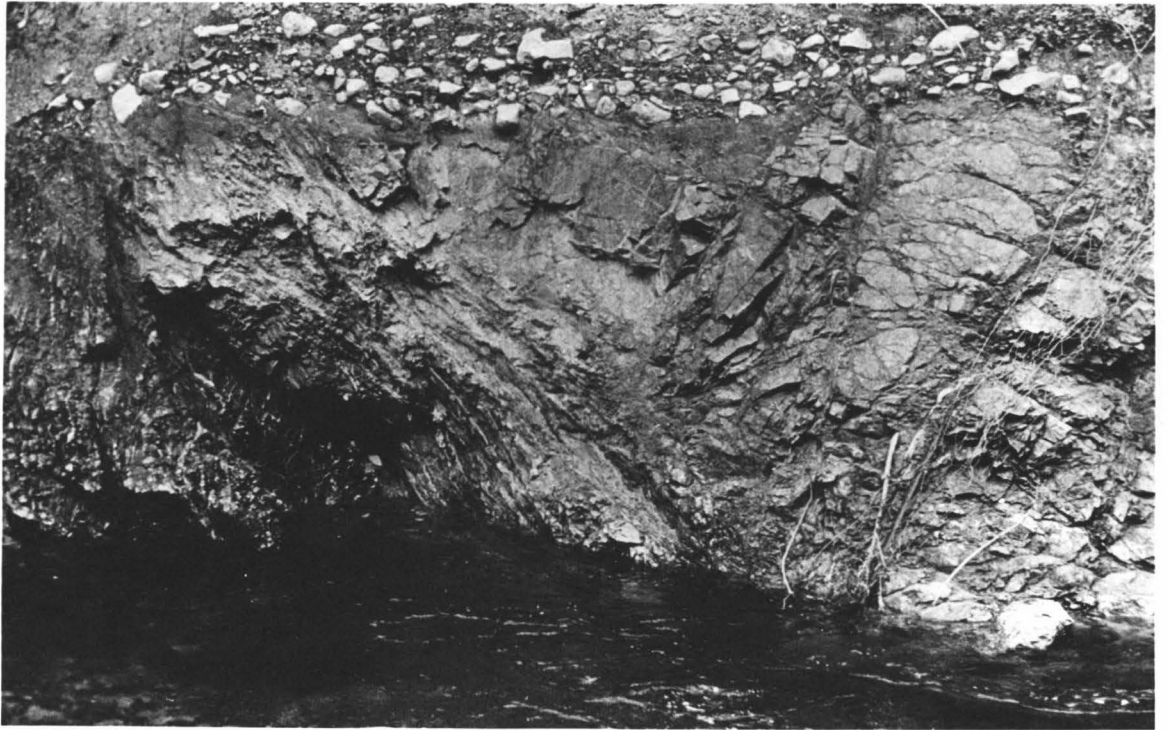


Figure 3-2b: Hematite-red metabasite with pillows (P). Pillows have a maximum diameter of 50 centimetres and are facing right way up.
Abbots Creek S27A/ 9969 0874,
geological hammer 31 cm long.





endiopside/augite compositions were determined by electron microprobe analyses (see Appendix VIII for relevant analysis), with individual grains being relatively homogenous. Two varieties of sphene occur in the interstitial regions after iron oxide minerals, the most common being a "normal" sphene and the other a Fe-Al rich sphene (determined by electron microprobe). Disseminated pyrite mineralization is rare. The groundmass is dominantly chlorite with some sericite, red oxide grains and clay. Glass occurs in sample 17056.

The metabasite shows variolitic and sub-ophitic to ophitic textures. Variolitic textured metabasites exhibit thin plagioclase laths arranged in subradial or "bow-tie" sheaves. Laths are generally less than 0.7mm in length (17042, 17053, 17057), and show simple twinning. Fine grained colourless clinopyroxene (<0.1mm) and green chlorite pseudomorphs after euhedral olivine (<0.4mm) occur studded between plagioclase laths (17058; 17059 and 17061 respectively). Interstitial Al-sphene and magnetite are common. In sample 17056, celadonite is found in patches surrounded by pumpellyite and Al-Fe rich sphene with glass.

Sub-ophitic to ophitic textured metabasite contain large well developed tabular plagioclase laths, often not twinned, up to 2.5mm by 1.25mm in size, being partially or wholly enclosed by pinkish to colourless, anhedral to sub-hedral clinopyroxene grains (17045, 17055, 17060, 17062). Clinopyroxene grains range up to 3.25mm by 2.5mm in size (17045), are commonly fractured and in the majority of cases are partly altered to chlorite (fibrous blue variety) and pumpellyite (determined by electron microprobe analyses).

Minerals associated with metamorphism will be discussed later.

3.1.2 Red argillite

Red to brownish-red argillite crops out within metabasite sequences and as clasts within melange. Clasts are sub-angular to

rounded, generally only millimetres in diameter but can range up to 6 metres as at S26D/ 1180 1342.

In thin section the rock consists of minor amounts of equant monocrystalline quartz grains (0.02mm; 17100) set in dark red to brown clay-size particles. Secondary sericite, chlorite and calcite can be distinguished. Sample 17096 contains fine grained polycrystalline quartz aggregates in circular regions up to 0.8mm in diameter, possibly recrystallized radiolaria.

3.1.3 Chert

Chert occurs as a mappable unit cropping out over more than 50 metres (S26C/ 0610 1208), as fragments within melange and at S27A/ 9969 0881 as a 2cm by 2cm clast surrounded by metabasite. Fragments within melange range from clasts, millimetres in diameter, to blocks, one being 8m in length (S26D/ 1129 1705). Most cherts are hematite stained and red in colour (17074, 17078, 17079, 17095), however white (17086), grey (17092) and green (17098) coloured varieties occur. Beds ranging from 5mm to 5cm are seen, defined by fine dark silty partings between layers. Some bedded cherts are folded.

The chert consists of microcrystalline quartz grains (less than 0.02mm in diameter), which form recrystallized mosaics. Fine disseminations of pyrite occur, occasionally in clusters, with individual cubes ranging from 0.02mm to 0.3mm in diameter (17074). Recrystallized radiolarian skeletons are found in several cherts (17078, 17079, 17098), and show a tendency to be abundant in the Fe-rich hematite-stained units. Radiolarian skeletons were successfully extracted from sample 17078 (S26C/ 0610 1208); see Chapter 5.

3.1.4 Limestone

Limestone occurs as sub-angular to rounded clasts within melange. Clasts range up to 1m in diameter, are grey in colour when fresh and

weather to a light grey or white colour, having negative relief relative to the surrounding rock type. Calcite veining which developed prior to incorporation within the melange is common, often with a number of veins cross-cutting each other. Stylolites, indicating deformation through pressure solution mechanism, are abundant, while pyrite mineralization is often associated with the clasts.

In thin section, the limestones vary from micrite to fossiliferous micritic and sparite (1-10% allochems). Within the latter bryozoa and mussel fragments, foraminifera and echinoid plates are visible (17081,17082-Harmsen pers. com. 1983). The broken allochem assemblage indicates redeposition of the allochems into micritic material. One micritic clast (17097) displays burrows, less than 0.5mm in diameter, which are infilled with darker micritic material. This burrow rich section grades into a fine grained layered micrite, indicating a change in depositional environment, to one of increased energy.

3.2 METABASITE GEOCHEMISTRY

To characterize the metabasites which occur in the Tararua Range and determine their eruptive environment, 16 metabasites from various sites were analysed for major and trace elements. Analyses are listed in Table 3-1.

During alteration and metamorphism of basalts, a large number of elements are mobile eg. K,Ca,Mg,Na,Si,Fe,Al,Ba,Sr (Pearce 1975). Therefore only elements which are considered immobile, that is, resistant to mobilization and alteration are used for discrimination of basalt types and their tectonic setting eg. Ti,P,Zr,Y,Nb,La (Pearce & Cann 1973, Pearce 1975, Erlank & Kable 1976, Saunders 1979). Chemical variations of metabasalts from the Torlesse are described by Roser (1983).

Division into alkaline and tholeiitic magma types can be made

TABLE 3-1a: Analysis of metabasites from the Tararua Range

Analysis	(1)	(2)	(3)	(4)	(5)	(6)	(7)	(8)
Sample No.	17048	17046	17045	17047	17054	17055	17043	17040
Major Oxides (wt%)								
SiO ₂	49.38	44.22	43.58	41.29	48.37	44.34	40.28	43.52
TiO ₂	1.59	3.01	2.99	4.06	2.24	3.22	1.57	1.66
Al ₂ O ₃	16.64	17.02	16.95	14.55	15.20	14.59	14.12	15.93
Fe ₂ O ₃ T	9.36	11.39	12.11	13.19	7.61	13.07	8.56	8.81
MnO	0.20	0.25	0.26	0.33	0.18	0.26	0.19	0.16
MgO	3.61	6.67	6.95	6.39	4.99	3.53	3.24	2.70
CaO	6.66	6.10	6.25	8.32	8.26	7.28	15.54	12.33
Na ₂ O	5.05	4.22	4.11	3.90	5.27	3.81	4.75	4.49
K ₂ O	1.59	0.70	0.80	0.15	0.11	0.40	0.64	1.74
P ₂ O ₅	0.77	0.74	0.71	0.76	0.41	0.79	0.33	0.34
Loss	5.16	5.23	5.26	6.56	7.50	8.29	10.36	8.20
TOTAL	100.01	99.55	99.97	99.50	100.14	99.58	99.58	99.88
Trace Elements (ppm)								
Ba	460	272	275	123	100	123	94	214
Ce	107	87	93	99	45	66	25	30
Cr	98	102	110	20	147	13	212	305
Cu	18	44	39	61	18	25	46	51
Ga	29	23	21	24	18	26	13	16
La	59	40	46	46	18	24	8	13
Nb	83	60	58	65	31	42	18	19
Ni	67	59	57	41	112	14	75	106
Pb	7	5	1	4	8	3	1	1
Rb	19	15	15	3	2	17	14	46
Sc	13	26	24	41	23	28	30	25
Sr	454	638	698	553	424	416	335	359
Th	9	7	6	7	3	3	1	1
U	3	3	2	2	1	1	1	1
V	78	235	238	339	185	252	194	168
Y	37	34	34	43	29	50	25	29
Zn	110	112	107	141	69	157	78	128
Zr	537	342	342	409	226	409	145	156

TABLE 3-1b: Analysis of metabasites from the Tararua Range

Analysis	(9)	(10)	(11)	(12)	(13)	(14)	(15)	(16)
Sample No.	17041	17042	17052	17049	17050	17044	17053	17051
Major Oxides (wt%)								
SiO ₂	39.25	34.11	51.49	54.38	50.49	51.75	34.27	44.00
TiO ₂	1.58	1.41	0.97	1.04	0.95	0.85	1.10	1.32
Al ₂ O ₃	15.01	12.63	12.83	10.32	9.97	17.39	15.61	16.37
Fe ₂ O ₃ T	8.77	7.16	8.31	9.01	7.69	11.56	11.48	14.87
MnO	0.35	0.14	0.16	0.13	0.13	0.35	0.25	0.34
MgO	3.04	2.81	1.99	1.88	2.53	3.94	2.27	4.42
CaO	15.75	20.50	14.89	13.97	17.12	2.68	16.72	10.80
Na ₂ O	3.65	2.96	2.33	1.72	0.55	6.24	2.93	1.56
K ₂ O	1.29	1.88	0.06	0.03	0.01	0.41	0.89	0.04
P ₂ O ₅	0.34	0.34	0.10	0.11	0.10	0.07	0.11	0.15
Loss	10.68	15.71	6.82	6.03	10.13	4.52	13.93	5.79
TOTAL	99.71	99.65	99.95	98.62	99.67	99.76	99.56	99.66
Trace Elements (ppm)								
Ba	181	275	46	37	91	193	301	145
Ce	30	19	12	11	9	6	17	17
Cr	267	210	152	102	121	345	385	185
Cu	46	32	65	21	254	87	92	48
Ga	17	12	21	16	16	18	18	21
La	11	4	3	3	2	3	7	6
Nb	18	15	3	<2	<2	<2	<2	<2
Ni	80	76	51	48	36	61	153	80
Pb	1	1	2	1	2	7	3	11
Rb	32	49	1	1	1	16	33	1
Sc	32	25	30	30	33	45	40	48
Sr	340	319	173	128	169	429	270	102
Th	2	2	2	1	1	1	2	2
U	1	1	1	1	1	1	1	1
V	233	160	315	304	257	266	262	378
Y	29	28	23	23	24	30	31	39
Zn	118	74	89	80	69	127	104	166
Zr	134	130	66	72	64	37	80	74

using Y/Nb ratios, where basalts with ratios less than 1 are alkaline; ratios between 1-2 are transitional; ratios greater than 2 are tholeiitic (Pearce & Cann 1973). Samples analysed from the Tararua Range are evenly split between the 3 types (Fig.3-3a). Confirmation of alkaline or tholeiitic character of the samples is given using a discrimination function based on the immobile elements Ti,P,Y,Nb and Zr, (Grapes & Palmer 1984). All 6 samples classified as tholeiitic on the basis of Y/Nb ratios are confirmed, as are 4 of 5 of the metabasites as alkaline (Fig.3-3b). The remaining alkali metabasite and 4 of 5 transitional samples are notionally tholeiitic. The Df values broadly confirm the Y/Nb ratios.

3.2.1 Tectonic setting

Basalts may be erupted in variety of tectonic settings such as back-arc basins, island arcs, ocean islands, intra-arc rifts and at mid-ocean ridges. Basalts from different settings can be delineated using immobile elements as discriminants (Pearce & Cann 1973; Pearce 1975).

Using Ti and V, Shervais (1982) separated island-arc basalts, mid-ocean ridge basalts (MORB) and alkaline-ocean island basalts by Ti/V ratios of <20, 20-50, >50 respectively, with minor overlap. Tararua samples defined by Y/Nb ratios (Fig. 3-3a) fall within two areas on the Ti/V plot (Fig.3-4). Transitional and alkaline samples have Ti/V ratios from 40 to 105, being reasonably distinct from MORB, and similar to alkaline and transitional basalts that form in ocean basins as oceanic islands and seamounts. A comparable setting is the Hawaiian Island tholeiites and alkaline basalts, which have Ti/V ratios of 42-60 and 50-110 respectively (Shervais 1982). Tholeiitic samples from my field area cluster round a Ti/V ratio of 20, suggesting that they have either MORB or island-arc basalts affinities.

Pearce and Cann (1973) utilized the immobile elements Ti,Zr and Y

Figure 3-3a: Determination of magma type using Y/Nb ratio

(after Pearce & Cann 1973).

Y/Nb < 1 = alkaline

Y/Nb 1-2 = transitional (between two vertical lines)

Y/Nb > 2 = tholeiitic

Range for Guadalupe Ocean Island - Engel et al. 1965

Galapagos Ocean Island - Pearce & Cann 1973

Hawaiian Tholeiites Ocean Island - Pearce & Cann 1973

Mid-Atlantic Ridge Ocean Floor - Sun et al. 1979

Isand Arc Tholeiites - Pearce & Cann 1973

Figure 3-3b: Determination of magma type using a discriminant function utilizing the abundances of Ti, P, Nb, Y and Zr (after Grapes & Palmer 1984).

The discriminant function is:

$$Df = -0.2163TiO + 7.2431P O + 0.0196Nb - 0.1047Y + 0.0019Zr - 0.8983$$

Df positive = alkaline

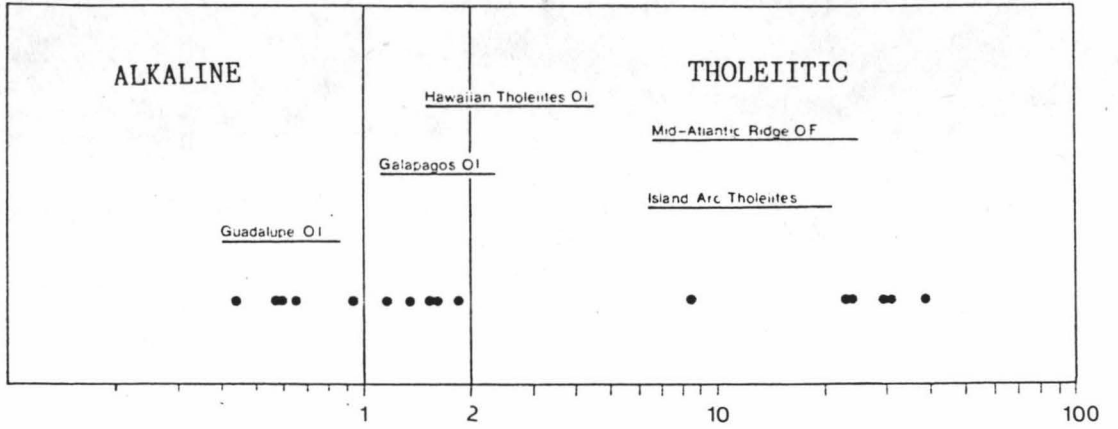
Df negative = tholeiitic

No transitional magma type by definition

Colours as from Figure 3-3a where:

- = alkaline
- = transitional
- = tholeiitic

A



B

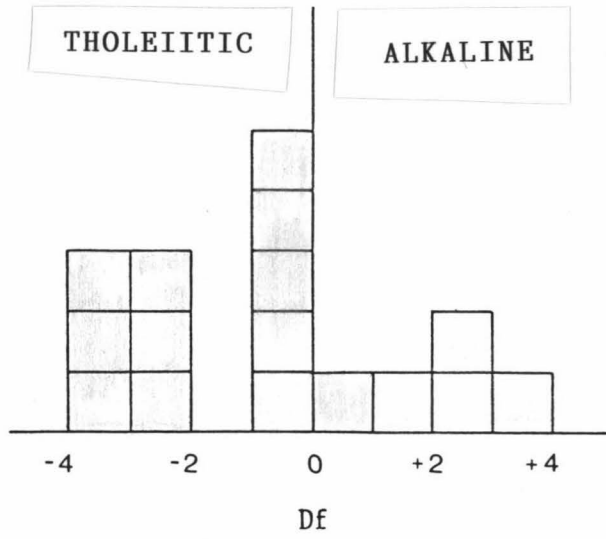


Figure 3-3

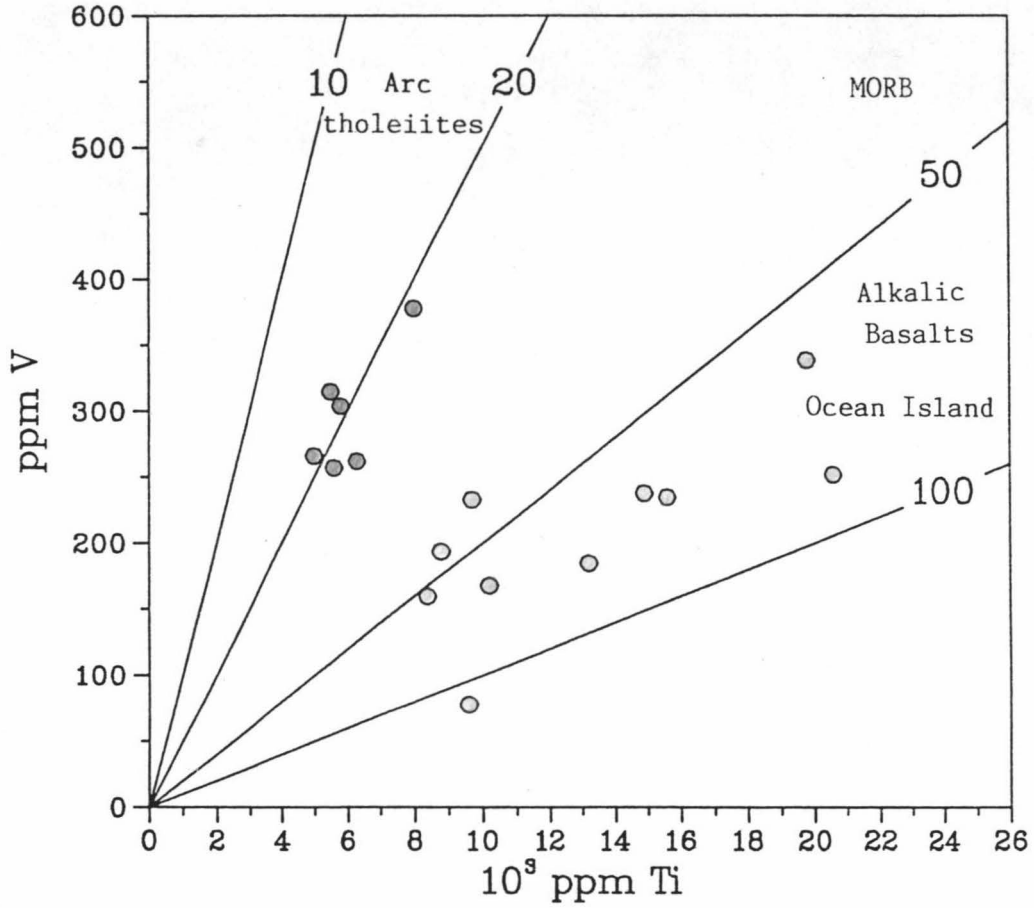


Figure 3-4: Ti-V discriminant plot for metabasite (after Shervais 1982).

Trend lines 10, 20, 50 and 100 are Ti/V ratios.

Colours as from Figure 3-3a where:

- = alkaline
- = transitional
- = tholeiitic

discrimination diagrams, to delineate four magmatic fields. These fields are:

- 1) intra-plate basalts (IPB);
- 2) ocean-floor basalts (OFB);
- 3) island-arc low potassium tholeiites (LKT);
- 4) calc-alkaline basalts (CAB);

were: IPB= alkaline-ocean island basalt; OFB= mid-ocean ridge basalt; LKT= island-arc basalt; CAB= island-arc basalt of Shervais (1982). The terminology of Pearce and Cann (1973) and Shervais (1982) is used throughout the geochemical discussion of metabasite for other binary axes discrimination plots.

On a Ti-Zr-Y diagram (Fig.3-5a) the transitional and alkaline samples plot mainly within the IPB field, with slight overlap into the OFB field by some transitional basalts. The tholeiite samples fall within the OFB field. Prestvik (1982) noted that basalts from tectonically anomalous ridge systems fell within the IPB field as well as the OFB field on the Ti-Zr-Y diagram, and concluded that this represented a trend from "primitive" to "evolved" basalts, with "primitive" basalts falling within field B, to "evolved" basalts falling in fields D and C. Two samples from the Tararua Range fall outside the fields on Fig.3-5a and could represent a "primitive" and "evolved" basalt, as they plot near the extension of the trend line of Prestvik (1982).

The fields for LKT and CAB overlap with that of OFB on Fig.3-6a, but further separation can be made using the binary plots Ti versus Zn and Zr versus Zr/Y. After plotting samples categorised as OFB on Fig.3-5a alone on a Ti-Zr diagram (Fig.3-5b; Pearce & Cann 1973), the transitional samples and one tholeiitic sample fall within the OFB field, while the eruptive settings of the other tholeiitic samples cannot be differentiated because they plot within the field common to all basalts.

Figure 3-5a: Ti-Zr-Y discriminant plot (after Pearce & Cann 1973).

A + B = low-potassium tholeiites (LKT)

B = ocean-floor basalts (OFB)

B + C = calc-alkaline basalts (CAB)

D = intra-plate basalts (IPB)

Trend line from "primitive" to "evolved" basalts (Prestvik 1982)

Figure 3-5b: Ti-Zr discriminant plot (after Pearce & Cann 1973).

Only OFB metabasites from Figure 3-5a have been plotted.

A + B = low-potassium tholeiites (LKT)

B + C = calc-alkaline basalts (CAB)

B + D = ocean-floor basalts (OFB)

Figure 3-5c: Zr/Y-Zr discriminant plot (after Pearce & Norry 1979).

A = Intraplate basalts

B = Mid-ocean ridge basalts

C = Island arc basalts

Colours as from Figure 3-3a where:

● = alkaline

○ = transitional

● = tholeiitic

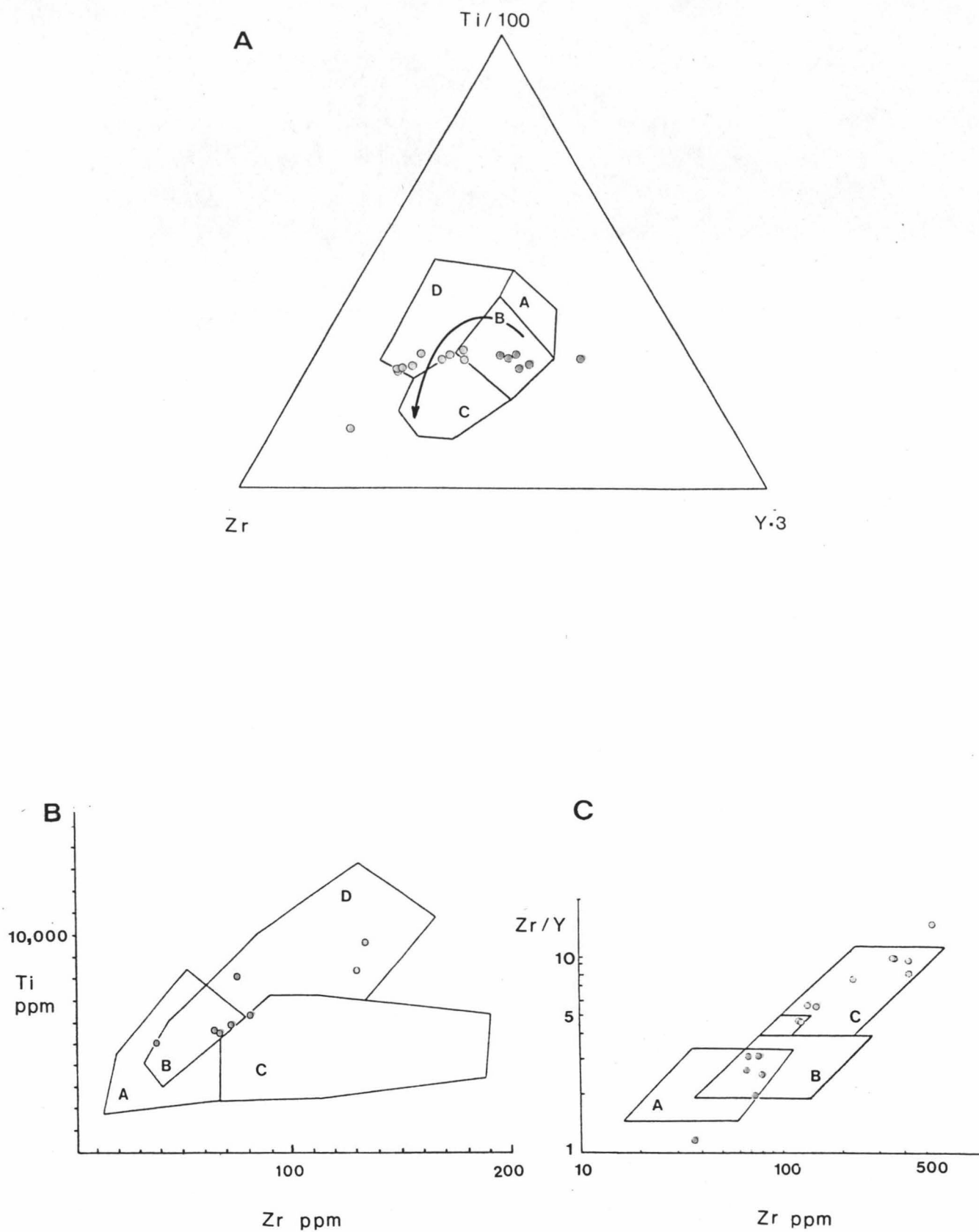


Figure 3-5

On a Zr/Y vs Zr diagram, (Pearce & Norry 1979), the results are again ambiguous with the tholeiitic samples falling within the field common to both island-arc and MORB (Fig.3-5c). An unequivocal setting cannot be determined for these 6 tholeiite samples using Figure 3-5a,b or c.

Saunders et al. (1979) however, proposed that island-arc basalts could be separated from ocean floor basalts by using La-Nb. The tholeiitic samples have very low La and Nb values and on a La-Nb diagram (Fig.3-6) they plot close to the regions defined by the lower detection limit for these elements. All samples from the Tararua Range, taken together show a trend similar to that defined for ocean floor basalts by Mid-Atlantic ridge segments at 36°N, 63°N and 45°N, rather than the island-arc trend seen in the South Shetland Islands or the West Mariana Ridge (Saunders et al. 1979)

Discrimination between island-arc tholeiites and abyssal tholeiites (OFB) can also be made using Ni contents, as island-arc tholeiites typically contain 0-30 ppm Ni and abyssal tholeiites 30-200 ppm Ni (Jakes & Gill 1970). From the La-Nb plot and the high Ni contents (36-156ppm), the tholeiitic samples are most likely to be ocean floor basalts.

Many workers have shown that the composition of clinopyroxenes vary according to the chemistry of their host lavas (eg. Kushiro 1960; Le Bas 1962). The composition of relic calcic clinopyroxenes from altered and metamorphosed basalts can be used to discriminate different magmatic settings. Basalts from four magmatic settings were separated by Nisbet and Pearce (1977) using clinopyroxene analyses. The settings recognised are:

- 1) ocean floor basalts (OFB: MORB of Shervais 1982);
- 2) volcanic arc basalts erupted above subduction zones in island arcs or at active continental margins (VAB: island-arc basalt

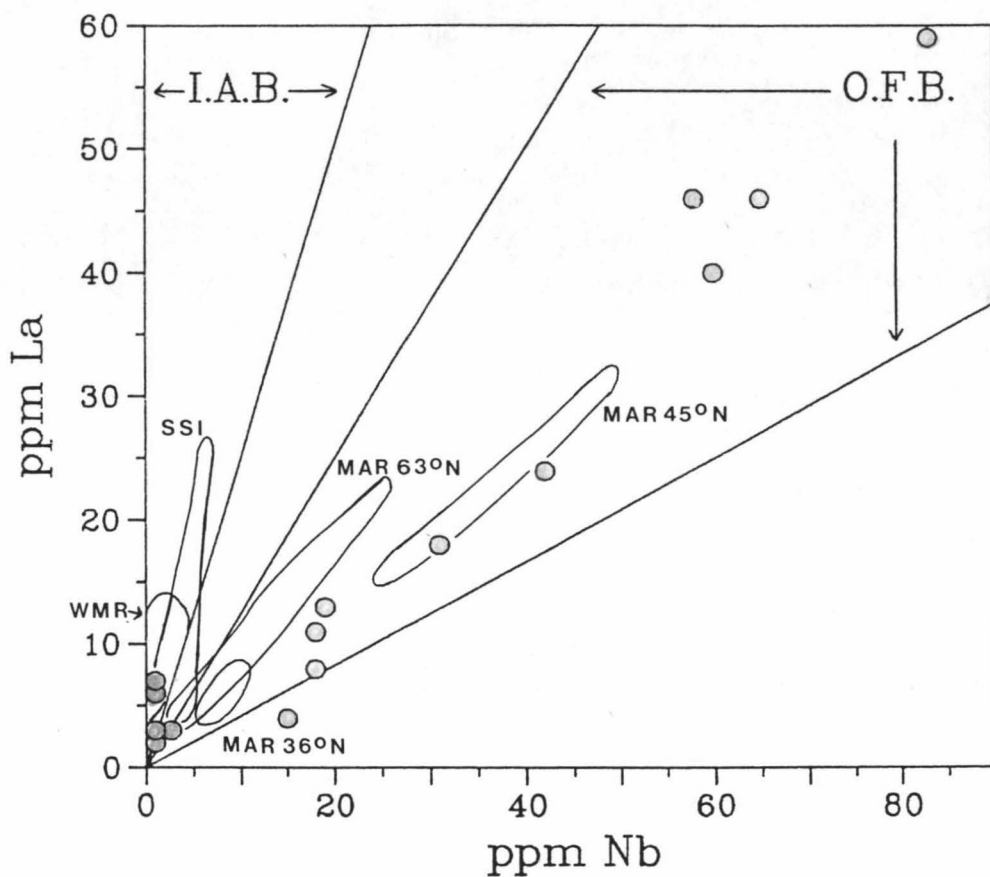


Figure 3-6: La - Nb discriminant plot (after Saunders et al. 1979).

Fields from Saunders et al. (1979) where:

- IAB = Island arc basalts
- OFB = Ocean floor basalts
- SSI = South Shetland Islands
- WMR = West Mariana Ridge
- MAR = Mid-Atlantic Ridge

The lower limit of detection for Nb = 2ppm

La = 3ppm

of Shervais 1982);

- 3) tholeiitic basalts erupted within plates in oceanic islands or continental rifts (WPT: MORB & alkaline-ocean island basalt of Shervais 1982);
- 4) alkalic basalts erupted within plates (WPA: alkaline-ocean island basalt of Shervais 1982).

Clinopyroxene grains from three alkaline samples (17045, 17056, 17062) were analysed by electron microprobe. On a $\text{TiO}_2\text{-MnO-Na}_2\text{O}$ discrimination plot (Nisbet & Pearce 1977) the clinopyroxene analyses fall mainly within the field unique to WPA (Fig. 3-7). Two analyses fall within the field common to all magma types, but as other clinopyroxenes from the same sample fall within the WPA field, these two can also be considered to represent WPA. Unfortunately clinopyroxene grains were not observed in the tholeiitic metabasite.

Geochemical and microprobe analyses indicate that the metabasites from the study area represent both intra-plate volcanics (eg. seamounts) and oceanic crust (ocean floor basalts, MORB). Such magmatic settings are in agreement with other workers (Sporli 1978; Roser 1983).

3.3 ORIGINAL ENVIRONMENT OF FORMATION

Within metabasite, clasts of chert and red argillite are found (at Abbots Creek: S27A/ 9969 0880 and Waiohine River: S26D/ 1105 1935), while in other areas, metabasite and red argillite have conformable contacts (at S26D/ 1108 1950). The field relationships between rocks of the volcanogenic association imply a related environment of deposition. Many other workers have inferred an associated depositional environment for these rock types (Andrews *et al.* 1976, Sporli 1978).

The presence of radiolaria skeletons and the clay-size detritus in

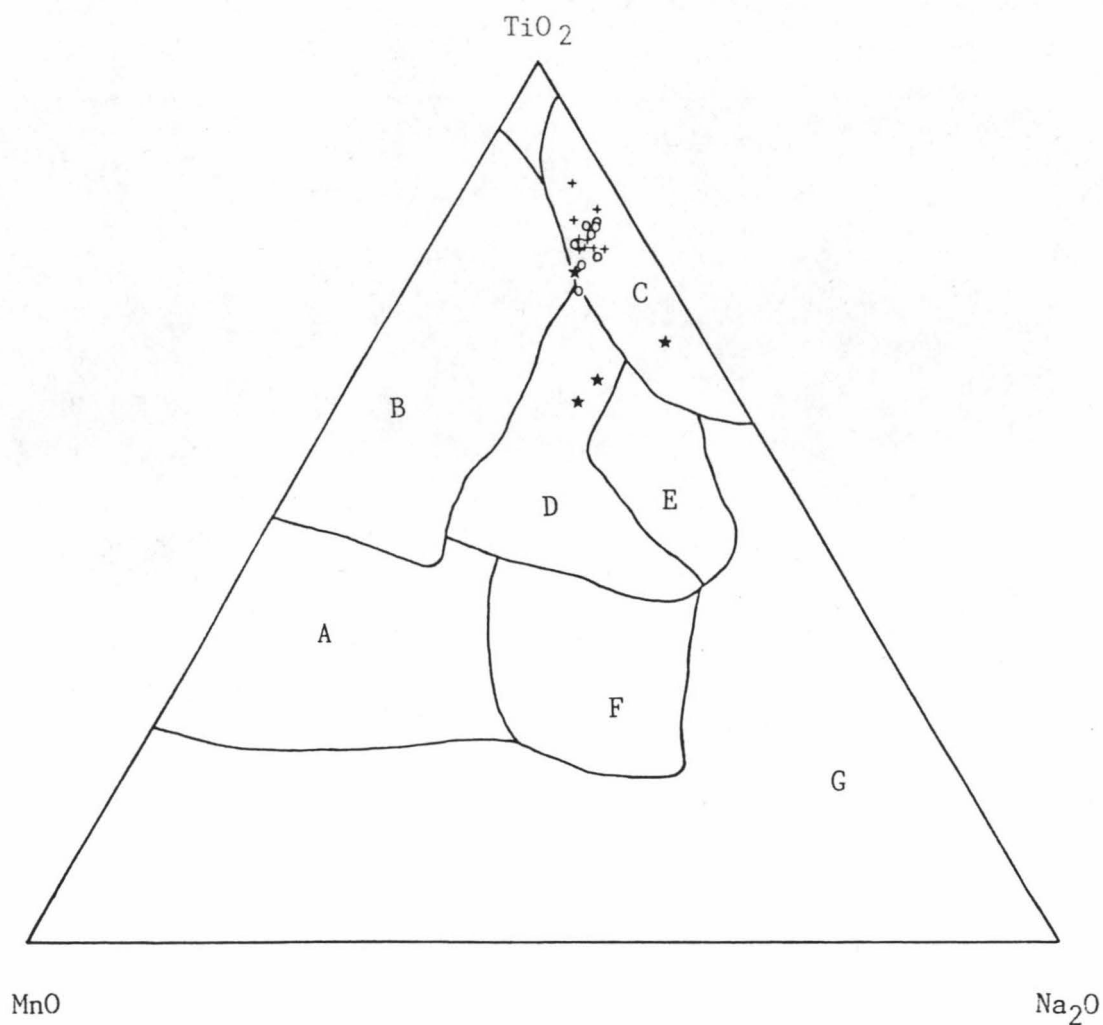


Figure 3-7: TiO_2 - MnO - Na_2O discriminant plot (after Nisbet & Pearce 1977).

Symbols + = 17043

★ = 17058

o = 17062

A' = VAB

B = OFB

C = WPA

D = ALL

E = VAB + WPT + WPA

F = VAB + WPA

G = WPA

thin sections of the red argillite and chert indicate an hemipelagic depositional environment. Coloured claystones occur in a number of marine environments such as at spreading ridges, at seamounts, forming as a result of hydrothermal solutions, or as a result of halmyrolytic degradation of oceanic basalt (Jenkyns & Hardy 1976, Jenkyns 1978). Reed (1957a) considered the coloured argillite at Red Rocks to be in part of tuffaceous origin. Roser (1983) updated the work done by Reed and considered that the coloured argillite to represent a mixture of normal terrigenous sediment (black argillite) and Al-Ti poor sediment from an active spreading ridge. On the basis of geochemical analyses, George (1983) proposed that the red argillite at Island Bay, Wellington, represented a mixture of oceanic basaltic material and pelagic clays. All these workers indicate that coloured argillites are deposited in an hemipelagic environment, with the sediment being affected by volcanic activity, either directly (ie. by degradation of basalt) or indirectly (ie. by input from regions affected by hydrothermal solutions; eg. at spreading ridges).

Chert is considered by Garrison (1974) to be deposited in two ways, either as abyssal radiolarian oozes, unrelated to igneous activity, or as by products of submarine volcanism. During submarine volcanism cherts can form either by precipitation of silica, with silica being supplied from the magma (directly or by leaching of the magma), or by silica which is released during subaqueous volcanism enhancing the productivity and/or preservation of radiolaria (Garrison 1974). Many workers view the cherts within the Torlesse as having formed with close affinity to submarine basalts (Reed 1957a, Bradshaw 1972, Sporli & Bell 1976, Roser 1983).

The limestones, being micrite to sparite with broken allochems and burrow traces, indicate deposition in a marine environment. As these

features can be found in both shallow marine and deep marine environments, the depositional site cannot be further defined.

As seen from Chapter 3.2, the metabasites are considered to have erupted in oceanic environments, forming mid-ocean ridges (eg. Mid-Atlantic ridge) and seamounts (eg. Hawaii). Such settings in modern environments (and by analogy ancient environments) often have associated coloured argillites, chert and limestone deposits eg. Line Island and the East-Pacific Rise (Garrison 1974, Jenkyns 1978). The rocks of the volcanogenic association from the Tararua Range are therefore thought to have been deposited in an oceanic environment, in part related to volcanic seamounts and mid-ocean ridges. This setting is unrelated to the depositional site of the rocks of the sedimentary association.

CHAPTER FOUR

METAMORPHISM

Rocks of the Tararua Range, including those from the field area, exhibit a number of metamorphic minerals, these being: quartz, plagioclase (albite), chlorite, sphene, celadonite, pumpellyite and prehnite. Representative analyses of the metamorphic minerals from greywacke and metabasite are in Table 4-1. Relevant microprobe analyses are given in Appendix VIII.

Quartz

Metamorphic quartz in the study area is found as a vein mineral and as minute polycrystalline aggregates within the matrix of greywacke.

Plagioclase

All plagioclase grains, from both greywacke and metabasite are albite (range from An_{0.2} Ab_{99.2} Or_{0.1} to An_{2.1} Ab_{96.4} Or_{1.5} in metabasite; An_{0.4} Ab_{99.2} Or_{0.4} to An_{1.9} Ab_{97.5} Or_{0.7} in greywacke).

Chlorite

Chlorite is frequently found after detrital biotite and within the matrix of greywacke. In metabasite, chlorite is commonly found as an anomalous blue birefringent coloured fibrous variety replacing clinopyroxene, as complete pseudomorphs after olivine and in the matrix. Vein chlorite is also present.

Sphene

Sphene is most abundant in interstitial areas in metabasite, after iron oxide minerals. Analyses indicate sphene of two compositions one being quite alumina and iron rich, up to 29.9 weight percent Al₂O₃ and 15.1 weight percent Fe₂O₃ (total Fe), with another more "normal" sphene having weight percentage values of 3.0 Al₂O₃ and 5.8 Fe₂O₃. These are more iron rich when compared with sphene from zeolite and actinolite facies schist, Otago (Kawachi *et al.* 1983) although the

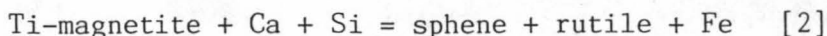
Table 4-1: Representative analyses of metamorphic minerals.

GREYWACKE		METABASITE					
PUMPELLYITE (17014)		SPHENE "normal" Al-Fe (17056) (17056)		CELADONITE (17056)	PUMPELLYITE Al-rich Fe-rich (17062) (17056)		PREHNITE (17058)
SiO ₂	37.37	31.83	43.26	56.58	44.23	39.04	41.98
Al ₂ O ₃	25.25	3.32	5.41	7.84	27.01	19.11	18.84
TiO ₂	0.01	33.04	6.98		0.02	1.20	0.01
FeO ⁺	9.92			14.71	0.94	11.84	
Fe ₂ O ₃ ⁺		2.67	15.06				7.40
MnO	0.37			0.05	0.64	0.09	0.02
MgO	0.05	0.17	6.93	6.40	1.04	2.71	0.01
CaO	23.40	26.68	21.49	0.21	18.39	16.53	25.76
Na ₂ O			0.38		3.11	0.01	0.09
K ₂ O		0.34	0.10	6.40	0.03	0.73	0.01
	-----	-----	-----	-----	-----	-----	-----
Total	96.37	98.05	99.61	92.19	95.41	91.26	94.12

+Total iron as FeO or Fe₂O₃.

Prehnite occurs as a vein mineral within metabasite.

"normal" sphene from this study does have similar compositions (Fig. 4-1a). Possible sphene forming reactions are:



(Offler *et al.* 1981).

Celadonite

Celadonite, bright emerald green in colour is found only within metabasite in close association with chlorite and Fe-rich pumpellyite in amygdules (17056).

Pumpellyite

Pumpellyite occurs as clusters of very fine needles in amygdules and replacing clinopyroxene grains (in metabasite), within the matrix of both metabasite and greywacke and as a vein mineral (17062). Analyses indicate a wide compositional variation in terms of Al and Fe where, FeO (total Fe) weight percent ranges vary from 0.25% (17062) to 11.84% (17059) while Al₂O₃ ranges from 20.56 weight percent (17059) to 29.79 weight percent (17062). Pumpellyites from Prehnite-Pumpellyite Facies rocks from N.S.W, Australia (Offler *et al.* 1981) show similar compositional variations (Fig. 4-1b). It has been suggested by Coombs (1953) and noted by Surdam (1969) that the darker coloured blue-green pumpellyites are characteristically iron-rich, while colourless pale pumpellyites tend to be iron-poor. Pumpellyites from the study area show this relationship.

The compositional range of pumpellyite has been interpreted by some workers to reflect the metamorphic grade of formation; the pumpellyite becomes more Al-rich with increasing metamorphic grade (eg. Kawachi 1975; Evarts & Schiffman 1983). However work by Offler *et al.* (1981) has shown that pumpellyites can have a wide variety of compositions within rocks of the same metamorphic grade. Therefore,

Figure 4-1a: Al - Ti - Fe variation diagram for sphene.



= Field of sphene from zeolite and pumpellyite-actinolite schist, Otago, New Zealand (Kawachi et al. 1983).

● = sphenes from this study

Sphenes from this study show wide compositional variation, with some being much more aluminous and iron rich in comparison with "normal" sphenes and those from Otago, New Zealand (from Kawachi et al. 1983).

Figure 4-1b: Al - Fe - Mg diagram showing compositional variation in pumpellyites.

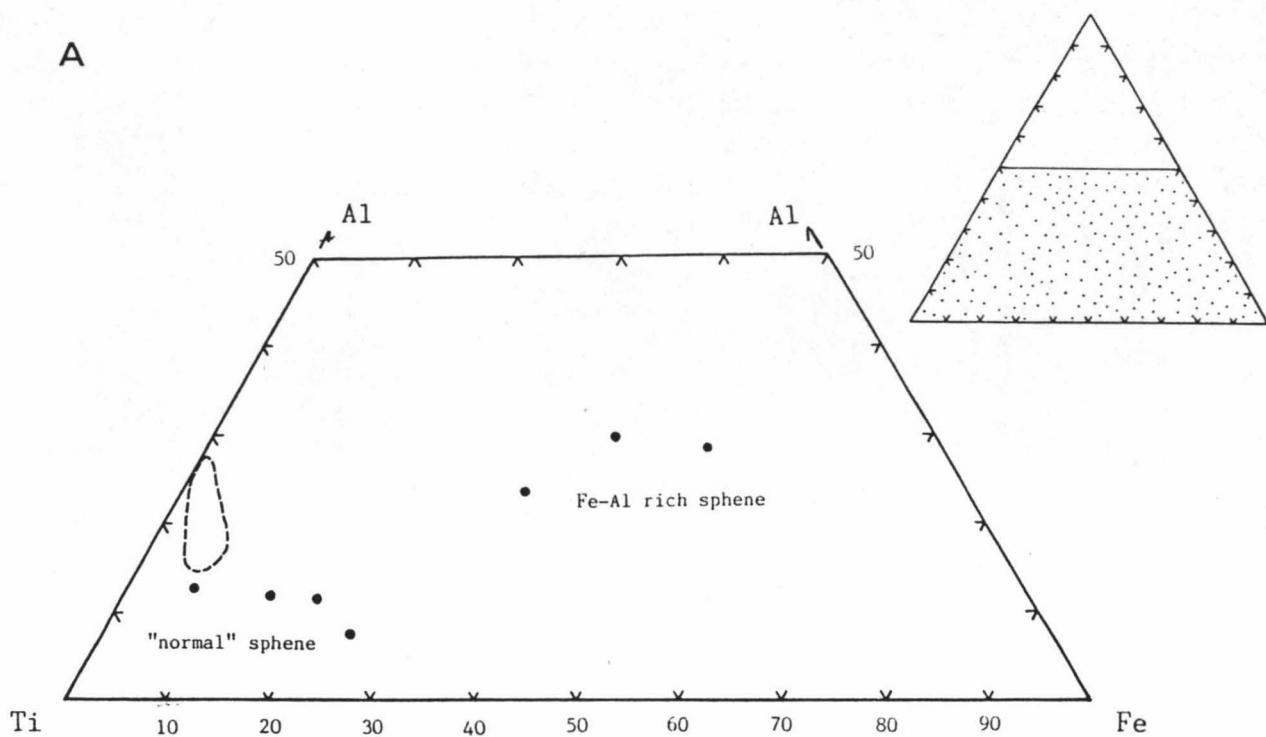
○ = pumpellyites from greywacke

● = pumpellyites from metabasite



= compositional field of pumpellyites from prehnite-pumpellyite facies rocks, N.S.W, Australia (Offler et al. 1981).

Analyses from this study fall within the compositional field of pumpellyites described by Offler et al. (1981).



B

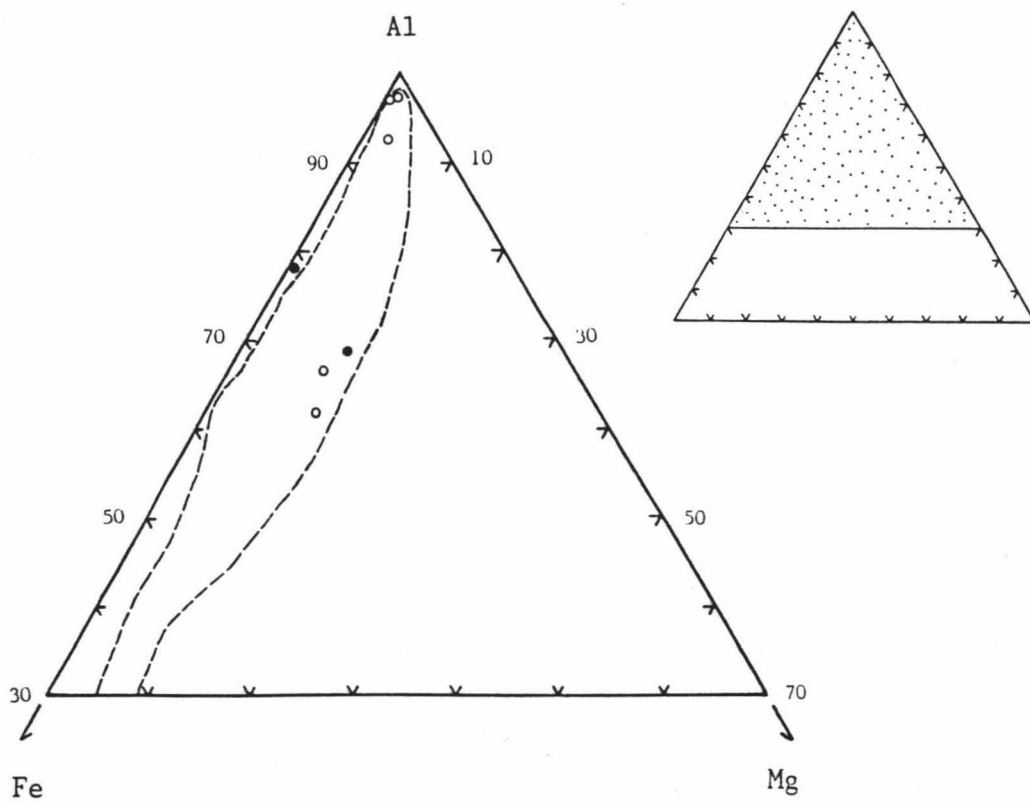


Figure 4-1:

interpretations of metamorphic grade based on Fe and Al composition should be made with caution.

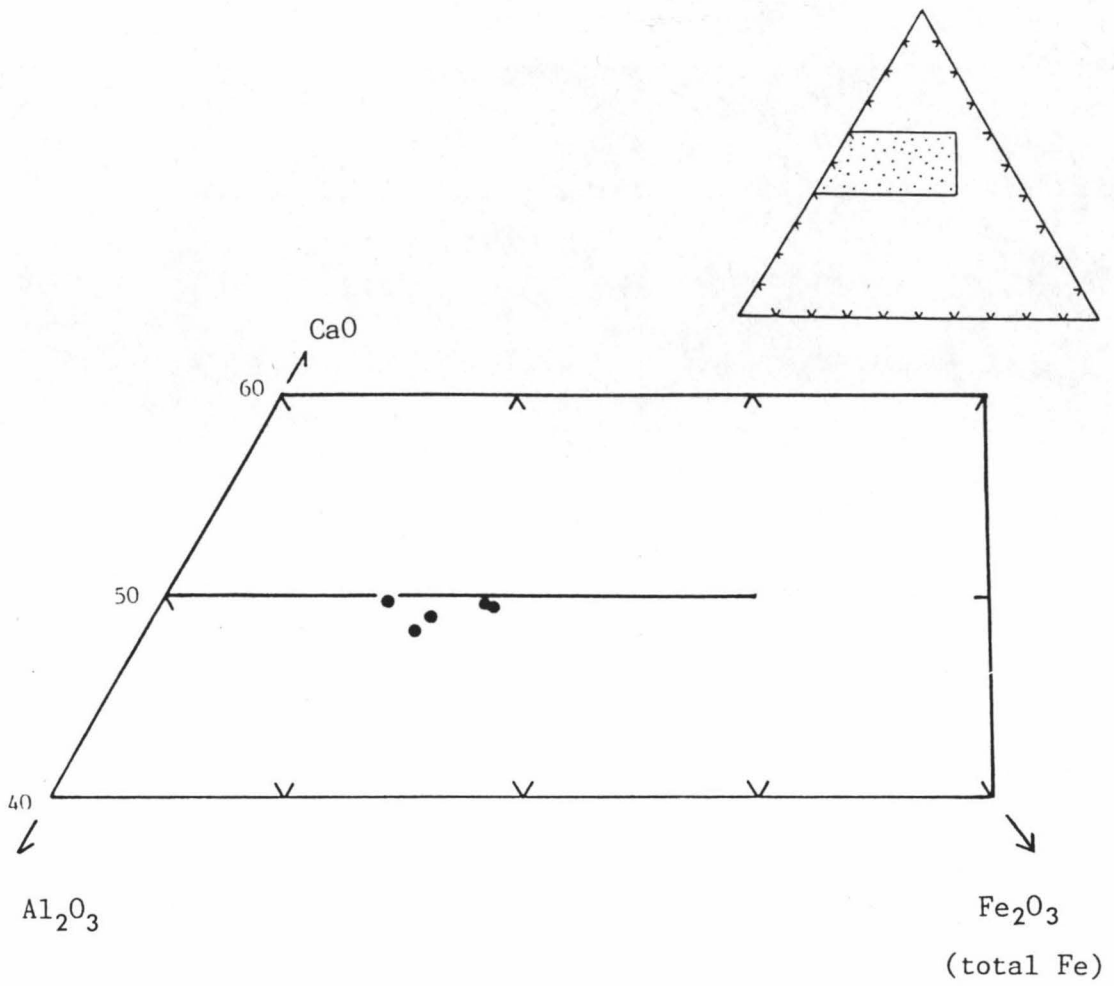
Prehnite

Prehnite occurs as fan-shaped aggregates and large irregular laths (1.3mm by 0.5mm; 17058) within veins. No prehnite was seen within the matrix of either metabasite or greywacke. Grains are colourless to pale yellow colour in thin section, and commonly exhibit undulatory extinction. Prehnite is associated with calcite, quartz and pumpellyite. Analyses show prehnite to be a Fe-rich variety (Fig.4-2), with Fe_2O_3 (total Fe) content ranging from 5.03 to 7.43 weight percent, suggesting appreciable replacement of Al by Fe^{3+} and Fe^{2+} (Surdam 1969)

4.1 VEIN MINERAL ASSEMBLAGES

Veins are generally less than 0.3mm thick but range up to 3 cm in thickness. In greywacke, the most common vein minerals are quartz and calcite. Where generations of mineral growths are evident in veins, quartz is generally the first formed mineral, growing in the characteristic "dog tooth" manner, followed by later calcite mineralization (17102, 17103, 17104). Calcite is commonly found in the centre of veins which suggests that it is the latter mineral to develop. Such veins are often cross-cut by later calcite veining, indicating a number of generations of veining (17104). The mineral assemblage quartz + prehnite is observed in a few veins (17101, 17105), and in sample 17105 is cut by a later quartz vein.

Veins in metabasite have a more varied mineral assemblage with calcite, quartz, chlorite, prehnite and pumpellyite occurring. Veins containing all the above mentioned minerals show a sequence of mineral development, determined by overprinting relationships, where quartz is the first formed, followed by prehnite, pumpellyite and chlorite, and lastly calcite (17106). Vein mineral assemblages seen in metabasite



● = prehnite

— = compositional range of prehnite in the low-grade metavolcanic rocks,
British Columbia (Surdam 1969).

Figure 4-2: CaO - Al₂O₃ - Fe₂O₃ (total iron) variation diagram for prehnite.

are: 1) calcite; 2) quartz; 3) calcite + quartz; 4) calcite + chlorite;
5) calcite + prehnite + pumpellyite; 6) calcite + chlorite + pumpellyite;
7) quartz + calcite + chlorite + pumpellyite + prehnite.

4.2 METAMORPHIC GRADE

In both the metabasite and greywacke the metamorphic mineral assemblages are; 1) chlorite + pumpellyite + calcite; 2) chlorite + pumpellyite; 3) chlorite + pumpellyite + celadonite; as well as those mineral assemblages seen in veins (described above). As both rock types show the same metamorphic minerals, it is reasonable to assume that they have undergone the same metamorphic history.

The metamorphic mineral assemblages seen in the study area are indicative of the Prehnite-Pumpellyite Facies of Coombs (1960) and Winkler (1965).

CHAPTER FIVE

PALEONTOLOGY

Fossil localities within the Torlesse Supergroup in the southern North Island are notably few, being restricted mainly to the eastern portion, around the Wellington and Otaki Forks regions.

In the Wellington region Late Triassic (Oretian-Otamitan) annelids Torlessia and Titahia (Webby 1967; Speden 1976) and the trace fossils Scalarituba (Rowe in prep) have been found, whilst at Otaki Forks, Late Triassic (Warepan) Monotis occur (Grant-Taylor & Waterhouse 1963; Speden 1976; Rattenbury 1983).

No in situ fossils have previously been recorded in the field area, apart from an indentation of ?organic material in ?breccia from the Tauherenikau Valley (N.Z.M.SI 866490; Speden 1976)

5.1 FOSSIL LOCALITIES WITHIN THE STUDY AREA

In this study area, fossils were found within limestone and chert.

Limestone

Limestone, fossiliferous micrite and sparite, contained bryozoa and mussel fragments, foraminifera and echinoid plates (Chapter 3.1.4). These fossils were distinguished in thin-section and no taxonomic identifications could be made.

Chert

In thin-sections of chert from the study area, radiolaria skeletons were commonly observed, often as recrystallized circular to oval shapes, some with well preserved structures visible.

Recent work by Pessagno and Newport (1972) and Feary and Hill (1978) have shown that radiolaria can be successfully extracted from chert. Both groups of workers stressed that unless radiolaria were abundant and have well preserved structures present in thin-section there is very little chance of extracting identifiable radiolaria from the

chert.

Examination of numerous radiolaria chert samples from the study area show an overall tendency for the red-hematite rich cherts to contain the most abundant and better preserved radiolaria in thin-section. Abundant and well preserved radiolaria skeletons were observed in a thin-section of sample 17078, from which radiolaria skeletons were successfully extracted by digesting the sample in hydrofluoric acid (technique outlined below). This same technique was applied to two radiolaria-rich samples from the same outcrop in the Manawatu Gorge (17109, 17110) and three samples from Red Rocks, Wellington. However, only one sample from the Manawatu Gorge yielded radiolaria.

Extraction technique

The extraction technique broadly follows that described by Pessagno and Newport (1972). The method used is outlined below:

- 1) samples were lightly crushed with pestle and mortar,
- 2) sieved through a #10 mesh sieve,
- 3) the coarse fraction was etched in 40% hydrofluoric acid.

Etching time ranged from seven hours to seven days depending on the sample,

- 4) sample thoroughly washed with tap water through a 100 um mesh,
- 5) sample dried in drying cabinet or under heat lamp,
- 6) dried sample put through a #100 mesh sieve, (the plus #100 mesh fraction may be saved for re-etching), then checked for radiolaria skeletons using normal micropaleontological techniques.

Picking of radiolaria from the washed and dried residue was a time consuming process and the amount of sample to be checked was greatly reduced by etching only the coarse fraction from step 2 (thus removing a large amount of fine chert particles), and checking only the #100 um mesh fraction (step 6).

The two sites from which the radiolaria were extracted are described below.

Tararua Range: sample 17078 (S26C/ 0610 1208) is a dark red chert from a horizon of red and pinkish-white coloured chert, that is exposed over 50 metres along a ridge. Chert cropped out as large in situ blocks, some with dimensions of tens of metres. Some portions of the chert were bedded, with beds ranging from 2 cm to 5 cm. Contacts with the surrounding greywacke and argillite were obscured.

Manawatu Gorge: sample 17109 (T24/ 492 949) comes from a very dark red-brown coloured chert from the Manawatu River. The chert appeared to be in a melange zone, although the contact with the surrounding rock types was obscured. The site is possibly the same one as described in Speden (1976).

5.1.1 Radiolaria

Radiolaria have two suborders, Spumellariina and Nassellariina, and to date, most work on Mesozoic radiolaria has been done on the suborder Nassellariina (eg. Pessagno 1977b; Pessagno & Whalen 1982).

In both samples (17078, 17109) over 70% of the observed radiolaria belong to the suborder Spumellariina, these being rounded, spherical to subspherical in shape. At present Mesozoic Spumellariina have not been described in any detail and therefore are of little use. Nassellariina have been described in detail by several workers (eg. Pessagno 1977; Yao 1982) and based on their descriptions Nassellariina (which comprise less than 30% of radiolaria observed) have been identified from the two samples. Systematic descriptions for all identified radiolaria are given below. A large number of specimens for which identifications could not be made are also described. Scanning electron photomicrographs of all these radiolaria can be found at the end of the systematic descriptions in Figures 5-2 to 5-4.

My identifications of these radiolaria have been sent to Mesozoic radiolaria specialists at the U.S.G.S Menlo Park, California for confirmation. A telegram stating "identifications and ages good" was received from B. Murchey on September 14, 1984. A follow up letter has not been received as yet.

Radiolaria assemblages

Sample 17078: (S26/ f14) In sample 17078 radiolaria skeletons are moderately well preserved and a total of five identifications have been made, four at generic level with two different species of one genus.

These identifications are:

Archaeodictyomitra sp. "C"

Archaeodictyomitra sp. "E"

Bagotum sp.

Parvicingula sp. "B"

Stichocapsa sp.

Also a number of unknown specimens (Unknown "A", "B", "C", "E", "F") were found. The genus Bagotum has a range of Lower Jurassic, and the Family Bagotidae has a range in age from Lower Jurassic to Middle Jurassic; based on other radiolaria present in the sample, for which identifications are more confident (Archaeodictyomitra and Parvicingula), a Middle Jurassic age is suggested for the assemblage (Fig. 5-1a).

Sample 17109: (T24/ f25) Sample 17109 contained well preserved radiolaria skeletons, with a total of ten taxa identified. These are:

Archaeodictyomitra sp. "A"

Archaeodictyomitra sp. "B"

Archaeodictyomitra sp. "C"

Archaeodictyomitra sp. "D"

Pseudodictyomitra sp.

Parvicingula sp. "A"

Tricolocapsa sp.

Zhamoidellum sp.

Eucyriidium sp.

Stihocapsa sp.

A number of unidentifiable radiolaria were also found (Unknown "C", "F"). Ranges for each genus is shown in Figure 5-1b, suggesting an age of Late Jurassic (Tithonian) to Early Cretaceous (upper Valanginian; lower Hauterian), for the assemblage.

The radiolaria assemblages from the chert blocks in the the study area and the Manawatu Gorge indicate ages of Middle Jurassic and Late Jurassic to Lower Cretaceous respectively.

5.2 SYSTEMATIC PALEONTOLOGY

Phylum PROTOZOA

Subphylum SARCODINA

Class RETICULARIA

Subclass RADIOLARIA

Order POLCYSTIDA

Suborder NASSELLARIINA

Family ARCHAEODICTYOMITRIDAE Pessagno 1976, emend. Pessagno 1977

Genus ARCHAEODICTYOMITRA Pessagno 1977.

Archaeodictyomitra sp. "A" (Fig. 5-2: 1-6)

Description: Skeleton subconical, with 10-11 costae visible in lateral view. Costae are without constrictions, converge towards the apex and occasionally wedge out. Post-cephalis chambers (all but the final chamber), increase moderately rapidly in width and length, but the final post-cephalis chamber decreases in width. Pore frames are oval. Towards the apex, the pores are arranged in transverse rows, each pore separated by costa; however on some post-cephalis chambers the pores have a diagonal or irregular arrangement.

Range: Middle Jurassic (Middle Bajocian) to Late Cretaceous (Maastrichtian); Pessagno & Whalen 1982.

Archaeodictyomitra sp. "B" (Fig. 5-2: 7-9)

Description: Skeleton is subconical, with a subrounded apex. Ten to eleven costae are visible in lateral view. The initial post-cephalis chambers increase slightly in width, and are then of more or less constant width. Final post-cephalis chamber decreases in width. Costae are without constrictions, some wedging out towards the apical region. Pores are rounded, arranged in transverse rows.

Remarks: Differs from Archaeodictyomitra sp. "A" by having; 1) a larger skeleton; 2) fewer discontinuous costae; 3) pores arranged in transverse rows, not in a diagonal or irregular arrangement.

Range: same as above.

Archaeodictyomitra sp. "C" (Fig. 5-2: 10-12)

Description: Subconical to rectangular in shape, with 10-12 costae visible in lateral view. Circumferential ridges slightly developed, possibly defined by pores being aligned transversely. The pores are rounded to oval.

Remarks: This species differs from Archaeodictyomitra sp. "A" and "B" by having 1) a more rectangular shape; 2) greater size; 3) slight development of circumferential ridges.

Range: same as above.

Archaeodictyomitra sp. "D" (Fig. 5-2: 13)

Description: Skeleton cigar shaped, with eleven costae visible in lateral view. Costae are continuous throughout, converging towards the apical region. Skeleton greatly increases in width from the apex to medial portion, with almost as great a decrease in width from the medial section to the last post-cephalis chamber. Pores are rounded to oval. Pores have a slightly irregular arrangement on the lower post-cephalis chambers, but are otherwise arranged in regular transverse rows between costae.

Remarks: Description is based on a single specimen. This skeleton differs from other species by; 1) having a cigar shape; 2) larger pore size.

Range: same as above.

Archaeodictyomitra sp. "E" (Fig. 5-2: 14)

Description: Apical region subconical, with skeleton having a constant width in the latter post-cephalis chambers. Twelve costae are visible in lateral view. Costae are continuous towards apical region, with slight constrictions which define the development of slight circumferential ridges. Pores are rounded, arranged in at least seven transverse rows.

Remarks: Description is based on a single specimen. Differs from other species by having the development of slight circumferential ridges.

Range: same as above.

Family BAGOTIDAE Pessagno & Whalen 1982

Genus BAGOTUM Pessagno & Whalen 1982

Bagotum sp. (Fig. 5-2: 15)

Description Skeleton ellipsoidal, with nine costae visible in lateral view. Both cephalis and the final post-cephalis chamber are bluntly rounded in shape. Pores are rounded, and aligned in transverse rows, with each pore separated by costae.

Remarks: Skeleton is very poorly preserved.

Range: Lower Jurassic to Middle Jurassic (Family)

Lower Jurassic (Genus); Pessagno & Whalen 1982.

Family EUCYRIDIIDAE Ehrenberg, 1847, emend. Petruskevaskaya 1971

Genus STICHOCAPSA Haeckel 1881.

Stichocapsa sp. (Fig. 5-3: 7-10)

Description: Skeleton consists of an apical section and an inflated subspherical post-cephalis chamber. The shape of the apical region shows considerable variation, from an almost conical shape to a subcylindrical dome shape. Skeleton contains uniformly distributed subspherical pores,

surrounded by hexagonal frames, in transverse rows. The rows are staggered with respect to each other.

Remark: Specimens are poorly preserved.

Range: Jurassic to Middle Cretaceous (Middle Cenomanian); Moore 1973; Foreman 1976; Yao 1980.

Family PARVICINGULIDAE Pessagno 1977.

Genus PARVICINGULA Pessagno 1977.

Parvicingula sp. "A" (Fig. 5-3: 4-5)

Description: Description is based on broken specimens. Contains at least four circumferential ridges. Pore frames are subcircular, arranged in three rows between circumferential ridges. The central row of pore frames are staggered, depressed with respect to those flanking in the outer rows. Pore frames of each outer row abut against circumferential ridges and slope gently toward the centre row. It appears that the circumferential ridges increase in width in the medial portion of the skeleton.

Range: Middle Jurassic (lower Bajocian) to Lower Cretaceous (upper Valanginian; lower Hauterivian?) Pessagno & Whalen 1982.

Parvicingula sp. "B" (Fig. 5-3: 6)

Description: Description, the same as for Parvicingula sp. "A" except that the pores are larger and have well developed hexagonal pore frames.

Range: same as above.

Family ~~PSEUDODICTYOMITRIDAE~~ Pessagno 1977

Genus Pseudodictyomitra Pessagno 1977

Pseudodictyomitra sp. (Fig. 5-2: 16)

Description: Skeleton conical, consisting of ten segments. Each segment is separated by circumferential strictures. The cephalis, thorax and abdomen are separated by single rows of pores, as are all but two of the post-abdominal chambers (between post-cephalis chambers six, seven and eight). The cephalis and thorax are smooth. On the abdomen, costae are weakly developed, but reasonably well developed on the post-abdomen chambers. Costae are discontinuous, slightly rounded in the medial portion and do not traverse the strictures.

Remarks: Identification has been based on a single specimen.

Range: Middle/Late Tithonian to Middle Turonian; Pessagno 1977.

Family WILLIERIEDELLIDAE Dumitrica 1970

Genus Zhamoidellum Dumitrica 1970

Zhamoidellum sp. (Fig. 5-3: 12-13)

Description: Subspherical cephalis and a greatly inflated spherical post-cephalis chamber. Both cephalis and post-cephalis chamber have small rounded pores arranged in regular tranverse rows. Between pore rows, small nodes or humps occurring randomly give giving the skeleton a knobbly appearance.

Remarks: Specimen is poorly preserved and the small nodes could be a function of preservation, rather than the original structure.

Range: ?Jurassic-Early Cretaceous (?Barremain); Foreman 1975.

CYRTOIDEA INCERTAE SEDIS

Genus TRICOLOCAPSA Haeckel 1881

Tricolocapsa sp. (Fig. 5-3: 1-3)

Description: Skeleton has dome shaped, bluntly rounded cephalis, with a greatly inflated subspherical post-cephalis chamber. Pores are present on both the cephalis and post-cephalis chamber. The pores are rounded, surrounded by a network of regular hexagonal frames in transverse rows. The rows are staggered resulting in a diagonal arrangement of the pores.

Range: ?Late Triassic-?Late Cretaceous; Yao 1979, De Wever et al. 1979.

Genus EUCRYTIDIUM Ehrenberg 1847

Eucrytidium sp. (Fig. 5-3: 11)

Description: Skeleton portion subspherical, consisting of eight costae visible in lateral view, costae without constrictions. With the exception of two ill defined pores, the skeleton is poreless.

Remarks: Description is based on a fragment of a skeleton.

Range: Jurassic to Recent; Pessagno 1977b.

RADIOLARIA INCERTAE SEDIS

UNKNOWN "A" (fig. 5-4: 1-4)

Description: Skeleton subspherical with small open circular aperture. Pores are rounded, surrounded by hexagonal pore frames, arranged in staggered rows. Hexagonal frame is not very well developed in some specimens.

UNKNOWN "B" (Fig. 5-4: 5)

Description: Skeleton multicrytoid with a post-cephalis chamber being greatly inflated. Two short horns protrude from the cephalis. Pores are subrounded, ill defined, set in hexagonal pore frames rows of which are

staggered with respect to each other.

UNKNOWN "C" (Fig. 5-4: 6)

Description: Very poorly preserved specimen however the original skeleton shape can be seen. Skeleton has a subconical to rounded apex that greatly increases in width towards the medial section. Basal portion from medial section decreasing in width, giving skeleton an ellipsoidal shape. Possibly a slight development of circumferential ridges.

UNKNOWN "D" (Fig. 5-4: 7-9)

Description : Skeleton subrounded to ellipsoidal. Both cephalis and post-cephalis chamber have an irregular distribution of medium size rounded pores.

UNKNOWN "E" (Fig. 5-4: 10-11)

Description: Portion of broken skeleton containing a horn.

UNKNOWN "F" (Fig. 5-4: 12)

Description: Very poorly preserved; apex conical to subconical, increasing in width towards medial section. Medial section greatly inflated. Basal portion of skeleton has a downward pointing subconical shape.

Figure 5-2:

- 1) Archaeodictyomitra sp. "A" x284 17109
- 2) Archaeodictyomitra sp. "A" x368 17109
- 3) Archaeodictyomitra sp. "A" x352 17109
- 4) Archaeodictyomitra sp. "A" x352 17109
- 5) Archaeodictyomitra sp. "A" x323 17109
- 6) Archaeodictyomitra sp. "A" x249 17109
- 7) Archaeodictyomitra sp. "B" x260 17109
- 8) Archaeodictyomitra sp. "B" x239 17109
- 9) Archaeodictyomitra sp. "B" x218 17109
- 10) Archaeodictyomitra sp. "C" x284 17078
- 11) Archaeodictyomitra sp. "C" x228 17109
- 12) Archaeodictyomitra sp. "C" x210 17078
- 13) Archaeodictyomitra sp. "D" x368 17109
- 14) Archaeodictyomitra sp. "E" x284 17078
- 15) Bagotum sp. x284 17078
- 16) Pseudodictyomitra sp. x210 17109



1



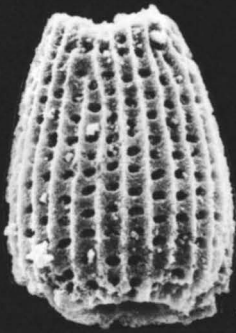
2



3



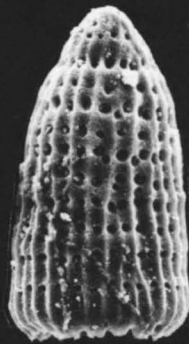
4



5



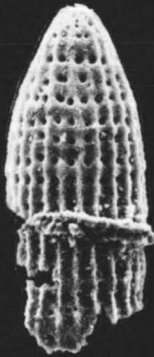
6



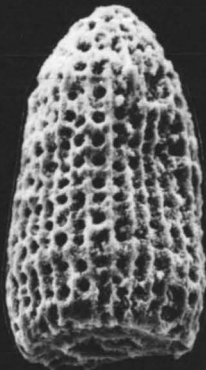
7



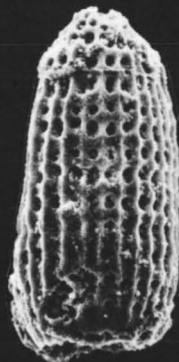
8



9



10



11



12



13



14



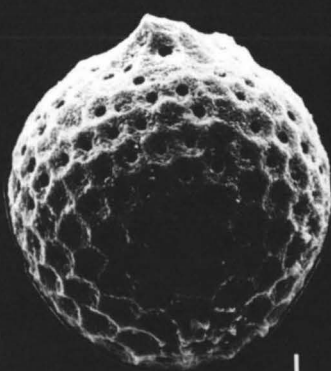
15



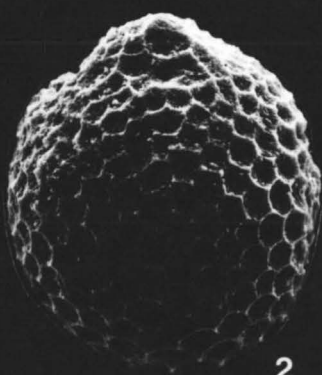
16

Figure 5-3:

- 1) Tricolocapsa sp. x476 17109
- 2) Tricolocapsa sp. x384 17109
- 3) Tricolocapsa sp. x543 17109
- 4) Parvingula sp. "A" x337 17109
- 5) Parvingula sp. "A" x438 17109
- 6) Parvingula sp. "B" x384 17078
- 7) Stichocapsa sp. x476 17078
- 8) Stichocapsa sp. x567 17109
- 9) Stichocapsa sp. x459 17078
- 10) Stichocapsa sp. x384 17078
- 11) Eucrytium sp. x543 17109
- 12) Zhamoidellum sp. x522 17109
- 13) Zhamoidellum sp. x620 17109



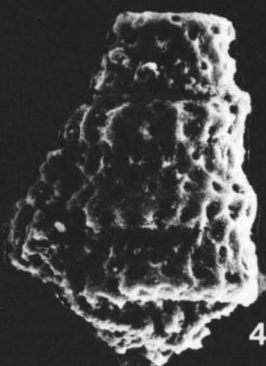
1



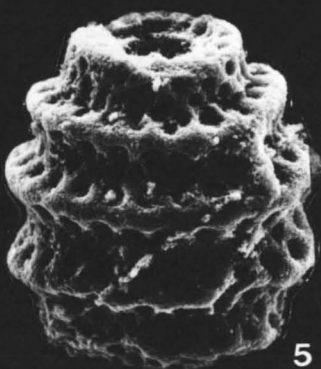
2



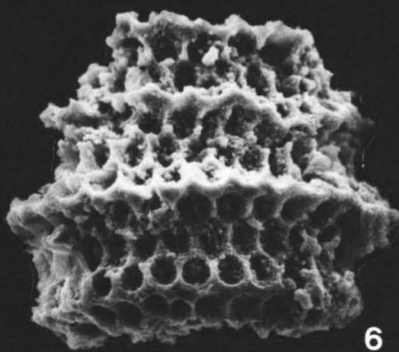
3



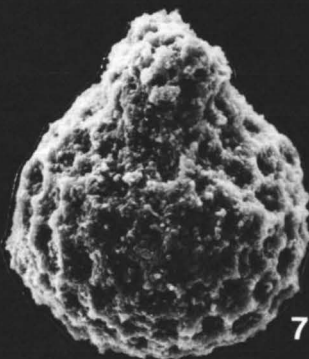
4



5



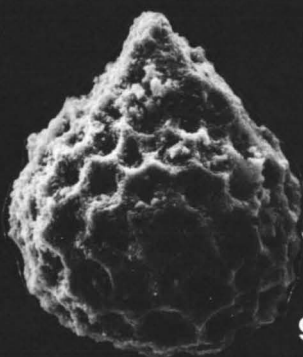
6



7



8



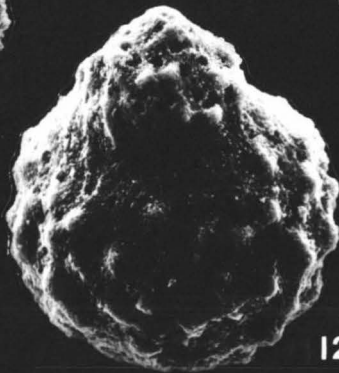
9



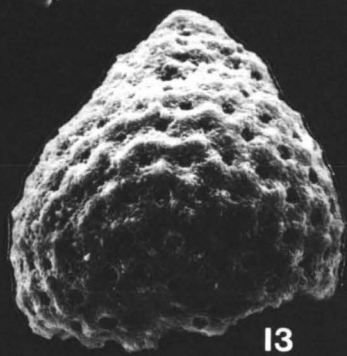
10



11



12



13

Figure 5-4:

- 1) Unknown "A" x438 17078
- 2) Unknown "A" x476 17078
- 3) Unknown "A" x352 17078
- 4) Unknown "A" x368 17109
- 5) Unknown "B" x459 17078
- 6) Unknown "C" x284 17078
- 7) Unknown "D" x297 17109
- 8) Unknown "D" x384 17109
- 9) Unknown "D" x401 17109
- 10) Unknown "E" x272 17078
- 11) Unknown "E" x384 17078
- 12) Unknown "F" x184 17078



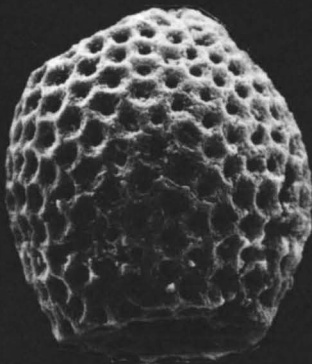
1



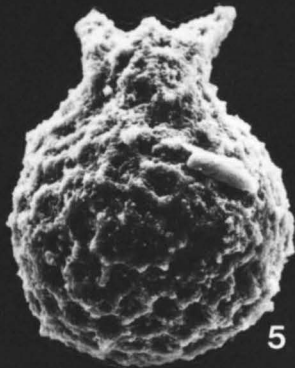
2



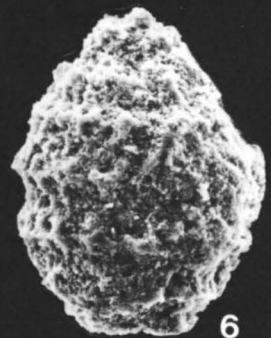
3



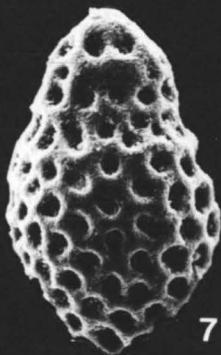
4



5



6



7



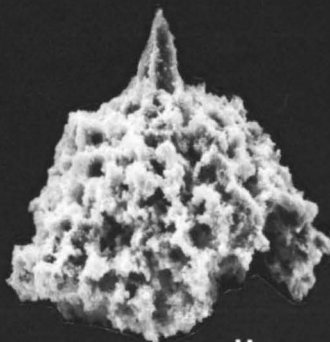
8



9



10



11



12

CHAPTER SIX

STRUCTURE

The aim of this chapter is to describe the deformation seen within the study area, to outline the possible sequence of deformation that the rocks have undergone, and to relate this sequence to deformation described in other regions of the Torlesse Supergroup.

Initially, mesoscopic structures (those which can be observed in outcrop) are described, and this is followed by a description of the macroscopic structures in the area, determined mainly by geometric analysis.

6.1 MESOSCOPIC STRUCTURES

Mesoscopic structures observed in outcrop are folds, shear foliation, faults and melange.

6.1.1 Folds

Folds are observed only in the eastern portion of the study area, cropping out within the lower Tauherenikau River and within melange in the Waiohine River. From field observations and overprinting relationships, there are at least three generations of folding within the study area.

The three different fold events can be inferred from observations within the melange:

- 1) a radiolarian chert block within the melange shows an early fold being refolded (Fig. 6-1a: first and second fold generations). These folds must have developed prior to the block being incorporated into the melange.

- 2) the melange has been folded (Fig. 6-1b: third fold generation).

Other folds observed within blocks in the melange can be ascribed to have formed prior to the third fold event. Hobbs et al. (1976) outlined how different fold events can produce similar fold styles, although in general, they noted that folds with the same style can often be assigned

Figure 6-1a: Light green radiolaria rich chert (17098) showing an isoclinal fold being refolded. Chert occurs as a block within melange and is surrounded by sheared argillite. Waiohine River S26D/ 1130 1710, compass 7 cm in diameter.

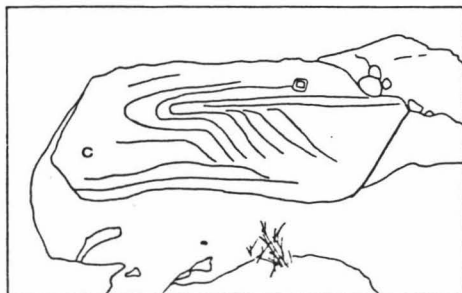
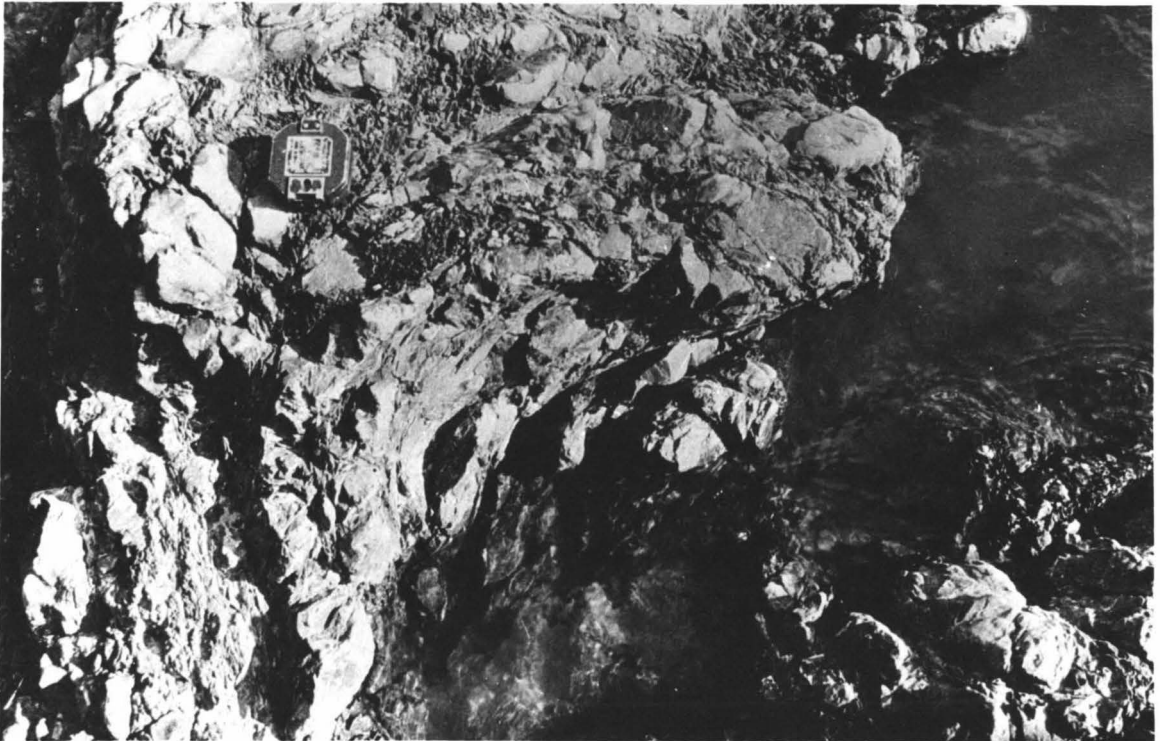


Figure 6-1b: Folded melange; with the fold defined by folded phacoids (P), lenses (L) and shear foliation. Waiohine River S26D/ 1126 1700, compass 7 cm in diameter.





to the same fold generation. Therefore, the folds in blocks within the melange which cannot definitely be attributed to either the first or second fold event (from overprinting relationships) have been grouped into the first fold event on the basis of their style. Based on structural relationships, folds observed elsewhere in the field area can be attributed to have formed during the third fold event.

Folds produced during the first fold event occur as single folds within blocks in melange (Fig. 6-2a). They are isoclinal to close (terminology of Fleuty 1964), and have angular hinges with some thickening in the hinge region and thinning in the limbs.

The second fold event produced a gentle fold. This generation is observed only in a single outcrop, where the limbs of the isoclinally folded chert have been refolded into a gentle fold (Fig. 6-1a). The fold is similar to those produced during the first fold event, being thicker in the hinge region although the hinge region is rounded.

The third fold event produced close to open folds, with these folds being defined by deformation of the melange and in isolated greywacke-argillite outcrops.

6.1.2 Shear Foliation

Throughout the field area, shearing is evident within argillite, producing a shear foliation. Shear foliation is defined by subparallel to anastomosing, discrete, shear fracture surfaces which have a scaly appearance in outcrop (Fig. 6-2b). In alternating greywacke and argillite sequences, the shear foliation is parallel or subparallel to bedding. Where argillite is the dominant rock type or matrix material, shear foliation is often the dominant mesoscopic structure present.

In thin section the shear foliation is defined by a concentration of darker and opaque minerals associated with the shear fracture surfaces. The concentration of darker minerals can be seen anastomosing

Figure 6-2a: A folded sandstone block within melange. The fold is close, defined by laminations in the fine-grained sandstone. Later faults (F) have displaced the block. Waiohine River S26D/ 1126 1702, compass 7 cm in diameter.

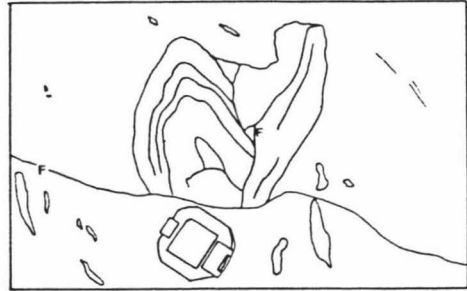
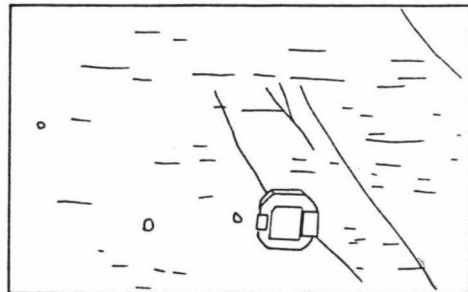
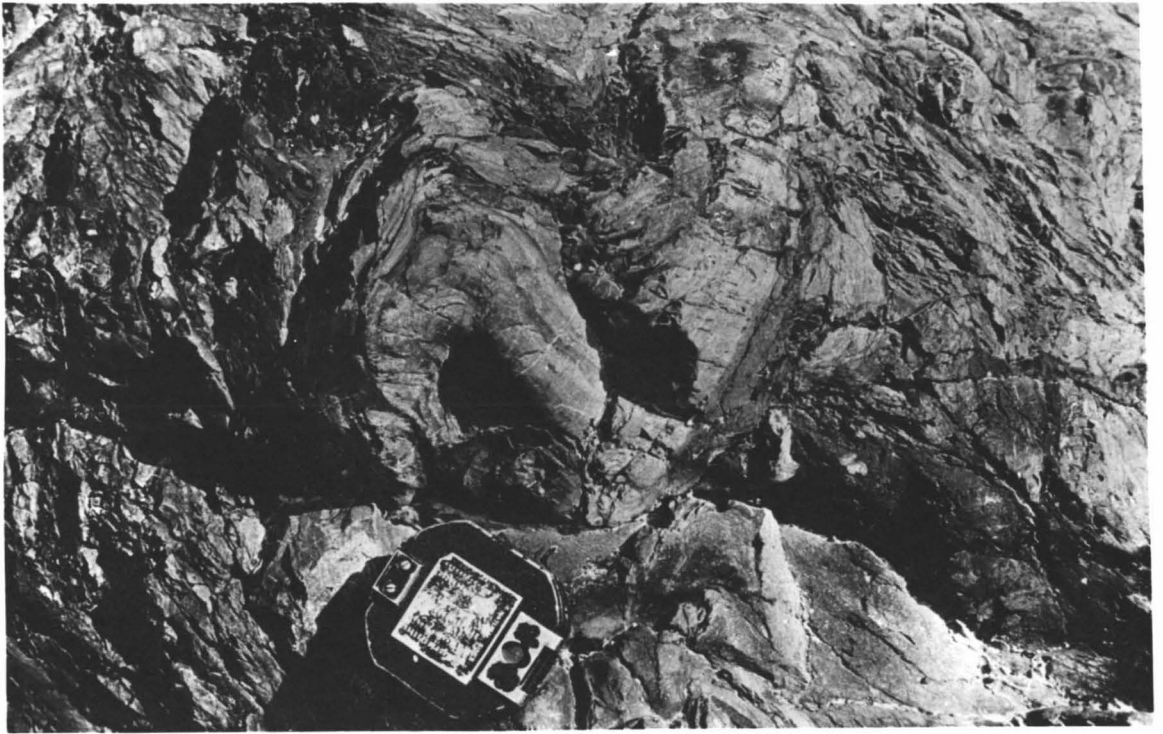


Figure 6-2b: Massive argillite with well developed shear foliation giving the outcrop a scaly appearance. Waiohine River S26D/ 1126 1695, compass 7 cm in diameter.





on the microscale. There appears to be no new mineral growth nor alignment of minerals associated with the development of shear foliation.

Similar shear surfaces have been described from the Esk Head Melange, South Island (shear fabric of Botsford, 1983) and the Franciscan Complex in California (D1 foliations of Cowan 1978; shear foliation of Korsch 1982).

6.1.3 Low-angle Faults

Faults at a low angle to bedding are common. They displace units parallel to bedding or at a low angle to the bedding plane, resulting in the anastomosing appearance and wedging in and out of beds (Fig. 6-3b). The surfaces of the fault planes are often smooth and polished in appearance, some of which have been the site of quartz and calcite mineral deposition. Later veins of these minerals are also found cross-cutting the fault planes at various angles.

Low-angle faults cut, and are cut by, shear foliation. The amount of movement along fault planes is hard to determine, but ranges from millimetres to larger than metres. Often, the wedging effect of beds makes the correlation of individual beds across some faults difficult.

6.1.4 High-angle Faults

Faults at a high angle to bedding are frequent. The high-angle faults often cut across bedding, shear foliation and low-angle faults. The fault planes are usually very sharp and hence are well defined, although, in some places, a small gouge zone of fine clays occurs.

These faults can define "packets" of beds, with beds on either side of the fault plane being slightly reorientated or rotated (Fig. 6-3a). Displacements along faults vary from millimetres to metres, and even to beyond outcrop scale. The occurrence of high angle faults outlining "packets" of beds are common on both the mesoscopic and microscopic scale. Both sinistral and dextral sense of displacement were

Figure 6-3a: High-angle to bedding faults (F) which are defining "packets" of beds. The "packets" of beds have slightly different orientations relative to each other giving the outcrop a "folded" appearance.

Waiohine Gorge Road S26D/ 1197 1783,
geological hammer 31 cm long.

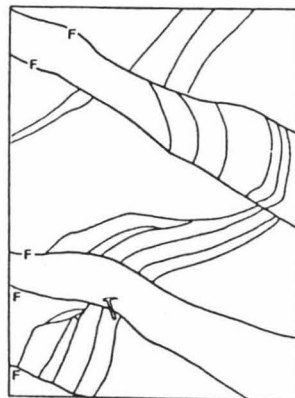
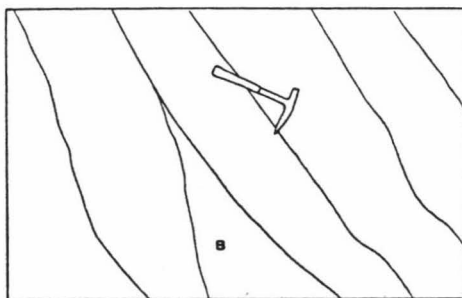


Figure 6-3b: Wedging of sandstone bed (B) caused by low-angle to bedding faults.

State Highway 2 S27A/ 0244 0559,
geological hammer is 31 cm long.





observed.

At some places, a high-angle fault is displaced by later faulting of the same style, inferring that either this fault type occurred over a period of time, or that there were at least two separate generations of high-angle faults.

6.1.5. Lozenges

Lozenges of greywacke occur within the field area, having a rhombic form sometimes with rounded corners. Lozenges are produced by the faulting, or jointing of beds, with each fault bounded segment of the bed being offset in relation to other segments, with slip occurring along the fault plane (Rast 1956). Figure 6-4 shows a cartoon interpretation of the development of lozenges. Initially the beds show a "kinked" outline (Fig. 6-5) and with increased displacement along the fault plane the segments can become completely separated from each other. Lozenges are frequently seen within melange in the study area and elsewhere (eg. Franciscan Complex, California; Korsch 1982).

6.1.6 Melange

The word melange is used here as a non-genetic descriptive term which describes mappable, internally fragmented and mixed rock bodies that contain a variety of inclusions, commonly in a pervasively-deformed matrix (after Silver & Beutner 1980). Thus melange can be used to describe any chaotic, mixed rocks.

Within the field area, melange is recognized at a number of localities. Within these melanges, there is a large variety in the shape, size and rock types of the inclusions. Inclusions range in size from millimetres to metres, while their shape varies in form from phacoids, lenses, lozenges, blocks and ellipsoids. The inclusions have sheared margins in contact with the surrounding melange matrix and irrespective of their shape are usually elongate with their long axis subparallel to

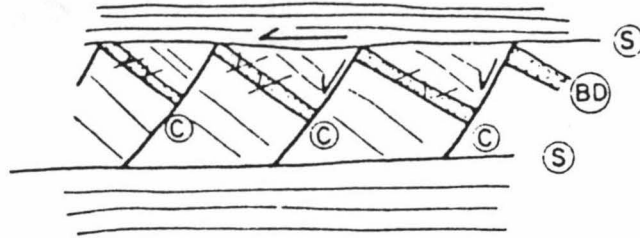


Figure 6-4: Cartoon interpretation of the development of lozenges

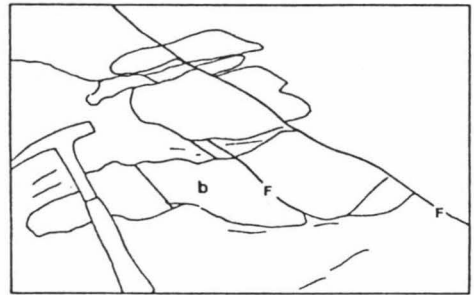
Lozenge shear fabric.

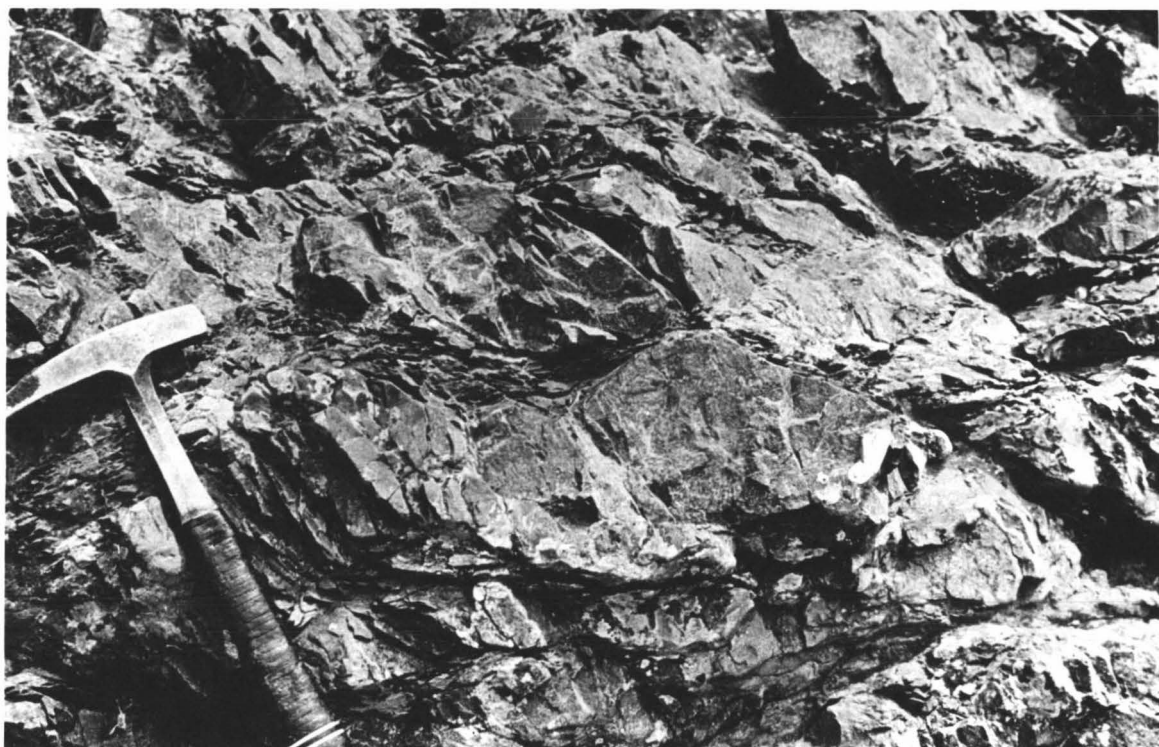
BD = bedding;

C = conjugate fault (dominant);

S = bedding shear.

Figure 6-5: Bed (B) in melange showing a "kinked" outline due to displacements along fault planes (F). This bed shows the beginning of lozenge development. Waiohine River S26D/ 1135 1719, geological hammer 31 cm long.





the shear foliation within the matrix (Fig. 6-6).

The most common forms of inclusions are lenses and phacioids where lenses occur up to metres in length and only centimetres in width, while phacioids are shorter, more squat in comparison with lenses and often have tapering ends. Lenses are commonly greywacke and calcareous siltstone, and bedding within these rock types is generally parallel to the long axis of the lenses, although in some lenses the bedding is at an angle to the long axis of the lenses.

Most of the largest inclusions are blocky (angular) and are often fractured. Bedding is often preserved intact within the greywacke and chert blocks. Lozenges (Rast 1956) have rhombic forms, although sometimes with rounded corners. Ellipsoids are roughly ellipsoidal in plan with their surfaces being slightly scalloped and frequently covered with fine scaly argillite and are present in the more argillite-matrix dominated sections of melange. These forms have been described as oblate ellipsoids by Cowan (1978).

Melange matrix

The melange matrix is sheared argillite, similar to the matrix of melanges described from the Franciscan Complex of California by Hsu (1968) and Cowan (1974) and from the Esk Head Melange (Botsford 1983). Weathering commonly emphasizes discrete shear planes. Contacts between the matrix and the inclusions are sharp and well defined. In melange at Waiohine River (S26D/ 1130 1710) where the inclusions have irregular margins the shear foliation in the matrix envelops, flows and swirls around the inclusions (Fig. 6-7). In some places, shear foliation cross cuts and is cut by faults both at a low-angle to bedding and at a high-angle to bedding.

Types of inclusions

Within melange all the rock types observed within the study area

Figure 6-6a: Melange. Note that the inclusions are generally elongate with their long axis subparallel to the shear foliation within the matrix.

Inclusion (I) contains beds at an angle to the dominant shear foliation.

Waiohine River S26D/ 1133 1716,
compass 7 cm in diameter.

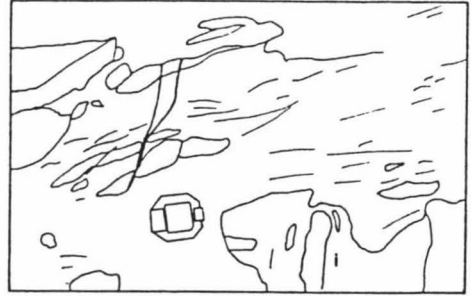
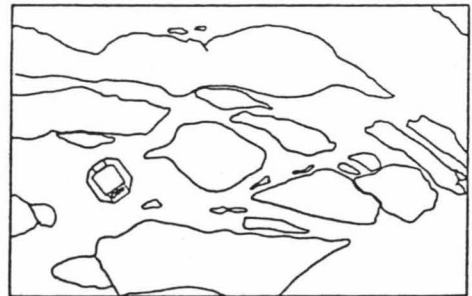


Figure 6-6b: Melange. Inclusions are predominantly greywacke, surrounded by a pervasively sheared matrix of argillite.

Contacts between inclusions and the matrix are sheared.

Waiohine River S26D/ 1133 1716,
compass 7 cm in diameter.



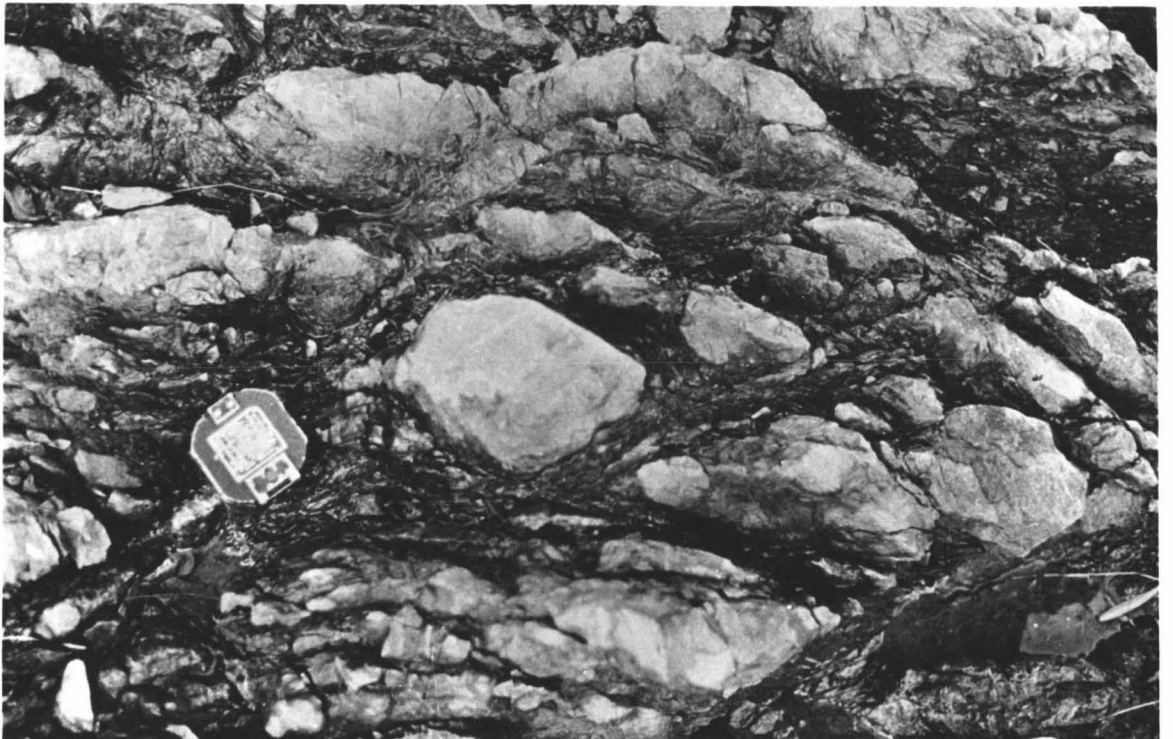
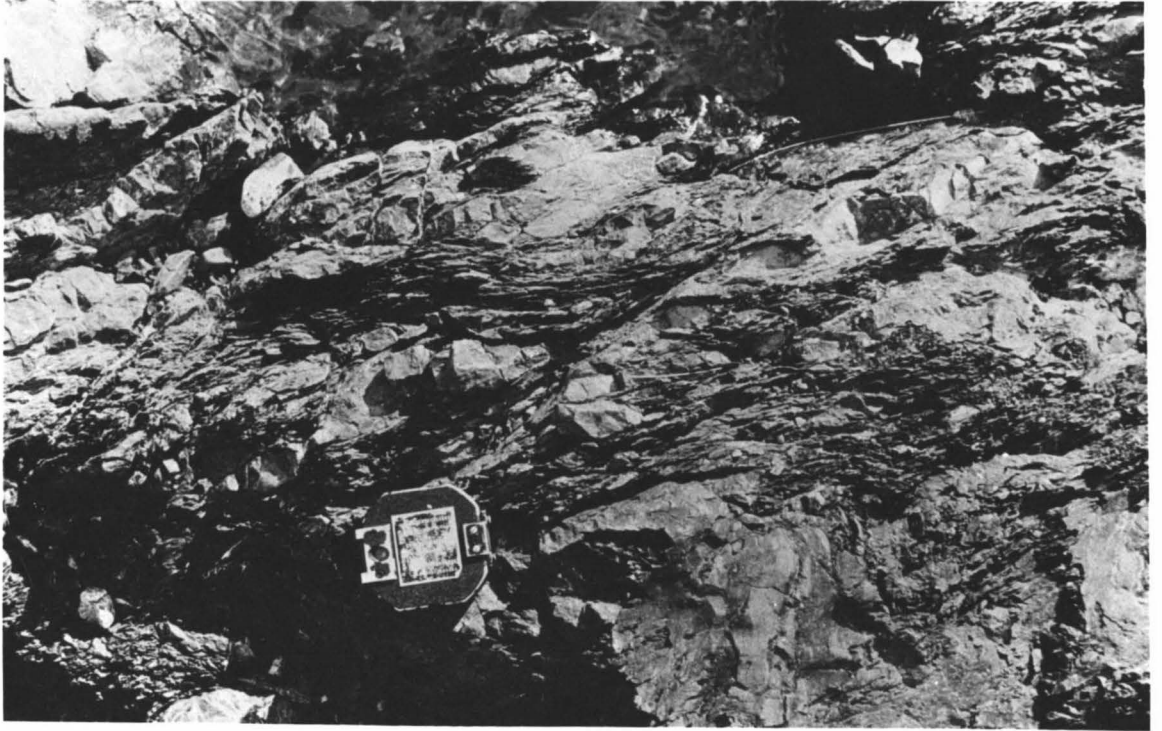


Figure 6-7a: Large chert block in melange, surrounded by a sheared argillite matrix. The chert block is elongate subparallel to the dominant shear foliation within the matrix. Figure 6-7b shows the contact between the chert and matrix in box B. Waiohine River S26D/ 1128 1704, geological hammer 31 cm long.

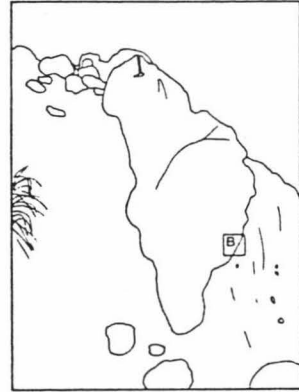
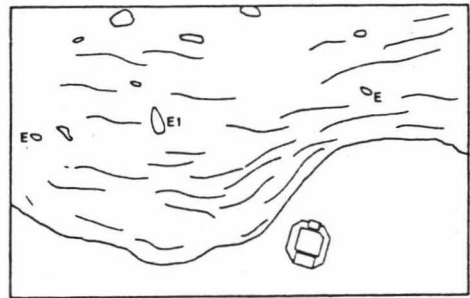
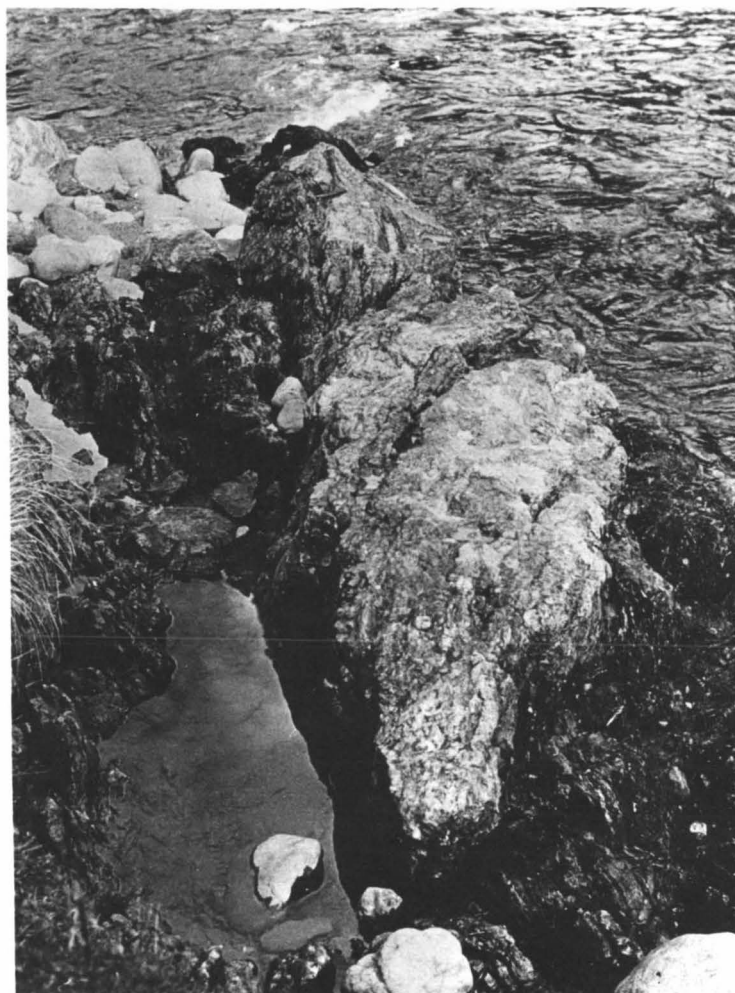


Figure 6-7b: Contact between the chert block and melange matrix. The shear foliation in the matrix flows around the irregular boundary of the chert block. Ellipsoids (E) occur, surrounded by matrix, most of which are elongate subparallel to the shear foliation. Note that ellipsoid (E1) is orientated almost perpendicular to the dominant shear foliation. Waiohine River S26D/ 1128 1704, compass 7 cm in diameter.





are present. The inclusions in order of decreasing abundance are: greywacke, argillite, calcareous siltstone, chert, metabasite, red argillite and limestone. However, individual rock types can be of more local importance within particular regions of melange ie. region dominated by chert and metabasite rather than greywacke.

Saleeby (1979) noted that in some regions of the Kaweah serpentinite melange, California, inclusions of similar rock types were clustered together. Although his melange is on a much larger scale than any melanges seen in the study area, I believe that the comparison is still valid. This clustering of similar rock types is pronounced only within the melange at Waiohine River where one section of the melange is dominated by greywacke inclusions, while another section contains abundant chert, metabasite and only minor greywacke inclusions.

The variation in rock types present as inclusions appears to be related to the amount of deformation present within melange. The more highly deformed sections contain more varied inclusion lithologies, whereas the least deformed sections are dominated by greywacke inclusions.

6.2 MESOSCOPIC DEFORMATION EVENTS

In attempting to define the relative timing of deformational events within basement rocks of the Tararua Range, the melange is an important unit because mesoscopic structures observed elsewhere can be correlated with structures within the melange. Within the melange at the Waiohine River (S26 / 1130 1710) most structures observed elsewhere in the study area are present and therefore the timing of structural events relative to the stages of melange formation can be inferred for the whole area. Mesoscopic structures can be separated into those that developed prior to the formation of the melange, those that developed during the melange formation and those that formed after the melange had developed

6.2.1 Pre-melange structure

Within melange, any deformation that occurred prior to the formation of the melange is recorded in the now discrete inclusions surrounded by melange matrix. At least two generations of folds are observed in the chert and greywacke blocks. The first generation folds are isoclinal and the limbs of these folds have been refolded during a second period of folding which have an open to gentle fold style (evident from a chert block; the folds have been described in chapter 6.1.1).

The initial deformations recorded in the study area are therefore shortening events represented by at least two periods of folding (ie. D1 and D2).

6.2.2 Structures produced during melange formation

Melange formation has been caused by the disruption and chaotic mixing of various rock types. During the formation of melange in the study area, faulting at both a low-angle to bedding and at a high-angle to bedding has occurred to such an extent that a chaotically disrupted unit was produced. Shear foliation has developed in response to the faulting and shearing.

The disruption produced by these structures is considered to be an ongoing process, with these structures forming concurrently and also alternatively with numerous episodes of faulting and development of shear foliation. Similar structures throughout the rest of the field area were most likely produced during the same deformational episode, although the deformation was intense enough to produce melange only in a few areas. Faulting at a low-angle to bedding in well-bedded alternating greywacke and argillite sequences represent the same deformation as seen in melange.

The type of strain or deformation which has formed the melange can be inferred quantitatively from the shape of the inclusions. The form of

most of the inclusions can be related to fracturing and faulting (that is, a rhombic shape) suggesting a shortening deformation while other inclusions, the ellipsoids can be produced during a flattening deformation. Detailed work on strain experienced by ellipsoids has been outlined by Flinn (1962) where he defined the parameter K for describing the shapes of ellipsoids, where $K=(a-1)/(b-1)$, and "a" is the ratio of the major to intermediate axes and "b" is the ratio of the intermediate to minor axes of the strain ellipsoid. A number of ellipsoidal inclusions were collected from the field area, measured and plotted on a Flinn diagram (Fig. 6-8). Most of the measurements fall within the region defined by the parameter of Flinn where $0 < K < 1$. Such a parameter defines a flattening type of strain. As the ellipsoids are predominantly aligned parallel to the shear foliation in the matrix, they have probably been shortened normal to, and extended parallel, to the shear foliation. Similar deformation and structures have been described by Cowan (1978) and Korsch (1982) for melange from the Franciscan Complex, California.

In the study area features of melange such as the disruption and mixing of rocks being related to faulting, suggest that the melange has been formed by deformation that is tectonic in origin, rather than forming due to sedimentary processes as has been proposed for some melanges (eg. Gucwa 1975). Melange from the study area is very similar to other melanges formed by tectonic deformation such as the Franciscan Complex, California described by Aalto (1981) and Korsch (1982).

6.2.3 Post-melange structure

Post-melange deformation in the study area has occurred because the melange fabric at the Waiohine River locality (S26D/ 1126 1700) has been folded. This deformation obviously occurred after formation of the melange because elongate lenses, phacoids and shear foliation of melange fabric are folded into close to open folds (described in chapter 6.1.1).

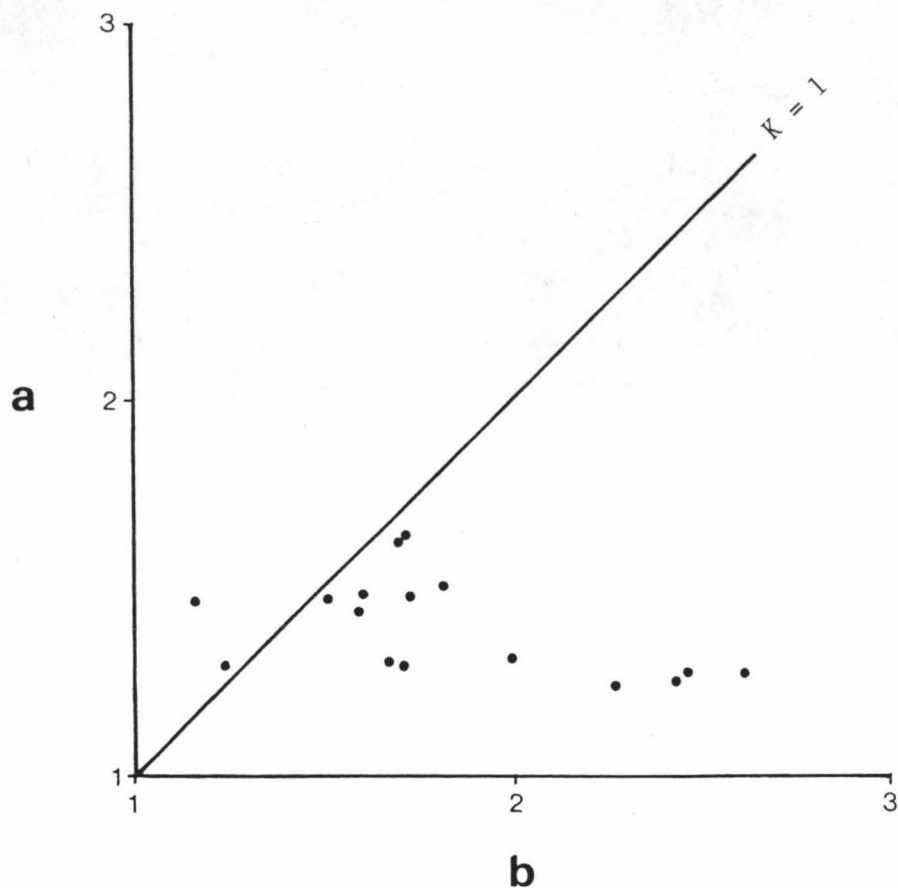


Figure 6-8: Flinn diagram showing the strain experienced by ellipsoids.

Most of the measurements fall within the region defined by the parameter $0 < K < 1$. This defines a "flattening" type of strain.

$$a = \frac{\text{major axes}}{\text{intermediate axes}}$$

$$b = \frac{\text{intermediate axes}}{\text{minor axes}}$$

6.3 MACROSCOPIC STRUCTURES

The monotonous nature of the greywacke and argillite beds and the paucity of facing evidence, coupled with the lack of marker beds in the Tararua Range, hinders the definition of macroscopic structures in the study area. The beds strike predominantly to the north-northeast and dip steeply either to the west-northwest or east-southeast.

In one region, S26 / 0695 1095, two macroscopic folds can be inferred from changes in the attitude of beds with younging direction. These folds will be discussed later.

Using the lithological associations defined in Chapter 2-1, the area can be divided into two "belts", which follow the dominant strike of bedding in the Tararua Range (Fig. 6-9).

Belt 1, the western belt, is dominated by massive to thick-bedded greywacke, along with conglomerate, olistostrome and minor massive argillite. Rocks of volcanogenic association (eg. metabasite, chert) occur in this belt, always having faulted contacts with the rocks of sedimentary association.

Belt 2, the eastern belt, contains rock sequences which are dominated by thinly-bedded, alternating greywacke and argillite beds, with only minor amounts of thick-bedded greywacke and massive argillite. Shear foliation and faults at a low-angle to bedding are common, and within this belt most of the fold structures are observed, possibly as a function of the bedded nature of the sedimentary material.

The contact between the two belts, in the Waiohine River is defined by a zone of melange over 20 metres wide, and elsewhere, where it was possible to observe the contact, it is either faulted or a zone of sheared argillite.

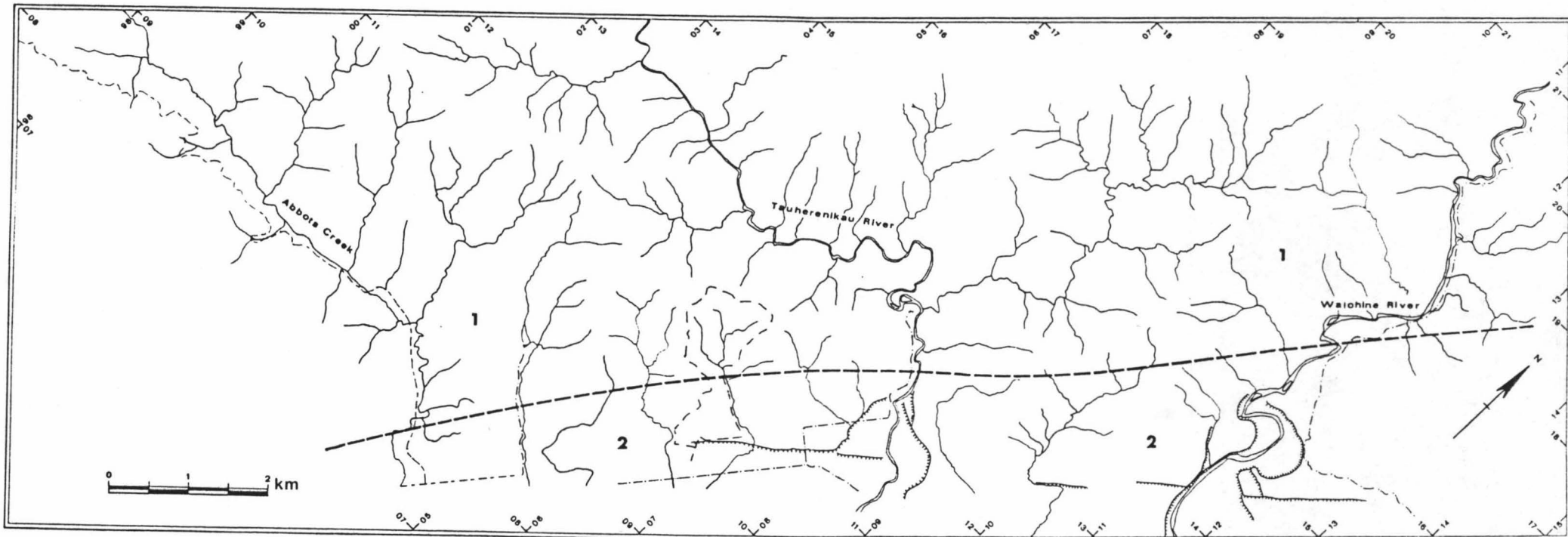


Figure 6-9: Macroscopic "belts" in the study area.

The two belts follow the dominant strike of bedding in the Tararua Range.

1 = Western belt: massive sandstone, conglomerate, olistostrome, and rocks of the volcanogenic association.

2 = Eastern belt: interbedded sandstone and argillite with minor massive sandstone and massive argillite.

6.4 MACROSCOPIC GEOMETRIC ANALYSIS

In determining the deformation on the macroscopic scale, the study area has been divided into fourteen "domains". The domain boundaries were determined by grouping adjacent, structurally-homogeneous outcrops into one domain. Orientation data have been plotted on equal-angle stereographic projections (Wulff nets) although a number of contoured diagrams, plotted on equal-area stereographic projections (Schmidt nets) were used to define some great circle traces. The location of the domains are shown in Figure 6-10.

Because the shear foliation is parallel or sub-parallel to bedding throughout the study area, both sets of orientation data have been plotted undifferentiated on the same net. Within individual domains the distribution of poles to bedding and shear foliation (πS_0) defines a great-circle girdle, implying that the beds have been cylindrically folded, and that they were planar prior to the deformational event which caused the folding. All domains display this pattern (Fig. 6-10). A synoptic net (Fig. 6-11) of fold axes (π pole) defined from πS_0 from each domain lie along a great-circle girdle with orientation $030^\circ/SE/85^\circ$. In comparing domains, the πS_0 girdles from individual domains show different orientations and each π pole has a different orientation. This implies that, before this deformation, beds within each domain were planar but that the beds had different orientations from one domain to another. Hence the rocks of the field area have undergone at least two folding events (if the area had only been folded once, the fold axes of all the individual domains theoretically should be the same).

Such a pattern seen in the synoptic net (Fig. 6-11) can be produced by two methods:

Alternative 1. The pattern results from an early fold system that has since been refolded. In this case, the orientations of πS_0 in each domain

Figure 6-10: Map of the field area showing structural domains.

Poles to bedding and shear foliation have been plotted for each domain (n So).

n = number of bedding and shear foliation orientations plotted.

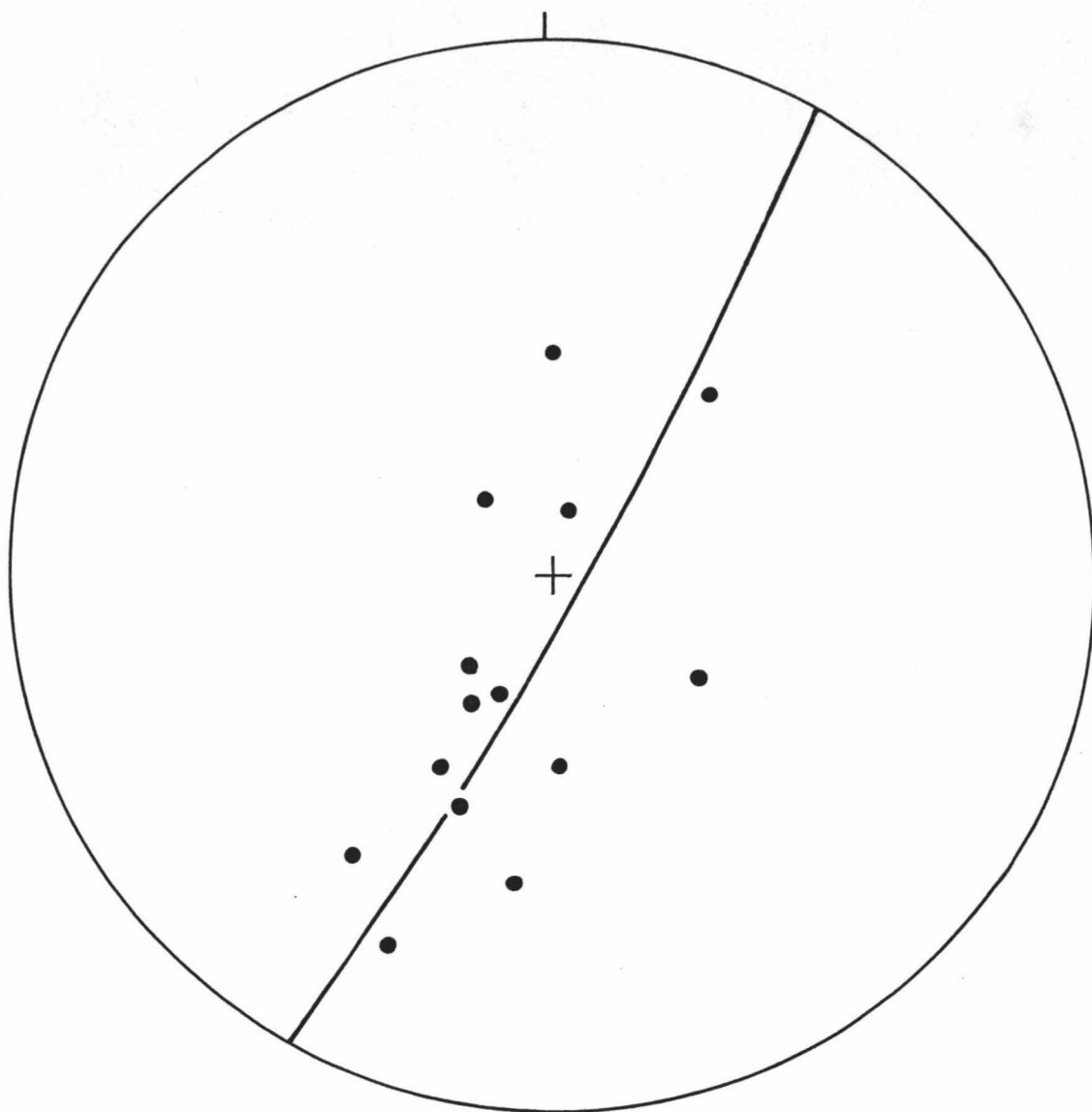


Figure 6-11: Synoptic net showing poles to πS_o for each domain.

are for the F1 folds (Fig. 6-12a). The different orientations of F1 for each domain (eg. area A, area B in Fig. 6-12a) are the result of refolding of the complete F1 fold by F2 and this refolding changes the orientation of the F1 folds. The synoptic great-circle defined by poles to π So in this alternative simply represents a plane in which the fold axes of F1 lie, and bears no relationship to the axial surface of either fold (F1 or F2).

Alternative 2: Folding of a non-planar form surface. If we assume that the now planar form surface was produced by a period of folding, then here the great-circle girdle of π So for each domain defines the fold axes F2 (Fig. 6-12b). In such a case, each domain (eg. area 1, area 2, area 3 in Fig. 6-12b) represents a segment which was originally planar prior to F2, with each domain having a different orientation relative to the others. In this alternative, the synoptic great-circle defined by F2 represents the axial surface of the second fold event (AS2).

To help constrain the possibilities outlined above, the geometry of mesoscopic folds can be used because these fold styles and axial surfaces should reflect those produced on the macroscopic scale (Hobbs et al. 1976).

Fold axes of close to open post-melange mesoscopic folds shown in Figure 6-13a lie along a NE-SW striking great-circle girdle. Axial surfaces of three of these mesoscopic folds from the Waiohine River have orientations similar to the great-circle defined by the fold axes (Fig. 6-13b). These axial surface orientations have very little variation and most likely represent the orientation of the axial surface of the later fold event. If these folds were produced during the earlier fold event, their axial surfaces should be folded and orientations would be expected to be more variable than they are. The axial surface traces also have a similar orientation to the great-circle girdle defined by poles to π So

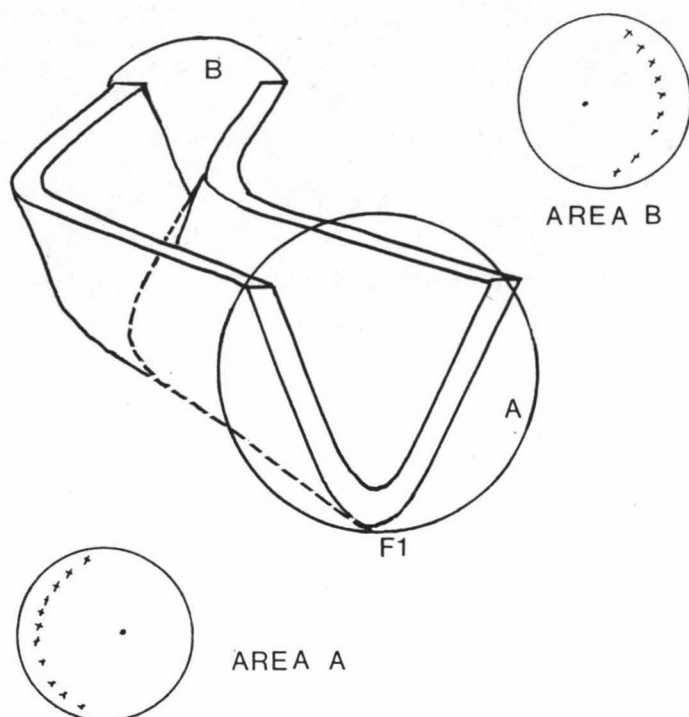
Figure 6-12a: Alternative 1: The pattern of poles to πS_0 is for an early fold system that has since been refolded. The orientations of πS_0 in each domain eg. area A, area B, are for the F1 folds.

$$\chi = \pi S_0$$

Figure 6-12b: Alternative 2: Folding of a non-planar form surface. The orientations of πS_0 in each domain eg. area A, area B, area C, are for the F2 folds. The synoptic great-circle defined by F2 represents the axial surface of AS2.

$$\chi = \pi S_0$$

a



b

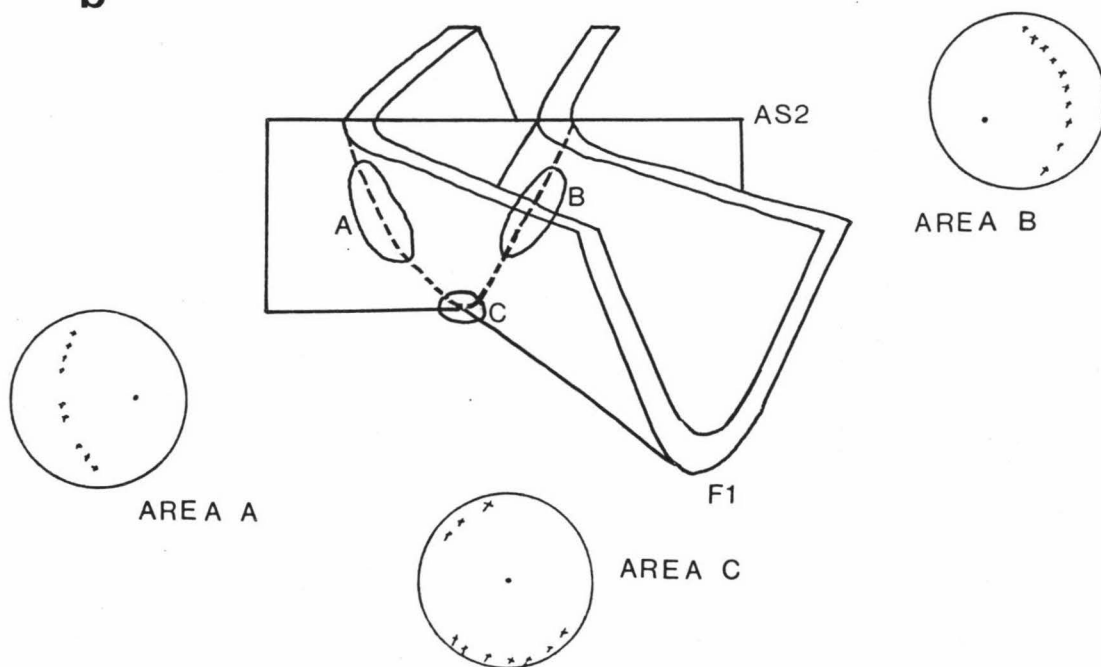


Figure 6-12

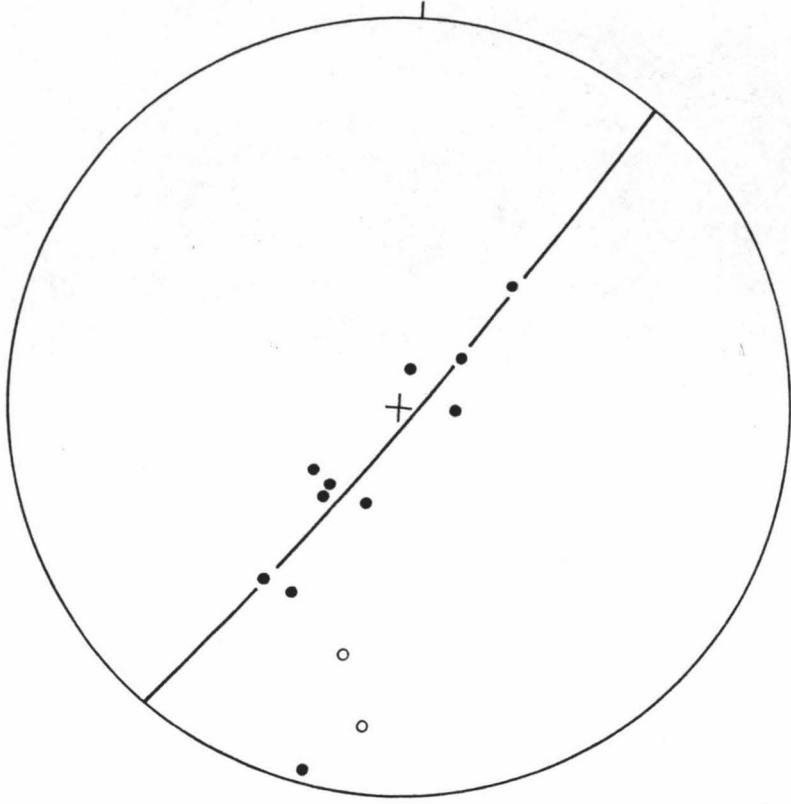
Figure 6-13a: Fold axes of mesoscopic and macroscopic folds
in the study area.

- = mesoscopic fold axes
- = macroscopic fold axes

Figure 6-13b: Axial surface orientations of mesoscopic folds.

Axial surface orientations of three post-melange folds from melange
in the Waiohine River.

a



b

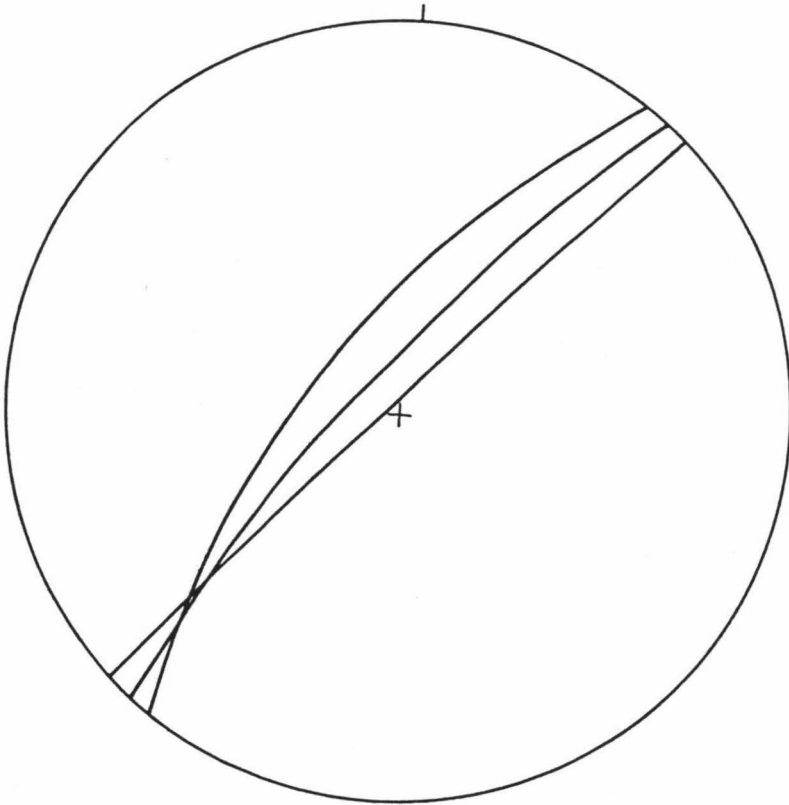


Figure 6-13

(Fig. 6-11), which suggests that the pattern of poles to πS_o represents alternative 2 described above. Macroscopic fold axes (Fig. 6-13a) lie near the NE-SW great-circle girdle defined by poles to πS_o and these may also be reflecting the later fold event.

6.4.1 High-angle faults

Poles to high-angle faults (πS_f) within individual domains are shown in Figure 6-14. Most of the domains show a scatter, although in some (domains 2, 3, 8, 12, 13) the poles define a great-circle girdle. This raises the possibility that the high-angle faults have been cylindrically folded, with the high-angle faults being planar and parallel prior to the fold event. This situation would then represent the case of two planar S-surfaces (S_o and high angle faults) being simultaneously folded, and producing a common axial surface, but having variable fold axes. Turner & Weiss (1963) described the geometry of simultaneous cylindrical folding of two planar surfaces, (Fig. 6-15) and showed that the axial surface of the folding event must contain the fold axes of the two originally planar surfaces. Following this, a great-circle girdle which contains the fold axes of πS_o and πS_f for individual domains should define the axial surface of the deformational fold event if these two surfaces (S_o and S_f) have been simultaneously folded. Great-circle girdles which contain the fold axes of πS_o and πS_f for domains 2, 3, 8, 12 and 13 show similar orientations, striking NE-SW (Fig. 6-16), which suggests that if these surfaces have been simultaneously folded, the deformational fold event had an axial surface which trended NE-SW.

6.4.2 Conclusions

The geometric analysis of the Tararua Range has been based mainly on πS_o diagrams, due to the scarcity of folds and absence of other structural features such as cleavage and lineations. Hence inferences

Figure 6-14: Map of the field area showing structural domains.

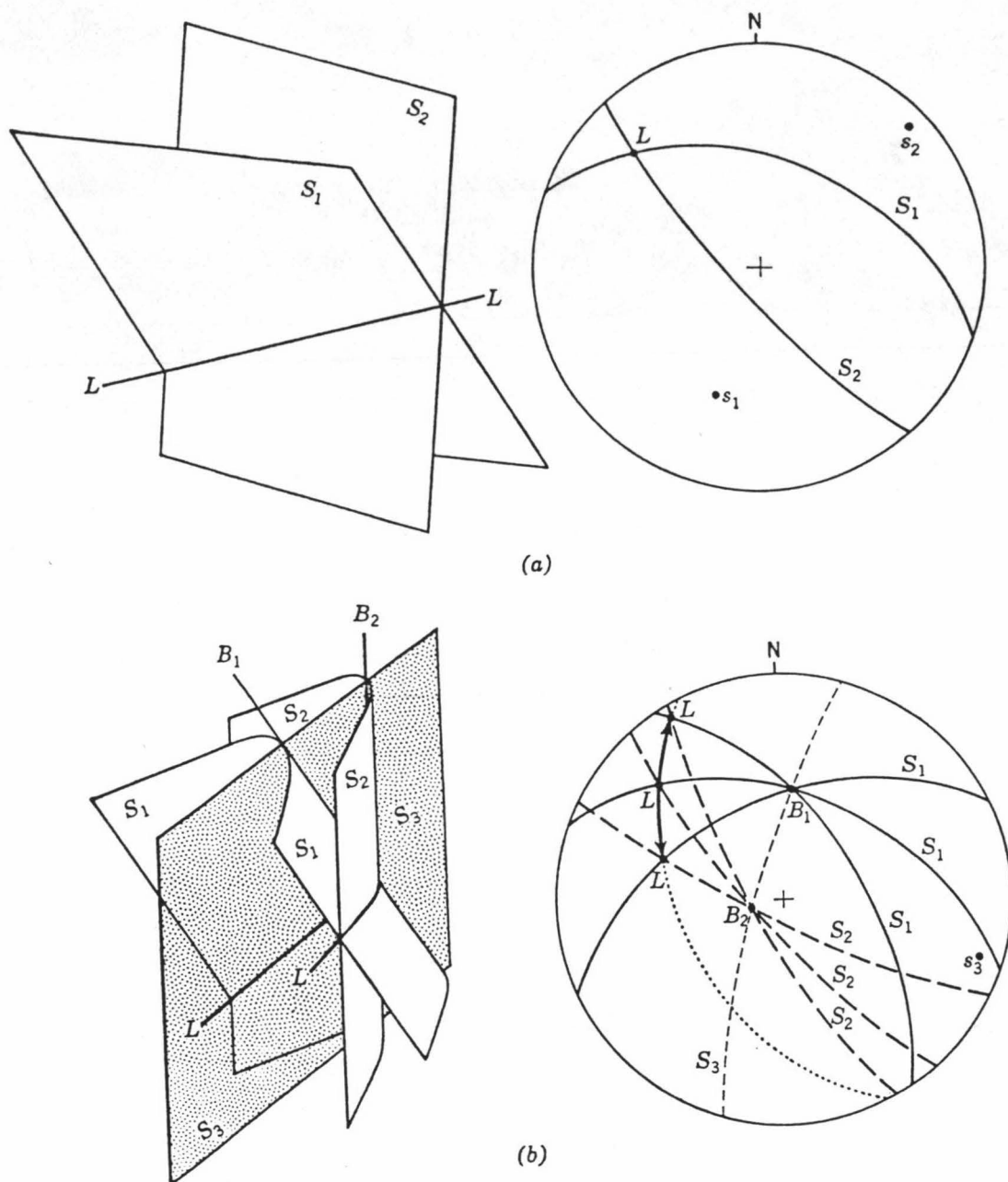
Poles to high-angle faults have been plotted for each domain (πS_f).

n = number of high-angle fault orientations plotted.

Figure 6-10: Map of the field area showing structural domains.

Poles to bedding and shear foliation have been plotted for each domain (n So).

n = number of bedding and shear foliation orientations plotted.



Simultaneous cylindrical folding of two planar surfaces S_1 and S_2 intersecting in a lineation L . S_1 is seen in b to be folded about B_1 and S_2 about B_2 . The folds share the same axial plane S_3 .

Figure 6-15: Simultaneous cylindrical folding to two planar surfaces from Turner & Weiss (1963).

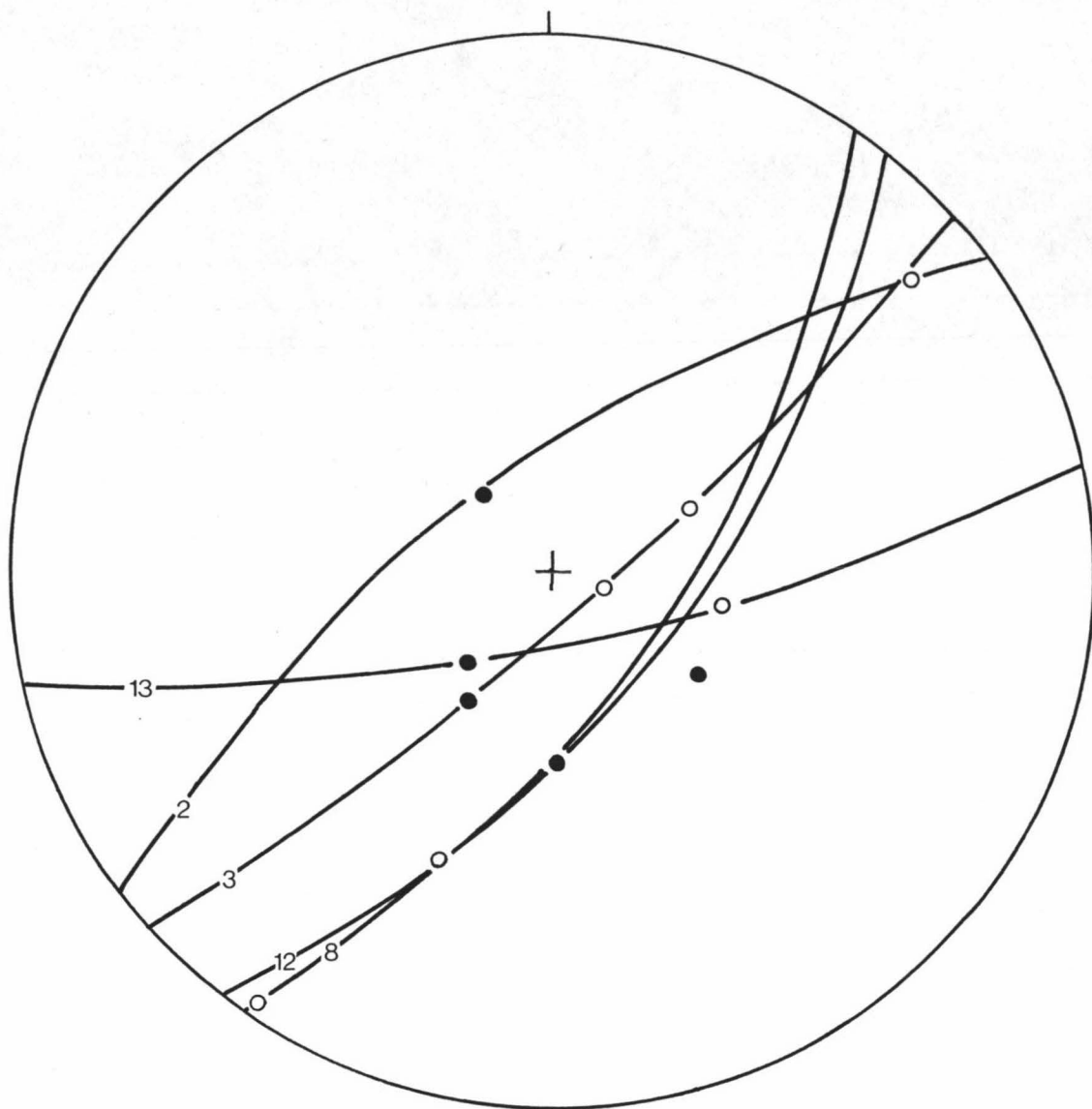


Figure 6-16: Net showing the great-circle girdles which contain the fold axis of S_o and S_f for domains 2, 3, 8, 12 and 13.

3 = domain number

● = fold axes for πS_o

○ = fold axes for πS_f

that can be made from the π So diagrams are that:

- 1) The area has been affected by at least two fold events; these events may be either discrete or two phases in a single progressive deformation.
- 2) the high-angle faults may have been planar and were folded along with So during at least one folding episode.
- 3) By comparing the mesoscopic fold axes with the π pole for individual domains, the net orientations for individual domains were most likely controlled by the second fold event. The axial surfaces of the mesoscopic folds, and the axial surfaces of the possible deformation event which simultaneously folded So and Sf strike NE-SW. This suggests that the synoptic net pattern (Fig. 6-11) of poles to π So reflects the later fold event.

On the synoptic diagram (Fig. 6-11) the π So lie along a great-circle girdle but show a slight spread away from the great-circle girdle. This scatter could be due to a number of factors, such as:

- 1) the shear foliation was not strictly planar prior to the fold event,
- 2) the folds are not purely cylindrical,
- 3) beds within individual domains were not totally planar prior to the second folding,
- 4) there may have been minor very late warping of the second fold event, but was not observed in the field.

6.5 RECENT DEFORMATION

Evidence for recent deformation in the Tararua Range is restricted to the presence of active faults. These faults can be distinguished by zones of soft gouge, ranging from centimetres to metres in thickness. The most obvious fault is the Wairarapa Fault although smaller recent faults can be found throughout the field area. These recent faults are plotted as planes in Figure 6-17. Data plotted on the net has a large scatter

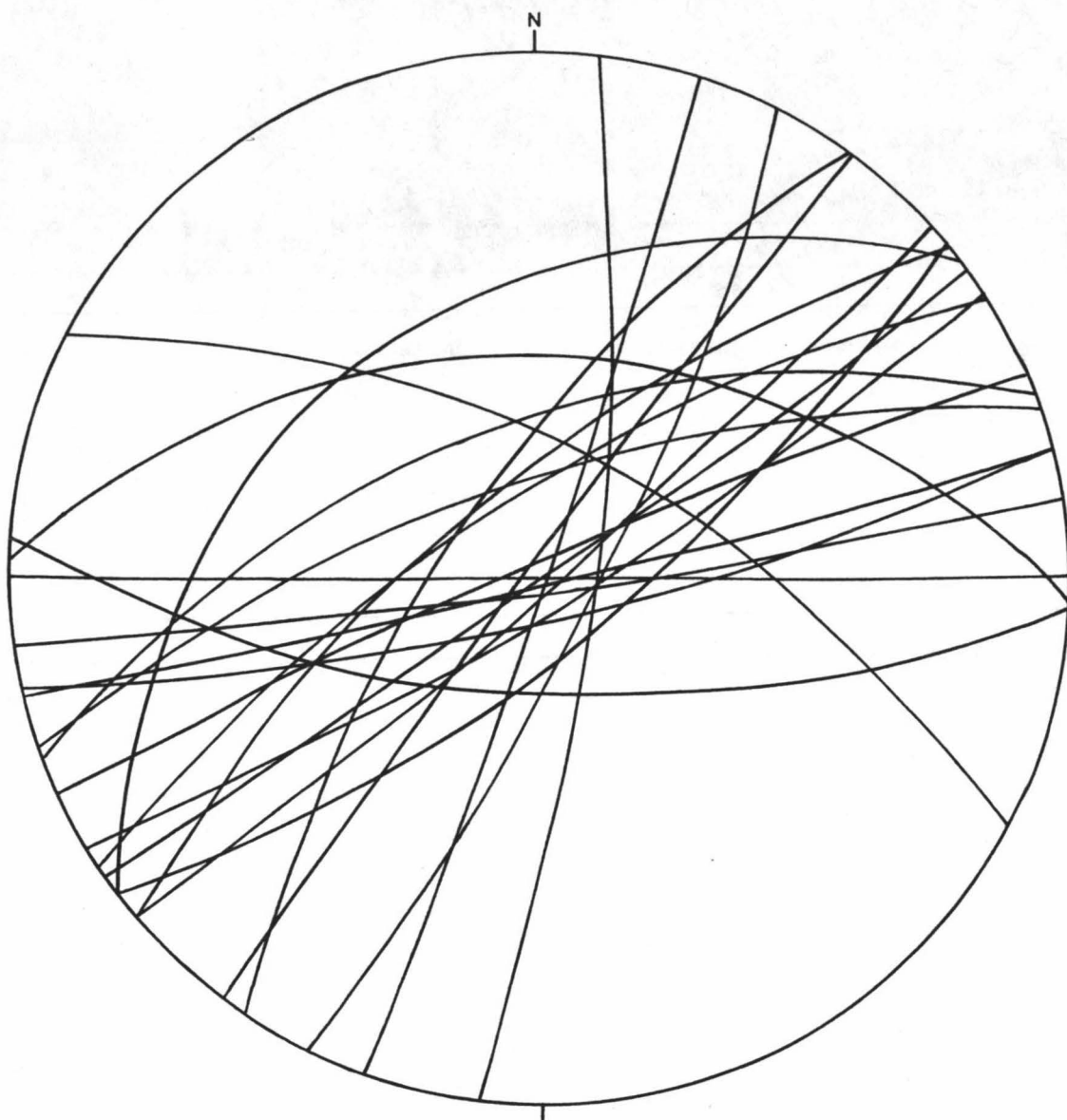


Figure 6-17: Recent faults plotted as planes on a Wulff net.

but overall strike northeast-southwest. The orientation of active faults from my study area show the same dominant trend as known active faults in the southern North Island which predominantly strike north-northeast to northeast. The Wairarapa Fault strikes at 035° (Grapes et al. 1984), while in the Tararua Range the Wellington Fault (Cotton 1912) strikes between 030° and 045° and overall in the southern North Island trends approximately to the northeast (Grapes et al. 1984). Recent faults described by Reed (1957b) from the Rimutaka-Tararua Range show a similar strike (eg. between 022° and 040°).

The Wairarapa Fault forms the southeastern boundary of my field area and is recognised in the field as a scarp up to 16 metres in height, and also as a zone of intense shearing with an associated gouge zone which is up to 20 metres wide where the fault crosses the Tauherenikau River S26C/ 0852 1187). A number of workers have discussed aspects of the Wairarapa Fault (Ongley 1943; Lensen 1958; Lensen & Vella 1971; Grapes et al. 1984) and apart from casual observations such as noting that approximately 50 metres to 100 metres of the greywacke and argillite adjacent to the Wairarapa Fault was intensely sheared, with the shears being parallel to the fault (eg. at Boar Creek and Tauherenikau River), I have not studied the fault in any detail.

The Wairarapa Fault has been correlated with the Clarence Fault of the South Island (Lensen 1958), and is thought to have been active during the Quaternary (Wellman 1969; Suggate 1978), with major strike-slip dextral displacements. Movement as recent as that associated with the 1855 earthquake has been attributed to the Wairarapa Fault, with a dextral horizontal displacement of 13 metres and a vertical displacement of 3 metres with the west side being upthrown being suggested (Ongley 1943).

The river terraces at the Waiohine River (S26D/ 1147 1430) display

a record of progressive fault movements along the Wairarapa Fault during the Quaternary. Detailed work on these faulted terraces by Lensen & Vella (1971) inferred that the Wairarapa Fault could possibly have a rate of vertical uplift and a rate of horizontal displacement of 0.9mm/year and 6.0mm/year respectively (Vella), or of 0.5mm/year and 3.4mm/year respectively (Lensen). These rates were based on the age, and hence displacement, of the Waiohine Surface (Vella 1963), thought to be 20,000 years by Vella, and 35,000 years by Lensen. Wellman (1972) however suggested an approximate age for the Waiohine Surface of 10,000 years, based on extrapolation from beach ridges at Turakirae Head, 50 kilometres south of the Waiohine River, and this would give an approximate average rate of horizontal displacement of 12mm/year along the Wairarapa Fault. Vella (pers. com. 1984) agrees with an age of 10,000 to 11,000 years for the Waiohine Surface. Recently, based on adopting an 11,000 year age for the Waiohine Surface, Grapes *et al.* (1984) have inferred the Wairarapa Fault, to have a rate of horizontal displacement of 11mm/year and a rate of vertical uplift of 1.7mm/year.

Lineaments

Figure 6-18 shows an interpretation of lineaments observed while viewing aerial photograph stereoscopic pairs. The Wairarapa Fault (lineament A; Fig. 6-18) is obvious. Other lineaments could represent recent faults, or be the eroded traces of now inactive faults. It is interesting to note that along the major lineament B (Fig. 6-18), there is a zone of rocks of the volcanogenic association. As these rocks (such as the metabasite) have faulted contacts with the surrounding clastic sediment, the lineament could be reflecting a zone of weakness initially caused by the occurrence of the volcanogenic association rock types.

Other lineaments can be related to recent crush zones (ie. lineament C; Fig. 6-18), although, not all lineaments seen on aerial

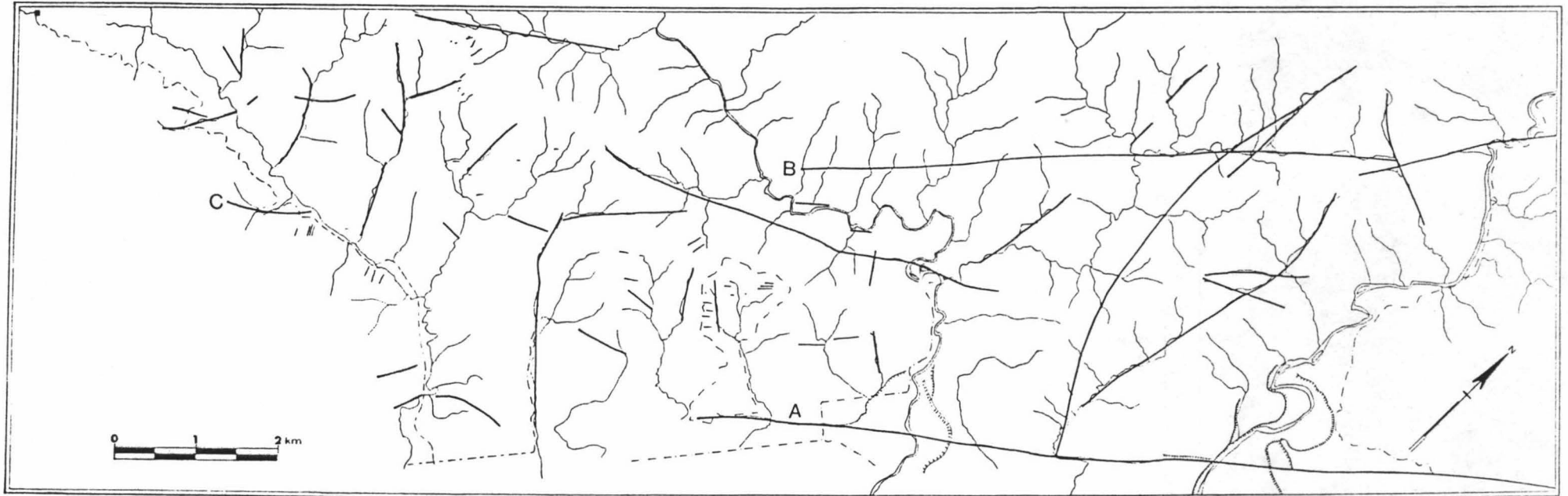


Figure 6-18: Lineaments observed while viewing aerial photograph stereoscopic pairs.

A = Lineament referred to in the text.

photographs could be related to features observed in the field.

Recent deformation in the study area, appears to be restricted to mainly dextral movement along the Wairarapa Fault, although some minor faults could also be active. Uplift of the Tararua Range has been occurring since the beginning of the Cenozoic, with major uplift being mainly a Quaternary event (Wellman 1969; Suggate 1978) and uplift is still ongoing. An uplift rate of 4mm/year for the Rimutaka-Tararua Range has been proposed by Wellman (1969) with the main uplift not taking place at the Wairarapa Fault (Lensen & Vella 1971).

6.6 SUMMARY

A number of deformational events produced the structures seen in the Tararua Range. These are outlined below in ascending chronological order.

The earliest deformational episode (either one event with two separate phases, or a single progressive deformation) was one of shortening and deformation of soft sediment, resulting in the production of at least two fold events with different axial surface orientations. This deformation is recorded in blocks within melange.

The second deformation is characterized by fragmentation and disruption of bedding. Structures produced by this deformation are:

- 1) faulting at a low-angle to bedding;
- 2) shear foliation;
- 3) faulting at a high-angle to bedding.

These structures do not occur in any specific order but rather as ongoing or alternating events with repeated faulting and development of shear foliation. In places, fragmentation has been so complete that melange has formed.

Post-melange deformation has produced folds. There is positive

evidence from field observations for one set of post-melange folds. However geometric analysis of bedding and shear foliation away from the melange indicate that two generations of folding has occurred (Fig. 6-11) and suggests that the latter fold generation and the mesoscopic post-melange folds were produced during the same deformational event. Nevertheless the timing of the early fold generation defined from geometric analysis is obscure. This event may have occurred either: 1) at the same time as the pre-melange mesoscopic folds, or alternatively, 2) after the melange had formed and hence is a post-melange fold but formed prior to the folds that can be seen deforming the melange.

Cenozoic deformation has resulted in uplift of the Torlesse Supergroup to form the Tararua Range, with deformation now being dominantly dextral strike-slip movement along the Wairarapa Fault.

6.6.1 Comparisons with other areas

The deformation determined in this study area can be related to deformation seen in other areas in the Torlesse Supergroup. Table 6-1 contains the deformational sequence determined by other workers in the Torlesse Supergroup, mainly from the southern half of the North Island and their possible relationships with other studies. The most obvious features to note in comparing the deformation seen in different regions are that:

- 1) often, the first recorded deformation is one of deformation of soft, unlithified, sediment.
- 2) a late deformation seen in all the studies (except in the Pohangina Melange, Sporli & Bell, 1976) has produced steeply plunging NE-SW trending folds.
- 3) where melange has developed, it was observed to occur after the soft sediment deformation, but before the deformation that produced the steeply plunging folds.

From Table 6-1 the structure and deformation seen within the study area, is similar to that observed elsewhere in the Torlesse Supergroup, thus implying that the deformation sequence affecting the rocks was of a regional scale.

This study	Sinclair Head (MacKenzie 1983)	Camp Bay (Webster 1982)	Sporli 1978	Pohangina Melange Sporli & Bell 1976	Axial Range Sporli & Bell 1976	Otaki Forks Rattenbury 1983	Esk Head Melange Botsford 1983
Late faulting	D4 minor warping on deformed limbs					Late faulting	Late faulting
?minor warping						Minor buckling on fold limbs	Gentle flexing on fold limbs
Folding NE-SW trending axes	D3 open tight folds steeply plunging	D3 folding NE-SW axes	D3 late steeply plunging folds		D3 late steeply plunging open folds (NE-SW striking axes)	Steeply plunging folds	Steeply plunging NE-SW trending folds
Melange formation	D2 subhorizontal tight-isoclinal folds	D2 folding on subhorizontal N-S axes	D2 strongly asymmetric folding & melange formation	D2 open, asymmetric folds with subhorizontal axes	D2 open asymmetric folds with subhorizontal axes	Open moderate plunging folds	Melange formation
	D1 tight gently plunging folds. Result of soft sediment deformation	D1 steeply plunging open folding	D1 steeply plunging folds	D1 steeply plunging isoclinal folds	D1 isoclinal steeply plunging folds	Faulting & melange formation Isoclinal folds	
D1 & D2 two generations of folding		Do soft sediment deformation		Melange formation		Soft sediment deformation	Folding & deformation of soft sediment

Table 6-1: Comparison of deformation seen in other areas
within the Torlesse Supergroup.

CHAPTER SEVEN

DISCUSSION

The advent of the plate tectonic theory has spawned a renewal of interest in rocks of the Torlesse Supergroup. Many authors have related features of the Torlesse Supergroup to processes associated with convergent plate margins (eg. Landis & Bishop 1972; Blake et al. 1974; Coombs et al. 1976; Sporli 1978; Bradshaw et al. 1981; MacKinnon 1983; Korsch & Wellman in press).

The aim of this discussion is to assess how my observations, data and analyses from the Tararua Range contribute to, or constrain, the various models proposed for the origin of the Torlesse Supergroup. Initially, rock types found within the Tararua Range are outlined, with suggestions as to their original source and environment of deposition. These rocks can be divided into two groups, those of a sedimentary association and those of a volcanogenic association, which have depositional environments that are not related (Chapter 2 & 3).

7.1 SOURCE OF THE SEDIMENTARY ASSOCIATION

Rocks of sedimentary association are predominantly sandstone and argillite with minor calcareous siltstone, conglomerate and olistostrome. From field observations, petrography and geochemical analyses, the rocks appear to have been derived from the same source. Greywacke from the Tararua Range contains detritus derived from an active continental margin which was shedding sediment of acid-volcanic and metamorphic origin (Chapter 2-3).

Although there is little dispute over the type of source rocks there are several ideas as to the site of these rocks. Initially, the Western Province was considered to be the source area of the Torlesse, because of its composition and proximity (Landis & Bishop 1972). However, detritus derived from the Western Province would have to cross the

Hokonui Association. It seems unlikely that this could be achieved without the detritus being modified by incorporation of Hokonui Association derived sediments (volcanic rich). There is no trace of any "by pass" systems (eg. submarine canyons) which would allow transportation of sediment through the Hokonui Association from the Western Province to the Torlesse Supergroup, and no positive record of Hokonui detritus in Torlesse rocks. Recently other possible source areas have been proposed, these being an eastern source (Bradshaw 1972; Bradshaw & Andrews 1973; Andrews 1974; Andrews et al. 1976; Kamp 1980) and a source to the south (Blake et al. 1974; Mackinnon 1983; Korsch & Wellman in press).

An eastern source for the Torlesse Supergroup has been based on regional sedimentological patterns. Andrews et al. (1976) argue that conglomerates and more shallow water sediments representing proximal sediments occur in the eastern portion of the Torlesse. Such observations have occurred not because of an actual abundance of conglomerate and shallow marine sediments in the eastern portion of the Torlesse Supergroup, but rather as these parts of the Torlesse are more accessible to workers (MacKinnon 1983). If such a continental landmass did exist to the east of the Torlesse, there is no evidence of it at present and it must have been removed, presumably by tectonic processes.

The third possible source is to the south, with detritus possibly being derived from Lesser Antarctica (Bradshaw et al. 1981; Dickinson 1982; MacKinnon 1983; Korsch & Wellman in press). A Lesser Antarctica (Gondwana) source is appropriate as it has rocks suitable for deriving detritus of Torlesse composition. MacKinnon (1983) and Korsch and Wellman (in press), have proposed a southerly source based on reconstructions of the New Zealand mass prior to offset by the Alpine Fault and associated faults. These reconstructions show that fossil zones in Torlesse

progressively young and wedge out towards the northeast, suggesting derivation of sediment from a source to the south.

7.1.1 Possible source of Tararua greywacke

Paleocurrent indicators (eg. flute casts, scours, groove casts) were not observed in the study area, although some constraint on the original source site is provided by petrographic modal data. During dispersal of detritus with increased distance from the source, changes in composition of sediments do occur (Pettijohn 1957). With transport the grains undergo abrasion (breaking down and fragmenting individual grains) and hence with increased distances of transport, the proportion of quartz should increase, as these grains are the least susceptible to abrasion (ie. compared to feldspar grains, Pettijohn 1957).

Greywacke of ?Middle Jurassic age (based on the age of radiolaria in chert, see below) from the Tararua Range have an average composition of Q33F48L19, whereas greywackes of similar age from the South Island contain less quartz (Q27F33L40, MacKinnon 1983). This suggests that greywacke from the Tararua Range has undergone more transportation prior to deposition relative to the greywacke of similar age from the South Island. A similar comparison can be made between sediments of known Late Triassic (Oretian-Otamitan) age from the Wellington area and the South Island. Here again, the average modal data from greywacke from Wellington (Q37F39L24, Rowe 1980) have more quartz relative to greywacke from the South Island (Q31F59L10, MacKinnon 1983).

7.1.2 Depositional environment for rocks of the sedimentary association

The rocks of the sedimentary association are interpreted as being deposited in a deep water marine environment (chapter 2-1). The majority of sediments within the Torlesse Supergroup have been deposited by turbiditic flows, although the lack of marker beds and the monotonous

alternating nature of the greywacke-argillite turbidite beds makes the extent and length of each individual turbidite impossible to define.

Several workers (Carter *et al.* 1978; Begg 1980; Hicks 1980; Howell 1980a; Botsford 1983; Rattenbury 1983; MacKenzie 1983) have interpreted the sediments seen within small regions in the Torlesse Supergroup in terms of a submarine fan system, with most sediments representing deposition in a middle to outer fan environment. These systems can occur in trenches or on the abyssal plains. Sediments accumulating in these two types of depositional environments are difficult to differentiate because they show similar features (Dickinson 1982). However it would be expected that abyssal plain sediments would contain a larger proportion of hemipelagic and pelagic sediments, while trench-fill deposits would contain a higher proportion of coarser detritus (eg. sandstone). In the Torlesse Supergroup, the sediments contain a high proportion of sandstone (MacKinnon 1983) and it is most likely that the turbidites have been deposited in a trench. Other workers (MacKinnon 1983; Korsch & Wellman *in press*) also suggest that the Torlesse sediments have been deposited in a trench. The modal differences of quartz, feldspar and lithic rock fragments described in Chapter 7.1.1 could be due to transportation of sediment from south to north in a trench.

7.2 ORIGIN OF THE VOLCANOGENIC ASSOCIATION

Rocks of the volcanogenic association, namely metabasite, red argillite, chert and limestone, can be regarded as representing sections of seafloor material. Based on geochemical analyses (chapter 3-2) the metabasites are oceanic in character, being erupted at mid-ocean ridges and also at intra-plate (ocean plate) settings, that is, seamounts. Other geochemical analyses of metabasites from the Torlesse Supergroup (Roser 1983) indicate also that they have erupted in oceanic settings. Chert,

red argillite and limestone all represent seafloor deposits (Chapter 3-3). Many workers have suggested that rocks of volcanogenic association elsewhere in the Torlesse Supergroup are seafloor material (eg. Sporli 1978; Botsford 1983; Roser 1983; MacKinnon 1983).

7.3 ORIGIN OF THE TORLESSE SUPERGROUP

Any model for the origin of the Torlesse Supergroup must explain how rocks of the volcanogenic association and rocks of the sedimentary association are now interleaved.

7.3.1 Proposed model of formation of the Torlesse

Recent models that discuss the origin of the Torlesse Supergroup all involve convergent plate margins. Bradshaw *et al.* (1981) view the older rocks of the Torlesse Supergroup as representing an exotic submarine fan system which was brought into contact with the New Zealand-Gondwana margin and added to the convergent margin, while the younger rocks represent sediments that accumulated in a trench seaward of the accreted submarine fan.

A model favored by several workers (Sporli 1978; MacKinnon 1983; Korsch & Wellman in press) is that the Torlesse Supergroup represents accretion in a migrating subduction system (terminology follows Karig & Sharman 1975). In subduction systems, which are often associated with active continental margins, seafloor material and trench-fill sediment are scrapped off, undergo decoupling from the subducting plate and are incorporated into the accretionary prism at the inner trench wall (Fig. 7-1). Deposition of sediment in a migrating subduction system will result in accretion of similar age sediments into "packets", with subduction migrating oceanward to keep pace with the "stacking" of "packets". Many subduction systems show a progression from oldest to youngest sediment seaward from a converging margin, eg. Alaska (Connelly 1978); Franciscan Complex, California (Blake & Jones 1974). Accretion of progressively

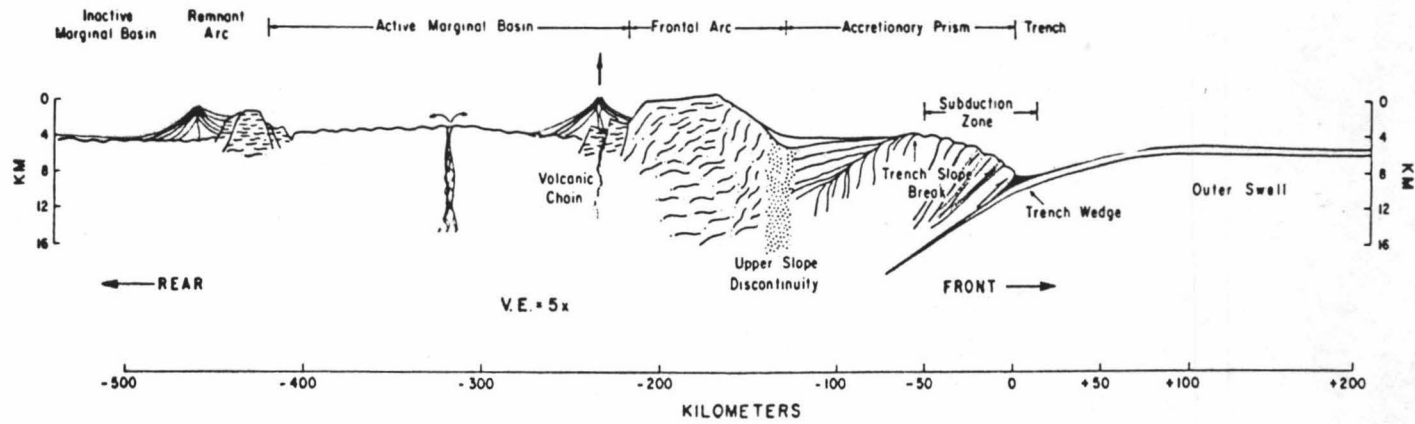


Figure 7-1: Subduction system (from Karig & Sharman 1975).

younger "packets" of sediment is typical of modern subduction systems (Karig & Sharman 1975).

Features of the Torlesse Supergroup indicative of accretion of sediment in progressively younger "packets" is the distribution of the mutually exclusive fossil zones which young to the east (Speden 1976; Sporli 1978; MacKinnon 1983) while within individual fossil zones the younging directions are predominantly to the west (Sporli & Bell 1976; Sporli 1978). These features infer accretion in a westward dipping subduction zone.

The model that the Torlesse Supergroup represents accretion is favored by several workers (eg. Sporli 1978; MacKinnon 1983; Korsch & Wellman in press) and appears to best "fit" what is at present known about the Torlesse. However there is some disagreement among workers as to the site of accretion.

Direct accretion of the Torlesse Supergroup onto the New Zealand mass has been proposed by Sporli (1978) and Korsch and Wellman (in press) with the contact between the Torlesse Supergroup and the Caples Group being seen as gradational. Sporli (1978) views the Torlesse as representing accretion of a large submarine fan with its source lying to the south. Alternately Korsch and Wellman (in press) suggest that the Torlesse has been deposited by long distance transport along a trench with subsequent accretion of these trench-fill sediments.

In contrast, MacKinnon (1983) suggested that the Torlesse was originally accreted to the Western Province-Gondwana margin, with deposition occurring in a trench fronting Gondwana and direct accretion onto the Western Province-Gondwana margin in that area. The Torlesse Supergroup was later "rafted" into its present position in part by strike-slip movement. In such a case, the contact between the Caples Group and the Torlesse Supergroup would be an abrupt break, such as a

major fault or suture but now it would be obscured somewhere in the Haast Schist.

Howell (1980b) has proposed that New Zealand is made up from at least four tectonostratigraphic terranes (1:Tuhua-Western Province, 2:Hokonui, 3:Caples, 4:Torlesse terranes). In such a model the Torlesse represents an "exotic" landmass which has been transported from its original site of formation and initially sutured to the Caples terrane, both of which were then sutured to the Hokonui and Tuhua terranes. Thus the Torlesse has been transferred by collision and suturing to the New Zealand mass.

7.4 SUBDUCTION ZONES

Factors affecting subduction and in particular the formation of the accretionary prism, need to be understood before inferences can be made about features seen within the Torlesse Supergroup.

7.4.1 Style of accretion

The growth and style of accretion within subduction systems varies, being a function of several variables, including the rate of subduction and the availability and nature of the sediment on the downgoing plate. From studies of ancient and modern subduction complexes Karig and Sharman (1975) have shown that the availability and rates of sediment supply onto the downgoing plate is more important than the rate of subduction.

The relative proportions of accreted turbiditic and ocean floor materials varies, some prisms being dominated by turbiditic, landward-derived, trench sediment, eg. Kodiak Island, Alaska (Byre 1982). Turbiditic sediment has a relatively low density and strength in comparison to that of seafloor material and Moore (1975) suggested that during subduction the lower density material would be preferentially accreted. Therefore where turbidite sediment influx into the trench is

high, shallow accretion would be dominated by low density turbiditic sediment with the denser seafloor material tending to be accreted at greater depths or subducted completely.

Other prisms, eg. Mutki, Turkey (Hall 1976) and Makran, Iran (McCall 1982), are dominated by seafloor material indicating little influx of sediment into the trench.

7.4.2 Mechanisms of emplacement

The processes involved in transferring the sediment pile from the subducting plate to the accretionary prism have been inferred from studies of modern and ancient subduction systems (Karig & Sharman 1975; Moore & Wheeler 1978). The sediment is thought to undergo the following sequence of events:

- 1) With initial subduction, the sediments are dewatered and lithified. Folding of the unconsolidated sediment may occur.
- 2) Sediment, being consolidated, passes through a "master" shear zone, which represents the initial dislocation of the sediment from the subducting plate.
- 3) Sediments are sheared, with development of foliation in response to underthrusting as sediment is accreted.
- 4) With subsequent accretion the sediment is tilted and rotated toward the land, with minor movement along thrust faults.
- 5) Later folding and shearing

(Karig & Sharman 1975; Moore & Wheeler 1978; Byrne 1982). It appears that the most intense deformation takes place at the beginning of subduction and detachment of the sediment from the subducting plate, with the amount of deformation decreasing as the sediment continues to be kneaded into the accretionary prism (Karig & Sharman 1975; Byrne 1982).

7.5 DATA FROM THE FIELD AREA

Many features of the Tararua Range are comparable with those inferred for accretionary prisms. Trench-fill detritus, derived from an active continental margin, and seafloor material being accreted in "packets" are often documented in subduction systems eg. Sunda Arc (Moore et al. 1982).

Within the Tararua Range rock types derived from a continental margin and also seafloor are juxtaposed (that is sedimentary association and volcanogenic association respectively). Also, the sequence of deformation in the study area is similar to that described for accretionary prisms. Therefore the data from the study area does not contradict an accretionary prism model. The implications of data from this study to the accretionary model are outlined below.

Within the study area, rocks of the volcanogenic association are approximately 2-3 % of the total rocks present. However to the west of the study area around Wellington and at the Otaki Forks region (Rattenbury 1983) the rocks are predominantly clastic sediments with negligible rock of seafloor origin.

In the Wellington region and the Axial Ranges of the southern North Island, there is an overall trend from west to east, to have an increased amount of rocks of the volcanogenic association ie. more rocks representing seafloor deposits, and a decrease in clastic trench deposits. This change in rock type across the Torlesse could indicate either:

- 1) a decrease in the sediment influx into the trench from the continental source,
- 2) that the rocks exposed at the eastern portion of the Torlesse are representing deeper depths within the accretionary prism,
- 3) the rate of subduction on the downgoing plate may have increased,

therefore not allowing sediment in the trench to build up before it is subducted.

If the eastern portion of the Torlesse Supergroup had been buried to greater depths, relative to the western portion of the Torlesse, it might be expected to have a higher grade of metamorphism. However as the Torlesse overall has a prehnite-pumpellyite metamorphic facies, proposition 2) is unlikely. Also the rate of the subducting plate does not appear to be an important feature of the style and growth of accretionary prisms (Karig & Sharman 1975) and therefore proposition 3) is doubtful.

I suggest that the first proposal is most probable, and that the change in rock types exposed throughout the Torlesse represents a decline in the influx of sediments into the trench with time, allowing more seafloor to be incorporated into the accretionary prism. It is interesting to note that sediment of Early Jurassic age has not yet been found within the Torlesse (MacKinnon 1983), which could be due to a lack of sediments in the trench at this time.

A significant aspect of this study is the occurrence, extraction and dating of radiolaria from chert blocks from the Tararua Range and the Manawatu Gorge as Middle Jurassic and Late Jurassic age respectively. The distribution of diagnostic and identifiable fossils are sparse in the North Island, with the fossil age zones in the Torlesse being much less well defined than in the South Island. Any additional information as to fossil localities and ages of the rocks within the Torlesse Supergroup can only aid the delineation of the fossil zones and possible tectonic reconstructions.

The paucity of recorded fossil localities within the Torlesse, and in particular the North Island, is probably a reflection on the amount of

work that has been done on the rocks, which is mainly controlled by their accessibility. Also, turbidites are notoriously fossil-poor. Most work to date has been done in the South Island, and in easily accessible parts of the Torlesse in the North Island ie. Wellington. With more work being done on the rocks of the Torlesse of the North Island it would be expected that the fossil zones will become better defined.

Feary and Pessagno (1980) found radiolaria from chert blocks in melange from the Raukumara Peninsula, North Island, where the radiolaria are of Ururoan (Pliensbachian-Toarcian) age while the surrounding clastic sediments based on macrofossils are Motuan (Albian) age. These rocks are thought to represent accretion in a subduction system (Feary & Pessagno 1980) which suggests that for at least some of the rocks in the Raukumara Peninsula there is approximately 80 million years age difference between the seafloor material (represented by the chert block) and the trench-fill sediments both of which were later accreted.

This gives a possible indication of the age difference between the two rock associations in the Tararua Range, in so much as, the rocks of sedimentary association may be millions of years younger than the age of the accreted seafloor material. This raises the possibility that the greywacke and other rocks of the sedimentary association may be of Late Jurassic or Cretaceous in age.

The age of radiolaria from chert in the study area suggests that part of the seafloor that was being subducted was of Middle Jurassic age and that the sediment being deposited in the trench and accreted with this seafloor material must be of Middle Jurassic age or younger (ie. Cretaceous). The same inference can be made about the sediments at the Manawatu Gorge, that they are either Late Jurassic in age or younger based on the age of radiolaria found in the chert block.

These ages based on radiolaria gives much better constraints as

to the locations of the fossil zones within the North Island, because the sediment associated with the chert blocks must be of Middle Jurassic (Tararua Range) or Late Jurassic (Manawatu Gorge) age or younger. Thus, the sediment would belong to fossil zone 5 (MacKinnon 1983) in the Torlesse Supergroup. A possible delineation of fossil zones within the North Island utilizing my data is given in Figure 7-2.

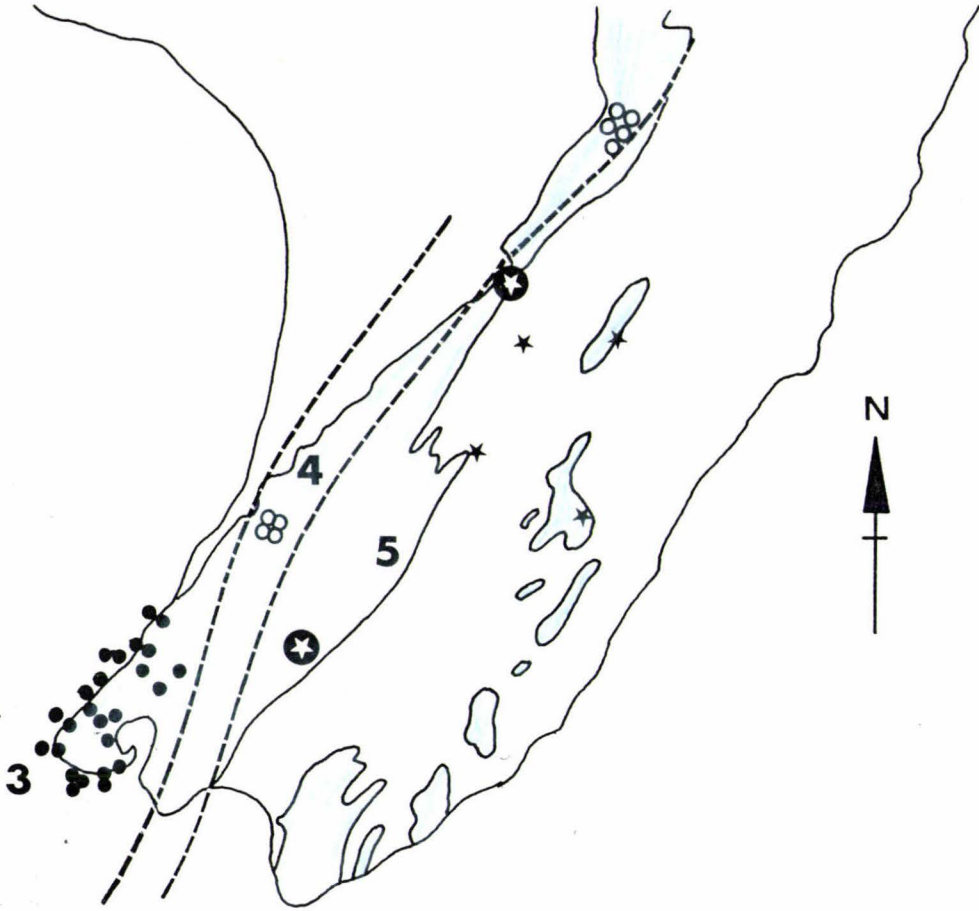


Figure 7-2: Delineation of fossil zones in the southern North Island.

Symbols



Torlesse Supergroup (exposed)



inferred fossil boundary



fossil localities from this study



Monotis localities (from Speden 1976)



Torlessia and Titahia localities

(from Speden 1976)

Fossil Zones

5

Late Jurassic-Early Cretaceous

4

Monotis, Late Triassic (Warepan)

3

Torlessia, Late Triassic (Oretian-Otamitan)

REFERENCES

- Aalto, K.R. 1981: Multistage melange formation in the Franciscan Complex, northernmost California. Geology 9: 602-607.
- Andrews, P.B. 1974: Deltaic sediments, Upper Triassic Torlesse Supergroup, Broken River, North Canterbury. New Zealand journal of geology and geophysics 17: 881-905.
- Speden, I.G.; Bradshaw, J.D. 1976: Lithological and palaeontological content of the Carboniferous-Jurassic Canterbury Suite, South Island, New Zealand. New Zealand journal of geology and geophysics 19: 791-819.
- Barnes, C.J. 1979: The structure and petrography of the Rimutaka greywackes and associated rocks. Unpublished B.Sc. (Hons) project, Geology department library, Victoria University of Wellington, 59 p.
- Begg, J.M. 1980: Sedimentology and paleogeography of some Kaihikuan Torlesse rocks in mid-Canterbury. New Zealand journal of geology and geophysics 23: 439-445.
- Blake, M.C., Jr.; Jones, D.L. 1974: Origin of franciscan melanges in northern California. In: Dott, R.H., Jr.; Shaver, R.H. ed: Modern and ancient geosynclinal sedimentation. Society of economic paleontologists special publication 19: 345-357.
- Blake, M.C., Jr.; Jones, D.L.; Landis, C.A. 1974: Active continental margins: Contrasts between California and New Zealand. In: Burk, C.A.; Drake, C.L. ed. The geology of continental margins. Springer-Verlag, New York, 1009 p.
- Botsford, S. 1983: Structural geology of the Esk Head Melange, South Island. Unpublished M.Sc. thesis, University of Canterbury. 249 p.
- Bouma, A.H. 1962: Sedimentology of some flysch deposits. Elsevier Amsterdam. 168 p.
- 1964: Turbidites. In: Bouma, A.F.; Brouwer, A. ed: Developments in sedimentology 3. Elsevier Amsterdam 247-256.
- Bradshaw, J.D. 1972: Stratigraphy and structure of the Torlesse Supergroup (560-561) Canterbury. New Zealand journal of geology and geophysics 15: 71-87.
- Bradshaw, J.D. 1973: Allochthonous Mesozoic fossil localities in melange within the Torlesse rocks of North Canterbury. Journal of the royal society of New Zealand 3: 161-167.
- Andrews, P.B. 1973: Geotectonics and the New Zealand geosyncline. Nature physical science 241: 14-16.
- Bradshaw, J.D.; Adams, C.J.; Andrews, P.B. 1981: Carboniferous to Cretaceous on the Pacific margin of Gondwanaland: the Rangitata phase of New Zealand. In: Cresswell, M.M.; Vella, P. ed: Gondwana Five. A.A. Balkema Rotterdam: 217-221.

- Byrne, T. 1982: Structural evolution of coherent terranes in the Ghost Rocks Formation, Kodiak Island, Alaska. In: Legget, J.K. ed: Trench-Forearc geology. Geological society of London special publication 10: 229-242.
- Campbell, J.W.; Warren, G. 1965: Fossil localities of the Torlesse Group in the South Island. Transactions of the Royal Society of New Zealand geology 3: 99-137.
- Carter, R.M.; Hicks, M.D.; Norris, J.R.; Turnball, I.M. 1978: Sedimentation patterns in an ancient arc-trench-ocean basin complex: Carboniferous to Jurassic Rangitata Orogen, New Zealand. In: Stanley, D.J.; Kelling, G. ed: Sedimentation in submarine canyons, fans and trenches. Dowden, Hutchinson, Ross Pennsylvania: 340-361.
- Carver, R.E. 1971: Procedures in sedimentary petrology. John Wiley & Son: 653 p.
- Chayes, F. 1956: Petrographic modal analysis. John Wiley & Sons. New York 113 p.
- Connelly, W. 1978: Uyak Complex, Kodiak Islands, Alaska: A cretaceous subduction complex. Geological society of America bulletin 89: 755-769.
- Coombs, D.S. 1953: The pumpellyite mineral series. Minerological magazine 30: 113-135.
- Landis, C.A.; Norris, R.J.; Sinton, J.A.; Borns, D.J.; Craw, D. 1976: The Dun Mountain ophiolite belt, New Zealand, its tectonic setting, construction and origin, with special reference to the southern portion. American journal of science 276: 561- 603.
- Nakamura, Y.; Vuagnat, M. 1976: Pumpellyite-actinolite facies schist of the Taueyanne Formation near Loeche, Valais, Switzerland. Journal of petrology 17: 440-471.
- 1960: Lowergrade mineral facies in New Zealand. 21st international geological congress 13: 339-351.
- Cotton, C.A. 1912: Recent and sub-recent movements of uplift and subsidence near Wellington. New Zealand. Scottish geographic magazine 28: 306-312.
- Cowan, D.S. 1974: Deformation and metamorphism of the Franciscan subduction zone complex northwest of Pacheco Pass, California. Geological society of America bulletin 85: 1623-1634.
- Cowan, D.S. 1978: Origin of blueschist-bearing chaotic rocks in the Franciscan Complex, San Simeon, California. Geological Society of America Bulletin 89:1415- 1423.
- Crook, K.A.W. 1974: Lithogenesis and geotectonics: the significance of compositional variations in flysch arenites (greywackes). Society of economic paleontologists and mineralogists

special publication 19: 304-310.

- Dickinson, W.R. 1970: Interpreting detrital modes of greywacke and arkose. Journal of sedimentary petrology 40: 695-707.
- 1982; Compositions of sandstone in Circum-Pacific subduction complexes and forearc basins. American association of petroleum geology bulletin 66: 121-137.
- Dickinson, W.R.; Suczek, C.A. 1979: Plate tectonics and sandstone compositions. American association of petroleum geologists bulletin 63: 2164-2182.
- Dickinson, W.R.; Valloni, R. 1980: Plate settings and provenance of sands in modern ocean basins. Geology 8: 82-86.
- Dickinson, W.R.; Ingersoll, R.V.; Cowan, D.S.; Helmold, K.P.; Suczek, C.A. 1982: Provenance of Franciscan greywackes in coastal California. Geological society of America bulletin 93: 95-107.
- Dickinson, W.R.; Beard, L.S.; Brakenridge, G.R.; Erjavec, J.L.; Ferguson, R.C.; Inman, K.F.; Knepp, R.A.; Lindberg, F.A.; Ryberg, P.T. 1983: Provenance of North American Phanerozoic sandstones in relation to tectonic setting. Geology society of America bulletin 94: 222-235.
- Erlank, A.J.; Kable, E.J.D. 1976: The significance of incompatible elements in Mid-Atlantic Ridge Basalts from 45°N with particular reference to Zr/Nb: Contributions to mineralogy and petrology 54: 281-291.
- Evarts, R.C.; Schiffman, P. 1983: Submarine hydrothermal metamorphism of the Del Puerto Ophiolite, California. American journal of science 283: 289-340.
- Feary, D.A.; Pessagno, E.A. 1980: An Early Jurassic age for chert within the Early Cretaceous Oponae Melange (Torlesse Supergroup), Raukumara peninsula, New Zealand. New Zealand journal of geology and geophysics 23: 623-628.
- Fleuty, M.J. 1964: The description of folds. Geological association proceedings 75: 461-492.
- Flinn, D. 1962: On folding during three-dimensional progressive deformation. Quarterly journal of the geological society of London 118: 385-428.
- Flores, G. 1955: Discussion. In: Beneo, B. ed: Les resultats des etudes pour la recherche petroliere en Sicilie (Italie). 4th world petroleum congress, Rome 1: 121-122.
- Folk, R.L. 1974: Petrology of sedimentary rocks. Hemphill publishing co. Texas 182 p.
- Foreman, H.P. 1975: Radiolaria from the North Pacific, deep sea drilling project, 32. Washington, U.S. government printing office. 579-676.

- George, A. 1983: The geology of Eastern Island Bay, South Wellington. Unpublished B.Sc.(Hons) project, Geology dept. library, Victoria University of Wellington, 82 p.
- Garrison, R.E. 1974: Radiolarian cherts, pelagic limestones and igneous rocks in eugeosynclinal assemblages. In: Hsu, K.J.; Jenkyns, H.S. ed: Pelagic sediments: on land and under the sea. International association of sedimentologists special publication 1: 367-399.
- Grant-Taylor, T.L.; Waterhouse, J.B. 1963: Monotis from the Tararua Range, Wellington. New Zealand journal of geology and geophysics 6: 623-627.
- Grapes, R. Palmer, K. 1984: Magma type and tectonic setting of metabasites, Southern Alps, New Zealand, using immobile elements. New Zealand journal of geology and geophysics 27: 21-25.
- Grapes, R.H.; Hardy, E.F., Wellman, H.W. 1984: The Wellington Mohaka and Wairarapa Faults. Victoria university of Wellington, 32 p.
- Gould, H.R. 1951: Some quantitative aspects of Lake Mead turbidity currents. Society of economic paleontologists mineralogists special publication 2: 34-52.
- Gucwa, P.R. 1975: Middle to late Cretaceous sedimentary melange, Franciscan Complex, northern California. Geology 3: 105-108.
- Hall, R. 1976: Ophiolite emplacement and the evolution of the Taurus suture zone, southeastern Turkey. Geological society of America bulletin 87: 1078-1088.
- Hicks, M.D. 1981: Deep-sea fan sediments in the in the Torlesse zone, Lake Ohau, South Canterbury, New Zealand. New Zealand journal of geology of geophysics 24: 204-230.
- Hobbs, B.E.; Means, W.D.; Williams, P.F. 1976: An outline of structural geology. Wiley International: 571 p.
- Howell, D.G. 1980a: Submarine fan facies in the Torlesse terrane, New Zealand. Journal of the Royal society of New Zealand 11: 113-122.
- Howell, D.G. 1980b: Mesozoic accretion of exotic terranes along the New Zealand segment of Gondwanaland. Geology 8: 487-491.
- Hsu, K.J. 1968: Principles of melanges and their bearing on the Franciscan-Knoxville paradox. Geological society of America bulletin 79: 1063-1074.
- Hsu, K.J. 1974: Melanges and their distinction from olistostromes. In: Dott, R.H.Jr.; Shaver, R.H. ed: Modern and ancient geosynclinal sedimentation. Society of economic paleontologists and mineralogists special publication 19: 321-333.

- Ingersoll, R.V. 1978: Submarine fan facies of the Upper Cretaceous Great Valley Sequence, Northern and Central California. Sedimentary geology 21: 205-230.
- Ingersoll, R.V.; Suczek, C.A. 1979: Petrology and provenance of Neogene sand from Nicobar and Bengal fans, D.S.D. P. sites 211 and 218. Journal of sedimentary petrology 49: 1217-1228.
- Jakes, P.; Gill, J. 1970: Rare earth elements and the island arc tholeiitic series. Earth and planetary science letters 9: 17-28.
- Jenkyns, H.C.; Hardy, R.G. 1976: Basal iron-titanium rich sediments from Hole 315A (Line Islands, central Pacific). In: Initial reports of the deep sea drilling project 33: 833-836.
- 1978: Pelagic environments. In: Reading, H.G. ed: Sedimentary environments and facies. Blackwell, Oxford: 314-371.
- Kamp, P.J.J. 1980. Pacifica and New Zealand: Proposed eastern elements in Gondwanaland's history. Nature 288: 659-664.
- Karig, D.E. 1974: Evolution of arc systems in the western Pacific. Annual review of earth and planetary sciences 2: 51-75.
- Karig, D.E.; Sharman, G.F. 1975: Subduction and accretion in trenches. Geological society of America bulletin 86: 377-389.
- Kawachi, Y. 1975: Pumpellyite-actinolite and contiguous facies metamorphism in part of Upper Wakitipu district, New Zealand. New Zealand journal of geology and geophysics 18: 401-441.
- Grapes, R.H.; Coombs, D.S.; Dowse, M. 1983: Mineralogy and petrology of a piemontite-bearing schist, western Otago. New Zealand. Journal metamorphic geology 1: 353-372.
- Kennedy, P.C.; Palmer, K.; Roser, B.P. 1981: Chemical analysis of eight U.S.G.S rock standards: BHVO-1, MAG-1, QLO-1, RGM-1, SCO-1, SDC-1, SGR-1, STM-1. Victoria University of Wellington geology department publication 21: 16 p.
- Kingma, J.T. 1967: Sheet 12, Wellington (1st ed) "Geological map of New Zealand 1:2,500,00". D.S.I.R., Wellington.
- Korsch, R.J. 1982: Structure of Franciscan complex in the Stanley Mountain Window, southern coast ranges, California. American journal of science 282: 1406-1437.
- Korsch, R.J.; Wellman, H.W. in press: The geological evolution of New Zealand and the New Zealand region. In: Nairn, A.E.M., Stehi, F.G. ed: The ocean basins and margins, volume 7A. The Pacific ocean. Plenum Press New York.
- Kushiro, I. 1969: Si-Al relation in clinopyroxenes from igneous rocks. American journal of science 158: 548-554.
- Landis, C.A.; Bishop, D.G. 1972: Plate tectonics and regional

- stratigraphic-metamorphic relations in the southern part of the New Zealand geosyncline. Geological society of America bulletin 83: 2267-2284.
- Coombs, D.S. 1967: Metamorphic belts and orogenesis in southern New Zealand: Tectonophysics 4: 501-518.
- Le Bas, M.J. 1962: The role of aluminum in igneous clinopyroxenes with relation to their parentage. American journal of science 260: 267-288.
- Lensen, G.J. 1958b: Note on fault correlations across Cook Strait. New Zealand journal of geology and geophysics 1: 263-268.
- Lensen, G.; Vella, P. 1971: The Waiohine River faulted terrace sequence. Royal society of New Zealand bulletin 9: 117-119.
- Mason, B. 1958: Principles of geochemistry: John Wiley & Sons. 310 p.
- Maynard, J.B.; Valloni, R.; Yu, H-S. 1982: Composition of modern deep-sea sands from arc-related basins. In: Leggett, J.K. ed: Trench Forearc Geology: sedimentation and tectonics on modern and ancient active plate margins. Geological society of London special publication 10: 551-561.
- McCall, G.J.H. 1983. Melanges of the Makran, southern Iran. In: McCall, G.J.H. ed: Ophiolitic and related melanges. Hutchinson Ross publishing company. Stroudsbury. 292-299.
- McKay, A. 1888a: On mineral deposits in the Tararua and Ruahine mountains. New Zealand geological survey report, geology exploration 1887-1888 19: 1-6.
- 1888b: On the Tauherenikau and Waiohine valleys, evolution of northern New Zealand and adjacent areas of the southwest pacific. New Zealand geological survey report, geology exploration 1887-1888 19: 37-48.
- Middleton, G.V.; Hampton, M.A. 1973: Sedimentary gravity flows: mechanics of flow and deposition. In. Turbidites and deep water sedimentation SEPM Pacific short course, Anaheim: 1-38.
- Moore, J.C. 1975: Selective subduction. Geology 3: 530-532.
- Moore, J.C.; Wheeler, R.L. 1978: Structural fabric of a melange Kodiak Islands, Alaska. American journal of science 278: 739-765.
- Curry, J.R.; Emmel, F.J. 1982: Sedimentation in the Sunda trench and forearc region. In: Leggett, J.K. ed: Trench-Forearc geology. London geological society special publication 10: 245-258.
- Nisbet, E.G.; Pearce, J.A. 1977: Clinopyroxene compositions in mafic lavas from different tectonic settings. Contributions to mineralogy and petrology 63: 149-160.
- Offler, R.; Baker, C.K.; Gamble, J. 1981: Pumpellyites in two low grade

- metamorphic terranes north of Newcastle, NSW Australia. Contributions to mineralogy and petrology 76: 171-176.
- Ongley, M. 1943: Surface trace of the 1855 Earthquake. Transactions of the Royal Society of New Zealand 73: 84-89.
- Orr, in prep: The geology of the Torlesse Supergroup, southern Tararua Range, North Island, New Zealand.
- Pettijohn, F.J.; Potter, P.E.; Siever, R. 1972: Sand and sandstone. Springer-Verlag New York. 618 p.
- Pessagno, E.A. 1977a: Lower Cretaceous radiolarian biostratigraphy of the Great Valley sequence and Franciscan Complex, California Coast Range. Cushman foundation for foraminiferal research. Special publication 15, 87 p.
- 1977b: Upper Jurassic radiolaria and radiolarian biostratigraphy of the California Coast Ranges. Micropaleontology 23: 56-113.
- Newport, R.L. 1972: A technique for extracting Radiolaria from radiolarian chert. Micropaleontology 18: 231-234.
- Whalen, P.A. 1982: Lower and Middle Jurassic radiolaria (multicyrtid Nassellariina) from California, east-central Oregon and the Queen Charlotte Islands, B.C. Micropaleontology 28: 111-169.
- Prestvik, T. 1982: Basic volcanic rocks and tectonic setting. A discussion of the Zr-Ti-Y discrimination diagram and its suitability for classification purposes. Lithos 15: 173-252.
- Rupke, N.A. 1978: Deep clastic seas. In: Reading, H.G. ed: Sedimentary environments and facies. Blackwell, Oxford: 372-415.
- Rast, N. 1956: The origin and significance of boundinage. Geological magazine 93: 401-408.
- Rattenbury, M.S. 1983: Geology of Otaki Forks, Tararua Range. Unpublished M.Sc.(Hons) thesis, University of Auckland 109 p.
- Roser, B.P. 1983: Comparative studies of copper and manganese mineralisation in the Torlesse, Waipapa and Haast Schist Terranes, New Zealand. Unpublished Phd thesis Geology dept. library, Victoria University of Wellington 491 p.
- Saleeby, J. 1979. Kaweah serpentinite melange, southwest Sierra Nevada foothills, California. Geological society of America Bulletin 90: 29-46.
- Saunders, A.D.; Tarney, J.; Marsh, N.G.; Wood, D.A. 1979: Ophiolites as ocean crust or marginal basin crust: A geochemical approach. In: Ophiolites proceedings of international ophiolite symposium, Cyprus. Cyprus geological survey department 193-204.

- Silver, E.A.; Beutner, E.C. 1980: Penrose conference report- melanges: Geology 8: 32-34.
- Suggate, R.P.; Stevens, G.R.; Te Punga, M.T. 1978: The geology of New Zealand. Government printer, Wellington, 2 vols, 820 p.
- Sun, S-S.; Nesbitt, R.W.; Sharaskin, A.Y. 1979: Geochemical characteristics of mid-ridge basalts. Earth and planetary science letters 44: 119-138.
- Surdam, R.C. 1969: Electron microprobe study of prehnite and pumpellyite from the Karmutsen Group, Vancouver Island, British Columbia. American mineralogist 54: 256-266.
- Taylor, S.R. 1965: The application of trace element data to problems in petrology. Physics and chemistry of the earth 6: 133-213.
- Turner, F.J.; Weiss, L.E. 1963: Structural analyses of metamorphic tectonites. McGraw-Hill Book Company, New York, 545 p.
- Yao, A. 1979: Radiolarian fauna from the Mino Bely in the northern part of the Inayama Area, Central Japan Part II: Nassellariia. of geosciences, Osaka City University 22: 21-72.
- 1982: Middle Triassic to Early Jurassic radiolarians from the Inuyama area, Central Japan. Journal of geosciences, Osaka City University 25: 53-70.
- Vella, P. 1963: Upper Pleistocene succession in the inland part of Wairarapa Valley, New Zealand. Transactions of royal society of New Zealand 2: 63-78.
- Webby, B.D. 1967: Tube fossils from the Triassic of southwest Wellington, New Zealand. Transactions of the royal society of New Zealand 5: 181-191.
- Wellman, H.W. 1969: Tilted marine beach ridges at Cape Turakirae New Zealand. Tuatara 17: 82-93.
- 1972: Rate of horizontal fault displacement in New Zealand. Nature 237: 275-277.
- Webby, B.D. 1967: Tube fossils from the Triassic of southwest Wellington, New Zealand. Transactions of the royal society of New Zealand geology 5: 181-191.
- Winkler, H.G.F. 1965: Petrogenesis of metamorphic rocks. Springer-Verlag Berlin. Heidelberg, 220 p.

APPENDIX I

MAPS

Topographic maps and aerial photographs used in this study are:

Topographic maps scale 1:25,000

N.Z.M.S 260 S26/C

N.Z.M.S 260 S26/D

N.Z.M.S 260 S27/A

Aerial photographs scale approximately 1:25,000

S.N 3672 4731/27

S.N 3672 4731/28

S.N 3672 4731/29

S.N 3672 4732/25

S.N 3672 4732/26

S.N 3672 4732/27

S.N 3672 4732/28

S.N 3672 4732/29

S.N 8171 F/5

S.N 8171 F/6

S.N 8171 F/7

APPENDIX II

MAJOR AND TRACE ELEMENT ANALYSES

Procedure

Thirty-four samples were analysed for major and trace elements contents. The rock samples were hydraulically crushed. Chips with obvious veining, weathering and other impurities were discarded. "Clean" chips were reduced to a fine powder in a "tema" rock mill.

Analyses were determined in an automated Siemens SR S-1 X-Ray Fluorescence Spectrometer using fused glass discs (major elements) and pressed powder pellets (trace elements). Full details of the analytical procedures are contained in Kennedy et al. (1981).

APPENDIX III

POINT COUNTING PROCEDURES

Point counting procedures, follow the method of Glagoleu and Chayes (Carver 1971), where modal analysis were determined by point counting 500 grains noting grain composition (those listed in Table 2-2) from a standard thin-section using a Swift automatic point counter. As the total lithic rock fragment is low, an extra 150 point counts of lithics fragments alone was made. During the initial count of 500 points, quartz and feldspar grains within lithic fragments were assigned to the quartz and feldspar categories respectively, following Dickinson (1970). A few sandstone thin-sandstones contain mud-stone rip-up clasts and these clasts were not included in the point counts.

Theoretical reliability of values obtained is within 4.5% of true values at the 95% confidence level (Van der Plais & Tobi 1965).



APPENDIX IV

GRAIN SIZE

The grain size of fifteen sandstone samples (those which had modal analyses) was determined from thin-section measurement. The apparent long axis of 100 grains were measured using a graduated micrometre eyepiece. The grains being measured were determined by a Swift automatic stage (the same technique as for modal point counting except instead of noting grain composition, the apparent long axis of each grain was measured).

APPENDIX V

SAMPLE LIST

Samples are housed in the petrology collection, Geology Department, Victoria University of Wellington. For most rock samples there is a hand specimen lodged (* no rock sample), as well as specimens that are listed under the column "Sample Type" where:

T=Thin-section;

P=Powder;

M=Electron microprobe section.

V.U.W No.	SAMPLE TYPE	GRID REFERENCE	SHORT DESCRIPTION
17010	T	S26C/ 0560 1050	Very fine grained sandstone
17011	T	S27A/ 0180 0855	Very fine grained sandstone
17012	T	S26C/ 0515 1285	Fine grained sandstone
17013	T	S26C/ 0582 1293	Fine grained sandstone
17014	T P M	S27A/ 0048 0839	Fine grained sandstone
17015	T	S27A/ 9972 0783	Fine grained sandstone
17016	T	S27A/ 9800 0785	Fine grained sandstone
17017	T	S27A/ 9890 0838	Very fine grained sandstone
17018	T	S27A/ 0133 0931	Fine grained sandstone
17019	T	S27A/ 0100 0983	Fine grained sandstone
17020	T	S27A/ 0081 1000	Medium grained sandstone
17021	T	S27A/ 0080 1000	Fine grained sandstone
17022	T	S27A/ 0039 0960	Fine grained sandstone
17023	T	S27A/ 0053 0928	Very fine grained sandstone
17024	T	S26D/ 1104 1931	Fine grained sandstone
17025	P	S26D/ 1197 1783	Fine grained sandstone
17026	P	S26D/ 1197 1783	Very fine grained sandstone
17027	P	S26D/ 1197 1783	Argillite
17028	P	S26D/ 1125 1912	Fine grained sandstone
17029	P	S27A/ 0244 0559	Argillite
17030	P	S27A/ 0244 0559	Fine grained sandstone
17031	P	S27A/ 0244 0559	Argillite
17032	P	S26C/ 0770 1310	Fine grained sandstone
17033	P	S26C/ 0527 1065	Medium grained sandstone
17034	P	S26C/ 0688 1380	Very fine grained sandstone
17035	P	S26C/ 0378 1030	Very fine grained sandstone
17036	P	S27A/ 9965 0816	Argillite
17037	P	S27A/ 0455 0923	Very fine grained sandstone
17038	T	S27A/ 0040 0987	Calcareous siltstone
17039		S27A/ 0072 0903	Very fine grained sandstone
17040		S27A/ 9968 0852	Metabasite
17041	P	S27A/ 9968 0884	Metabasite
17042	T P	S27A/ 9962 0880	Metabasite
17043	T P	S27A/ 9970 0872	Metabasite
17044	T P	S27A/ 0044 0870	Metabasite
17045	T P M	S27A/ 0401 0789	Metabasite
17046	P	S27A/ 0401 0790	Metabasite
17047	P	S27A/ 0401 0790	Metabasite
17048	P	S27A/ 0400 0791	Metabasite
17049	T P	S26D/ 1108 1937	Metabasite
17050	T P	S26D/ 1104 1934	Metabasite
17051	P	S26D/ 1106 1937	Metabasite

V.U.W No.	SAMPLE TYPE	GRID REFERENCE	SHORT DESCRIPTION
17052	P	S26D/ 1106 1936	Metabasite
17053	T P	S27A/ 0180 0850	Metabasite
17054	P	S26D/ 1103 1953	Metabasite
17055	T P	S26D/ 1192 1799	Metabasite
17056	T M	S27A/ 9941 0882	Metabasite
17057	T	S27A/ 9968 0879	Metabasite
17058	T M	S27A/ 9960 0880	Metabasite
17059	* T	S27A/ 9956 0880	Metabasite
17060	* T	S27A/ 9975 0872	Metabasite
17061	T	S27A/ 9968 0873	Metabasite
17062	T M	S27A/ 9975 0872	Metabasite
17063	T	S27A/ 0071 0858	Fine grained sandstone
17064	T	S27A/ 0071 0858	Argillite
17065	T	S27A/ 0403 0788	Argillite
17066	T	S27A/ 0510 0813	Fine grained sandstone
17067	T	S27A/ 0403 0788	Argillite
17068	T	S27A/ 9836 0810	Medium grained sandstone
17069	T	S27A/ 9962 0825	Very fine grained sandstone
17070	T	S27A/ 9963 0820	Argillite
17071	T	S27A/ 0165 0935	Fine grained sandstone
17072	T	S26C/ 0428 1130	Conglomerate
17073	T	S26C/ 0382 1081	Argillite
17074	T	S27A/ 0435 0903	Red chert
17075	T	S26C/ 0581 1027	Very fine grained sandstone
17076	T	S26C/ 0521 1072	Very fine grained sandstone
17077	T	S26C/ 0530 1061	Very fine grained sandstone
17078	T	S26C/ 0601 1205	Red chert
17079	T	S26C/ 0620 1218	Red chert
17080	T	S26C/ 0790 1290	Olistostrome
17081	T	S26C/ 0789 1290	Limestone
17082	T	S26C/ 0788 1291	Limestone
17083	T	S26C/ 0640 1341	Medium grained sandstone
17084	T	S26C/ 0644 1346	Limestone
17085	* T	S26C/ 0532 1262	Very fine grained sandstone
17086	T	S27A/ 0547 0832	White chert
17087	T	S26C/ 0547 1278	Fine grained sandstone
17088	T	S26C/ 0547 1278	Olistostrome
17089	T	S26C/ 0547 1278	Olistostrome
17090	T	S26C/ 0446 1295	Fine grained sandstone
17091	T	S26C/ 0832 1590	Metabasite
17092	T	S26D/ 1151 1890	Grey chert
17093	T	S26D/ 1160 1889	Calcareous siltstone
17094	T	S26D/ 1108 1950	Argillite
17095	T	S26D/ 1180 1842	Red chert
17096	T	S26D/ 1192 1794	Red argillite
17097	T	S26D/ 1192 1794	Limestone
17098	T	S26D/ 1130 1710	Green chert
17099	T	S26D/ 1147 1605	Calcareous siltstone
17100	T	S26D/ 1155 1883	Red argillite
17101	T	S27A/ 9955 0837	Argillite
17102	T	S27A/ 0402 0789	Quartz vein
17103	T	S27A/ 0410 0988	Very fine grained sandstone

V.U.W No.	SAMPLE TYPE	GRID REFERENCE	SHORT DESCRIPTION
17104	T	S27A/ 0430 0957	Fine grained sandstone
17105	T	S26C/ 0549 1175	Very fine grained sandstone
17106	T	S27A/ 9795 0790	Very fine grained sandstone
17107	T	S26C/ 0709 1397	Fine grained sandstone
17108	T	S26C/ 0547 1278	Fine grained sandstone
17109			Chert (Manawatu Gorge)
17110			Chert (Manawatu Gorge)
17111		S26C/ 1130 1710	Greywacke ellipsoid
17112		S26C/ 1130 1710	Greywacke ellipsoid
17113		S26C/ 1130 1710	Greywacke ellipsoid
17114		S26C/ 1130 1710	Greywacke ellipsoid
17115		S26C/ 1130 1710	Greywacke ellipsoid
17116		S26C/ 1130 1710	Greywacke ellipsoid
17117		S26C/ 1130 1710	Greywacke ellipsoid
17118		S26C/ 1130 1710	Greywacke ellipsoid
17119		S26C/ 1130 1710	Greywacke ellipsoid
17120		S26C/ 1130 1710	Greywacke ellipsoid
17121		S26C/ 1130 1710	Greywacke ellipsoid
17122		S26C/ 1130 1710	Greywacke ellipsoid
17123		S26C/ 1130 1710	Greywacke ellipsoid
17124		S26C/ 1130 1710	Greywacke ellipsoid
17125		S26C/ 1130 1710	Greywacke ellipsoid
17126		S26C/ 1130 1710	Greywacke ellipsoid

APPENDIX VI

ELECTRON MICROPROBE ANALYSIS

Electron microprobe analyses were made using the Jeol 733 Superprobe in the Analytical Facility, Victoria University of Wellington. All polished mounts were carbon coated.

APPENDIX VII

CARBONATE DETERMINATION

Thin-sections were stained with alizarin red-S and potassium ferricyanide solution, to differentiate carbonates. For staining the thin sections were :

- 1) Etched in dilute (1.0%) HCl solution;
- 2) Immersed in a solution of alizarin red-S and potassium ferricyanide for 45-75 seconds;
- 3) Immersed again in a solution of alizarin red-S to further increase the colour differentiation of carbonate;
- 4) Washed in distilled water.

APPENDIX VIII

ELECTRON MICROPROBE ANALYSES

CLINOPYROXENE 17045									
SiO ₂	49.30	49.09	48.93	49.67	49.39	47.06	49.47	49.67	46.28
Al ₂ O ₃	3.70	3.68	4.17	3.54	3.93	6.03	4.02	4.18	6.59
TiO ₂	1.91	1.85	2.13	2.04	2.09	3.16	1.75	1.79	2.93
FeO	7.56	7.79	7.79	7.68	7.78	8.33	6.57	6.74	7.70
MnO	0.15	0.12	0.16	0.14	0.17	0.10	0.10	0.12	0.12
MgO	14.48	14.55	14.15	14.02	14.20	12.45	14.60	14.41	12.87
CaO	22.42	22.29	22.25	21.83	22.12	21.62	22.18	21.65	22.93
Na ₂ O	0.38	0.36	0.41	0.33	0.38	0.55	0.39	0.37	0.36
K ₂ O			0.01	0.01		0.04		0.07	0.02
Total	99.90	99.73	100.00	99.26	100.06	99.34	99.08	99.00	99.80

CLINOPYROXENE 17062									
SiO ₂	46.48	48.87	48.02	48.19	49.80	51.32	48.81	47.98	
Al ₂ O ₃	4.28	4.37	5.16	5.50	4.06	2.49	5.00	4.42	
TiO ₂	1.96	2.03	2.01	2.06	1.99	1.36	2.29	2.27	
FeO	7.47	7.53	6.77	6.83	7.83	7.22	7.46	8.52	
MnO	0.19	0.15	0.17	0.08	0.12	0.17	0.12	0.10	
MgO	13.89	13.86	13.78	13.79	14.05	15.20	13.63	13.46	
CaO	22.33	22.33	22.68	22.29	22.41	21.35	21.84	21.37	
Na ₂ O	0.43	0.45	0.39	0.40	0.38	0.32	0.42	0.44	
K ₂ O	0.03			0.03	0.04				
Total	99.06	99.59	98.98	99.17	100.68	99.43	99.57	98.56	

CLINOPYROXENE 17058				
SiO ₂	48.63	50.20	50.78	49.20
Al ₂ O ₃	6.42	4.80	4.82	4.87
TiO ₂	1.71	0.77	0.86	0.87
FeO	7.55	5.78	5.84	5.71
MnO	0.19	0.04	0.22	0.17
MgO	14.38	16.90	16.89	16.88
CaO	19.73	19.51	20.23	19.01
Na ₂ O	0.34	0.33	0.33	0.33
K ₂ O	0.01		0.01	
Total	98.96	98.33	99.98	97.04

PUMPELLYITE								
GREYWACKE			METABASITE					
17014			17056			17062		
SiO ₂	37.37	36.97	39.04	37.38	37.75	36.58	44.23	
Al ₂ O ₃	25.25	20.60	19.11	20.56	28.83	29.79	27.01	
TiO ₂	0.01	0.06	1.20	0.15	0.02	0.03	0.02	
FeO	9.92	8.82	11.84	10.37	0.59	0.24	0.94	
MnO	0.37	0.19	0.09	0.05	1.43	1.11	0.67	
MgO	0.05	2.66	2.71	2.27	0.34	0.59	1.04	
CaO	23.40	20.77	16.53	17.71	20.49	21.31	18.39	
Na ₂ O			0.01	0.06	0.03	0.02	3.11	
K ₂ O			0.73	0.38			0.03	
Total	96.37	90.07	91.26	88.93	88.48	89.67	95.44	

CELADONITE (17056)		PREHNITE (17058)				
SiO ₂	56.58	40.32	41.98	41.56	40.74	38.78
Al ₂ O ₃	7.84	19.96	18.84	18.87	20.55	20.53
TiO ₂		0.09	0.01	0.01	0.05	0.07
FeO	14.71					
Fe ₂ O ₃		6.06	7.40	7.42	5.03	5.80
MnO	0.05	0.05	0.02	0.07	0.09	0.06
MgO	6.40	0.02	0.01	0.01	0.05	
CaO	0.21	24.93	25.76	25.74	25.27	24.49
Na ₂ O		0.04	0.09	0.10	0.07	0.06
K ₂ O	6.40	0.03	0.01	0.01	0.01	0.01
Total	92.19	91.48	94.12	93.79	91.86	89.80

Total iron as FeO or Fe₂O .

SPHENE								
"NORMAL" 17056					AL-FE RICH 17056			
SiO ₂	31.83	29.67	32.41	28.60	31.14	43.26	38.96	
Al ₂ O ₃	3.31	2.88	2.99	2.81	5.09	5.41	6.78	
TiO ₂	33.04	26.81	29.78	25.04	14.25	6.98	10.73	
Fe ₂ O ₃	2.67	7.49	5.86	7.04	11.03	15.05	11.46	
MnO					0.18		0.31	
MgO	0.17	0.14	0.52	0.17	4.14	6.93	5.22	
CaO	26.68	25.56	25.52	25.30	21.33	21.49	19.65	
Na ₂ O		0.12			0.30	0.38	0.31	
K ₂ O	0.34	0.10	0.07	0.16	0.34	0.10	0.40	
Total	98.05	92.77	97.16	89.12	87.80	99.61	93.82	

